EPRI

Fiber Optic Sensors for Temperature and Strain Monitoring in Motors and Generators

Export Control U.S.

LICENSED MATERIAL

WARNING:
Please read the Export Control and License Agreement on the back cover before removing the Wrapping Material.

Technical Report

Fiber Optic Sensors for Temperature and Strain Monitoring in Motors and Generators

TR-101950-V2
2487-02

Final Report, April 1997

Prepared by
Battelle
505 King Avenue
Columbus, Ohio 43201

Authors
A. A. Boiarski
J. P. Kurmer

Prepared for
Electric Power Research Institute
3412 Hillview Avenue
Palo Alto, California 94304

EPRI Project Manager
J. Stein

Generation Group

DISCLAIMER OF WARRANTIES AND LIMITATION OF LIABILITIES

ORGANIZATION(S) THAT PREPARED THIS REPORT

BATTELLE

ORDERING INFORMATION

Requests for copies of this report should be directed to the EPRI Distribution Center, 207 Coggins Drive, P.O. Box 23205, Pleasant Hill, CA 94523, (510) 934-4212.

REPORT SUMMARY

Early detection of potential problems in motor and generator windings helps decrease outage time and reduces repair costs. This work demonstrates the use of fiber optic sensors for measuring temperature and strain in these and other electrical components

Background

Conductor temperature monitoring is important for safe, reliable operation of power plant equipment. For example, monitoring of stator or rotor winding temperature could help determine winding integrity. Techniques presently exist to measure average temperature of a stator coil or local stator temperature at specific points. However, no method exists for determining peak temperature by measuring temperature along the entire stator winding length. Further, present techniques can only measure rotor surface temperature. No internal rotor temperature monitoring is possible. End winding strain also is important to measure in operating motors and generators, especially during start-up and shut-down periods. In addition, an indication of loose winding conditions would be beneficial during continuous operation. To explore new methods of monitoring electrical power equipment, EPRI and The Consolidated Edison Company of New York, Inc., co-funded this effort.

Objectives

To demonstrate fiber optic approaches for temperature and strain monitoring in electric motors and generators.

Approach

For continuous temperature measurement over the entire stator or rotor surface area, researchers developed a distributed fiber optic temperature sensing (DFOTS) system and tested it in operating power plant equipment. This system consisted of a high-resolution optical time-domain reflectometer (OTDR) and a specially prepared optical fiber sensor. The sensor was formed by coating a proprietary, ultraviolet light-curable material onto a silica core glass during fiber production. Changes in Rayleigh backscattered light were used to indicate temperature changes along the fiber length. The system consisted of a 40 meter length of sensing fiber and an OTDR with length resolution capability of either 3, 8, or 30 cm. The research team installed the sensing fiber in the stator windings of a boiler feed-pump motor and an air-cooled turbine generator during winding repair. They also installed it in the rotor of a synchronous condenser unit using a special rotary joint connector.

The team demonstrated end-winding strain monitoring by developing and laboratory testing a strain sensor based on an optical fiber bending-loss approach. Researchers obtained a special commercial fiber that used transverse force to produce fiber bending loss. They mounted this fiber in a mechanical transducer that converted local strain into transverse loading on a short length of fiber. A simple emitter-detector combination measured changes in fiber loss. The fiber loss data indicated static and dynamic strain in a structure at the point where the transducer was mounted. The research team attached the strain sensor to an aluminum bar and subjected it to known static and dynamic strain conditions in a laboratory environment. These tests determined basic sensor performance.

Results

This effort demonstrated that fiber optic sensors can monitor temperature and strain in electrical power equipment**.** The distributed fiber optic temperature sensing (DFOTS) system measured winding temperature in operating motors and generators. The project first attempted winding temperature measurements in the rotor of a synchronous condenser motor. Sensing fiber damage prevented acquisition of operational temperature data. The rotary joint worked as expected indicating that rotor temperature measurements were feasible. After jacketing the fiber to minimize damage potential, temperature data were obtained in the stator winding of a boiler feed pump motor. Results indicated that no hot spots existed in the stator winding following a rewind operation. The project also obtained feed-pump results once the motor was installed in an operating power plant.

The strain sensor was tested under laboratory conditions using both static and dynamic loading conditions. For static loads, the sensor output was linear over a range from -1000 to + 1000 micro-inches per inch (microstrain). The measurement resolution was 5 micro-inches per inch. The project also obtained dynamic measurements at a fixed strain of 200 micro-inches per inch over a range from 5 to 140 Hz. These dynamic strain results indicated that the sensor response was constant up to 100 Hz. A small degradation in output response occurred above the 100 Hz oscillation frequency.

EPRI Perspective

Demonstration of a method for directly monitoring peak stator winding temperature and end winding strain will allow early detection of stator and rotor winding problems. Early detection could limit damage and extend winding life. Furthermore, measurement of local winding temperature throughout the generator and strain on the end windings will allow operators to more effectively control any winding malfunctions. Besides motors and generators, utilities also can apply fiber optic sensing approaches to temperature and strain monitoring of transformers, bus connectors, and transmission lines.

TR-101950-V2

Interest Categories

Fossil steam plant O&M cost reduction
Turbines and generators
Instrumentation and control

Keywords

Temperature sensors
Strain sensors
Electric motors / generators
Field testing
Stator / rotor windings
Fiber optics

ACKNOWLEDGMENTS

The sensor development and major field testing efforts were co-funded by EPRI and the Consolidated Edison Company of New York, Inc. Rotor temperature measurements were supported by PG&E. The authors wish to acknowledge several individuals for their valuable contributions made during this research effort.

Tim Fink, Gerald Pilate and Dennis Rielley of Con Edison are to be commended for their valuable assistance during the Hudson Avenue and Gowanus power station testing. Charles Koffler (Sytek Benkiser, Inc), Denise Sliker (Fibertron Inc) and Robert Davis of PG&E should be recognized for their assistance during the synchronous motor testing at the San Mateo substation.

Finally, a special thank you goes to Mr. Jan Stein of EPRI for his consultation and encouragement throughout the course of this project.

CONTENTS

LIST OF FIGURES

Figure **Page**

Figure **Page**

LIST OF TABLES

SUMMARY

The Contractor developed both a distributed fiber optic temperature sensor (DFOTS) system and a point fiber optic strain sensor. The DFOTS system was used to successfully obtain winding temperature distribution data in operating power plant environments. The point fiber optic strain sensor was demonstrated in a laboratory test environment as a method of measuring static and dynamic strain at selected points in a winding structures.

The DFOTS system demonstrations involved measurement of the temperature distribution in rotor and stator windings of motors and generators. The DFOTS system used commercial optical radar techniques, OTDR, to measure temperature at multiple points along a specially fabricated sensing fiber. Hot spots less than 10 cm long were measured over a 40-meter fiber length. This is equivalent to having four hundred point sensors located along the fiber. The sensor's temperature measurement range was 0 to 150°C and the accuracy was estimated to be at least ±5°C. The temperature sensor was formed by coating commercial silica core glass with a special low-index polymer using standard fiber production methods. The cladding was soft so a 1 mm diameter teflon™ buffer coating was added during manufacturing to provide basic protection. Modeling efforts showed that this polymer cladding, which contained scattering centers, functioned by changing its refractive index with temperature so that more or less core-transmitted optical power was present in the cladding material. The cladding was designed to scatter light, therefore, the backscattered signal becomes a sensitive function of temperature. The fiber transmission-loss coefficient itself also varied with changing fiber temperature.

Distributed temperature sensor calibration data were obtained on the sensing fiber by heating known lengths to known temperatures. Both changes in scattering signal and transmission loss were determined. A special, high-resolution OTDR was used during the sensor tests to interrogate the fiber and provide both temperature and position information. Results of the thermal tests demonstrated that the sensor results agreed with the clad-scattering model. A new sensor referencing approach was also identified. This new referencing method involved measurement of the back-scattering signal from both ends of the sensing fiber using a fiber optic switch arrangement. The new referencing method involved subtracting the mathematical inversion of the signal from one end from the regular signal obtained from the other fiber end. This advanced referencing scheme cancelled the fiber loss variation with temperature, therefore,

winding temperature data could be obtained by a simple algebraic manipulation of the scattering signal change.

The DFOTS system was used to obtain temperature data for three field test applications, namely: Rotor winding temperature in a synchronous condenser. Stator winding temperature in a boiler feed-pump motor, and stator winding temperature in an air cooled turbine generator. The DFOTS system was first used in a salient pole field winding monitoring application at PG&E's (Pacific Gas and Electric's) San Mateo sub-station. Four lengths of standard sensing fiber were installed in two V-Block regions in a serpentine fashion using epoxy. After installation, the fibers were tested in the rewind shop using the DFOTS system. Two of the fibers were severely damaged along the fiber length and at the connector (end termination). The other two installed fibers also experienced some damage resulting in additional transmission loss, but were still usable. Temperature data were obtained for one of the fibers by heating the V-Block region with a gas-fired blower. These shop check-out tests indicated that DFOTS determined temperature agreed with a standard contact-type thermocouple measurement . Following the shop tests, the instrumented rotor was shipped to the power station and installed. A rotary joint was used to provide optical interrogation of the fiber (from one end) during rotor rotation at 720 r/min. A feed-through connector was also required as a pressure seal for the fiber as it passed through the hydrogen-cooled condenser housing. DFOTS data were obtained for static, rolling (no load) and load conditions (air and hydrogen coolant). Data analysis indicated that the entire system functioned properly, however, the sensing fibers were severed during rotor installation in the condenser housing. Although not totally successful, this initial attempt at rotor temperature measurement indicated that the DFOTS approach to rotor temperature monitoring was feasible. After examining the difficulties encountered in these rotor tests, the fiber was henceforth jacketed with a standard loose-tube jacket containing kevlar material as a strength member. Standard connectors were also installed that mechanically attached to the jacket and provided a rigid end connection.

The second DFOTS system installation was performed on a boiler feed-pump motor from the Hudson Avenue power station (Consolidated Edison Company of New York, Inc.). A forty meter length of jacketed fiber sensor was sent to Con Edison's Van Nest shop where it was installed in the motor's stator winding after a standard rewind operation. The fiber was placed on the stator coil surface in every third slot by looping it back and forth throughout the winding. The fiber was held in place using lashing, epoxy, and silicone adhesive. The installed fiber was then painted with insulating paint. Following installation, the DFOTS system was set-up at the shop and the fiber was tested during a standard coil-loop check-out test. These shop tests revealed that the fiber had been damaged somewhat at positions where it entered and exited the motor housing, however, the damage did not compromise temperature measurements. DFOTS determined temperature data were obtained during the coil-loop testing. These data showed that no hot-spots were present in the winding. Further, the sensing-fiber temperature data agreed with values obtained from standard RTD devices located in several stator slot positions. Following these check-out tests, the stator was installed at the Hudson Avenue station and results were obtained for various pump load conditions. These field-test data indicated that the stator temperature was uniform and reached a peak value of 18°C above ambient at a no-load state. For maximum pump loading, the measured temperature rose to 28°C above ambient. Following these tests, fiber strain relief was provided at the fiber-motor / generator housing-interface points.

The final application of the DFOTS system to winding temperature monitoring was made at the Gowanus Power station (Con Edison) in New York city. In this case, the sensing fiber was installed in the stator of an air-cooled turbine generator following repair of the unit's rotor winding. During installation, the sensing fiber was placed along the surface of the top half of the coil in every third slot. Seven of the 36 stator slots were instrumented with fiber that was held in place with silicone adhesive and coated with insulating paint. In this installation, only short lengths of sensing fiber exited the generator's frame assembly and these short lengths were physically isolated for protection. System check-out tests indicated that only minor light losses were introduced in the fiber during this optimized installation process. These transmission changes occurred at points where the sensing fiber entered and exited the stator coil. A further installation refinement involved use of standard 40 meter fiber optic jumper cables to locate the OTDR equipment in a control room at a safe distance away from the generator. Stator temperature data were obtained for start-up and near steady-state operating conditions at full generator load. These measurements indicated that stator temperature was uniform (i.e., no hot spots) and the peak temperature was 23°C above the ambient air value.

No suitable commercial device was available at the beginning of this project so a new fiber optic strain sensor was developed by the Contractor to measure strain in end-windings during start-up, shut-down and continuous operating conditions. End-winding strain is related toN deflection of the end-winding structures. Based on some early internal research and development (IR&D) work, the sensor was constructed using a commercially available distributed bending loss sensor obtained from Herga Ltd. in the UK. Herga uses this fiber to manufacture optical switches for consumer safety applications. When axial force is exerted on the Herga fiber, at any point along its length, fiber bending loss occurs. A simple light emitting diode and solid state detector combination are used to indicate the degree of fiber loss (i.e., measure fiber transmission). In its early IR&D efforts, we noted that the amount of loss was proportional to the applied axial force. To produce a strain sensor, the Herga fiber was placed in a special mechanical device designed by the Contractor, that was mounted to the loaded structure. The small mechanism converted local strain on the base of this device into transverse force on a short length of the fiber inserted into the mechanism. This design produces a point strain sensor, where the measurement point can be changed by changing the location where the transducer device is mounted along the Herga fiber length. Several transducers could be mounted on the same fiber to provide a strain summation device. Further, a series of fibers, with one transducer each, could be used to determine the strain on a series of end-winding structures.

In laboratory tests, the strain sensor was mechanically attached to an aluminum bar and the bar subjected to both compressive and tensile strains over a wide range of values. Both static and dynamic strain were introduced using various laboratory equipment to generate known strain conditions. These laboratory tests determined the basic performance parameters for the new strain sensing device. For static loads in a cantilever loading configuration, the sensor output was found to be linear over a range from -1000 to +1000 micro-inches per inch (i.e., micro-strain units). The measurement resolution was ±5 micro-strain over this broad measurement range. Dynamic measurements were also made at a fixed strain of 200 micro-inches per inch. Both oscillating cantilever and axial dynamic loading conditions were used to test the frequency response of the sensor from 5 to 140 Hz. These dynamic strain results indicate that the fiber optic strain sensor's response was constant over a range from 5 to 100 Hz. From 100 to 140 Hz, a small decrease in sensor response was noted at the 200 micro-strain level.

Results in this study indicate that fiber optic sensors can measure winding temperature and end-winding strain in power generating equipment. The problems of fiber damage were overcome using commercial fiber jacketing and end-connection approaches. Successful fiber installation (retro-fit) was demonstrated in both stator and rotor applications. Further sensor and system development is required, but the sensors described herein could both be commercialized. Once in use, these sensors could provide monitoring of winding integrity and early detection of potential motor and generator winding problems. Monitoring may be useful for extending winding life. Also, early warning of problem conditions could help reduce unplanned outage time and reduce repair costs.

1

INTRODUCTION

Measurement of conductor temperature and end-winding strain provides important information for safe and reliable operation of power equipment. For example, temperature and strain monitoring of motor or generator rotor and stator windings could indicate winding integrity and give the operator warning of fault conditions.

Thermal damage to the conductor does not normally occur due to temporary overload conditions, however, higher than normal temperatures can have a cumulative effect of shortening insulation life. There are established methods for stator temperature measurement at selected points in motors and generators. On-line techniques to locate and measure the hottest stator winding section are, however, not available. Further, only average rotor temperature measurement capabilities exist. Therefore, improved temperature monitoring in motors and generators could minimize deterioration of insulation, and possibly help predict winding life.

Start-up and trips cause maximum deflection (hence strain) of end-winding structures. If these transient strain conditions could be rapidly measured, feed-back systems could minimize this strain by tailoring the detailed time history to minimize the effects of these transient events. Furthermore, repeated on/off cycling and/or extended use can cause the stator or rotor coils to loosen. This loose-coil problem can cause catastrophic damage to occur if not detected in a timely manner. Detection of a loose winding condition would be beneficial in preventing some major winding failures and allowing for timely repair. There are established methods for detecting end-winding deflection in stator coils, but these methods are expensive and they do not provide any direct strain measurements or give detailed frequency information regarding deflection phenomenon. Therefore, improved end-winding strain monitoring is also important in motors and generators.

Besides motors and generators, monitoring opportunities exist in other electrical equipment scenarios, namely: real-time thermal and strain monitoring in isophase buses and transformers, establishing temperature rise in feeder cables during a fault condition, and measuring tray cable temperatures. Strain and temperature in over-head transmission lines is another possible application for advanced sensing technology.

Although beneficial, the measurement of temperature and strain in electrical systems has some major constraints. The key constraint is that most transducers are electrically based. Therefore, the sensing devices are often incompatible with an electrical system environment. Furthermore, measurements need to be made at multiple points throughout an electrical system that is often many hundreds of meters in length and the spatial resolution of each measurement should be small (e.g., 0.1 meter or less)

To provide continuous, high-spatial resolution monitoring of temperature at many locations within a power system, the Contractor proposed to develop a high resolution distributed fiber optic temperature sensor (DFOTS) system. The key DFOTS advantage is the fact that one fiber can be used to obtain measurements at many points along its length. Further, optical fiber sensing does not perturb the electrical environment because of the nonmetallic nature of this sensing approach.

Overall measurement system goals are as follows:

- Temperature accuracy: ± 5°C
- Temperature range: 0 - 150°C
- Sensor length: ≥ 40 meters
- Length resolution: 0.1 meters.

Length resolution was a particularity stringent goal in that no other DFOTS method has even approached this resolution limit. The basic DFOTS technology was developed by the Contractor with support from EPRI and Con Edison(1). The first objective of the current project was to provide further demonstration of this high-resolution DFOTS system for specific motor and generator temperature measurement applications.

The need for strain monitoring in end-windings required that the Contractor develop a specialized fiber optic sensor that attaches to the end-winding structure. The overall specifications for this strain sensor are as follows:

- Strain resolution: ≤ ± 5 micro-strain
- Strain range: -500 to +500 micro-strain
- Gauge length: ≤ 1 cm
- Frequency response: 120 - 360 Hz
- System cost (8 sensors and readout): ≤ $30,000

The second objective of the current project was to develop a suitable fiber optic strain sensor and experimentally demonstrate that it met the above specifications.

In the text of this report, fiber optic temperature sensing is first discussed followed by strain sensing. In both cases, the recent literature is reviewed and any commercial devices are described. A description of sensor and read-out system architecture is provided and theoretical sensor models are discussed, where applicable. Further, calibration results are provided to demonstrate the performance properties of the two sensors and their read-out systems. In the case of the DFOTS system, field test data are also provided to demonstrate the temperature sensor and its associated measurement system can function in actual power plant environments.

2

BACKGROUND

In an earlier project (RP 2308-06), which ended in 1987, the Contractor confirmed the feasibility of a distributed fiber optic temperature sensor technique for measuring local temperature in electrical system applications. The basic sensing methodology depended on a unique fiber coating material (i.e., cladding) whose optical transmission loss increased with increasing temperature (see EPRI patent No. 5,052,820 dated October, 1991). Two types of coating materials showed promise; one material (a UV-curable acrylic) was compatible with high-volume production of sensing fiber. It was demonstrated that this special coating could be placed on a short length of fiber to obtain an indication of where a hot-spot existed.

Following this initial feasibility demonstration, the Contractor collaborated with Corning Glass Works to examine the problems of coating long lengths of optical fibers with the new temperature sensitive acrylic coating. Many meters of fiber were coated; however, beading occurred because of low coating viscosity. Therefore, no distributed temperature sensor data could be obtained. These previous efforts are discussed in EPRI Report EL-5568.

The current project (RP 2487-02) has been funded since 1988 and the current prototype sensor and read-out system was developed as a result of these project efforts. Several new, higher viscosity coating materials were examined and these materials were coated first onto borosilica glass (3M corporation) then on low-loss silica core material (Fiberguide Industries). Several kilometers of fiber were manufactured without beading problems. A description of the preferred material and early laboratory results, plus initial field demonstration data, are described in EPRI TR-101950 (i.e., reference [1] published in 1993). The cladding now contains scattering centers and functions differently than the initial sensing fiber. In the present case, the low-index cladding material changes its index of refraction with temperature so that more or less core-transmitted optical power is present in the cladding. Therefore, the backscattered light intensity, coupled back into the fiber core, changes with temperature. The fiber loss also changes, but the fiber actually becomes less lossy as temperature increases. This new temperature sensing fiber approach was patented by EPRI (US No. 5,191,206 dated March 2, 1993).

3

FIBER OPTIC SENSING IN ELECTRICAL POWER SYSTEMS

The Contractor adopted fiber optic sensing as the key technology for measurement of system parameters in the electric power industry. There are several advantages to this overall approach, namely:

1. Optical-based sensor does not perturb the electrical environment because it is non-conductive (sensor doesn't affect system)
2. Small sensor size and light weight
3. Rapid response to environmental changes
4. Major technology already developed for fiber optic communications industry.
5. Optical-based sensor output is not affected by EMI generated by electrical environment (system doesn't affect sensor)

Another advantage to fiber optic sensing is the availability of a "distributed sensing" strategy. In this case, the entire length of fiber senses a particular parameter (e.g., temperature). Using optical radar techniques, the distributed sensing methodology can be used to obtain local information at discrete, small intervals along the fiber length.

Distributed Fiber Optic Sensing

The approach employed for temperature measurement involved use of a distributed fiber-optic sensor, which is based on standard Optical Time Domain Reflectometry (OTDR) technology. The OTDR technology was initially developed by the telecommunications industry for the characterization of (e.g., fault location in) fiber-optic telephone systems. A light pulse transmitted by an optical fiber is gradually attenuated by a combination of absorption and Rayleigh scattering. Faults in the fiber produce points where rapid attenuation occurs. The scattered light returns in a direction opposite to the propagating light pulse (backscattered) as shown in Figure 3-1.

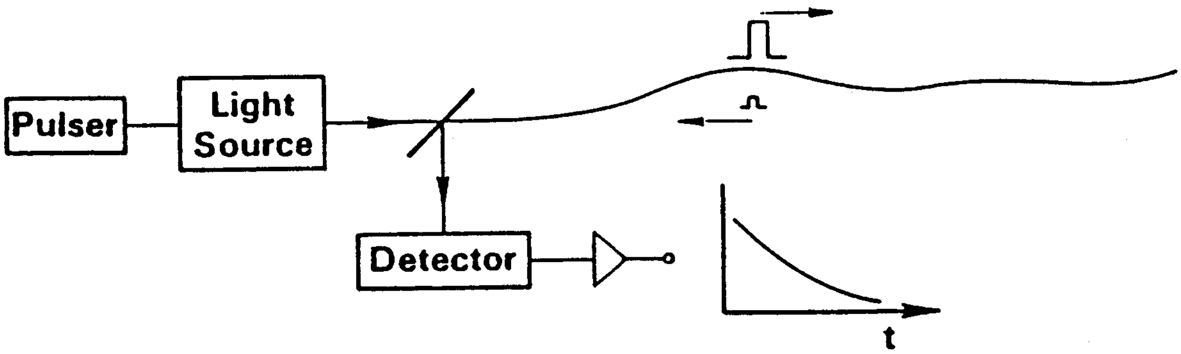

Figure 3-1
Block Diagram of Ranging in an Optical Fiber using the OTDR Approach

The signal characteristics of the backscattered light are such that the scattered light signal decreases exponentially over time (range). Therefore, the attenuation slope becomes linear when displayed on a logarithmic scale, as illustrated in Figure 3-2. This slope represents the local loss characteristic (dB/meter) of the optical fiber. If the slope is steep, the optical loss is large, whereas a gentle slope indicates that the loss characteristics of the optical fiber are good (i.e., low loss). A fault in the fiber is also indicated in Figure 3-2 by noting abrupt changes in the Rayleigh backscattered light.

The backscattering-based OTDR method permits attenuation and fault measurements of optical fibers without cutting the fibers and the measurement can be made from either end. Therefore, the method is simple and is useful in installation, processing, and maintenance of optical fiber communication systems. The distance of any particular change in an optical fiber transmission loss can be calculated by measuring the elapsed time of the returned pulse. If the time required to propagate back and forth is τ, then the location, L, of the change is given by

$$L = \frac{c\tau}{2n} \quad , \qquad (1)$$

where,

c = velocity of light in a vacuum (3×10^8 m/s), and
n = refractive index of the fiber ($n \approx 1.5$ for silica fibers).

Equation (1) indicates that light travels 1 meter out and back along a fiber in a total transit time of 10 nanoseconds (nsec).

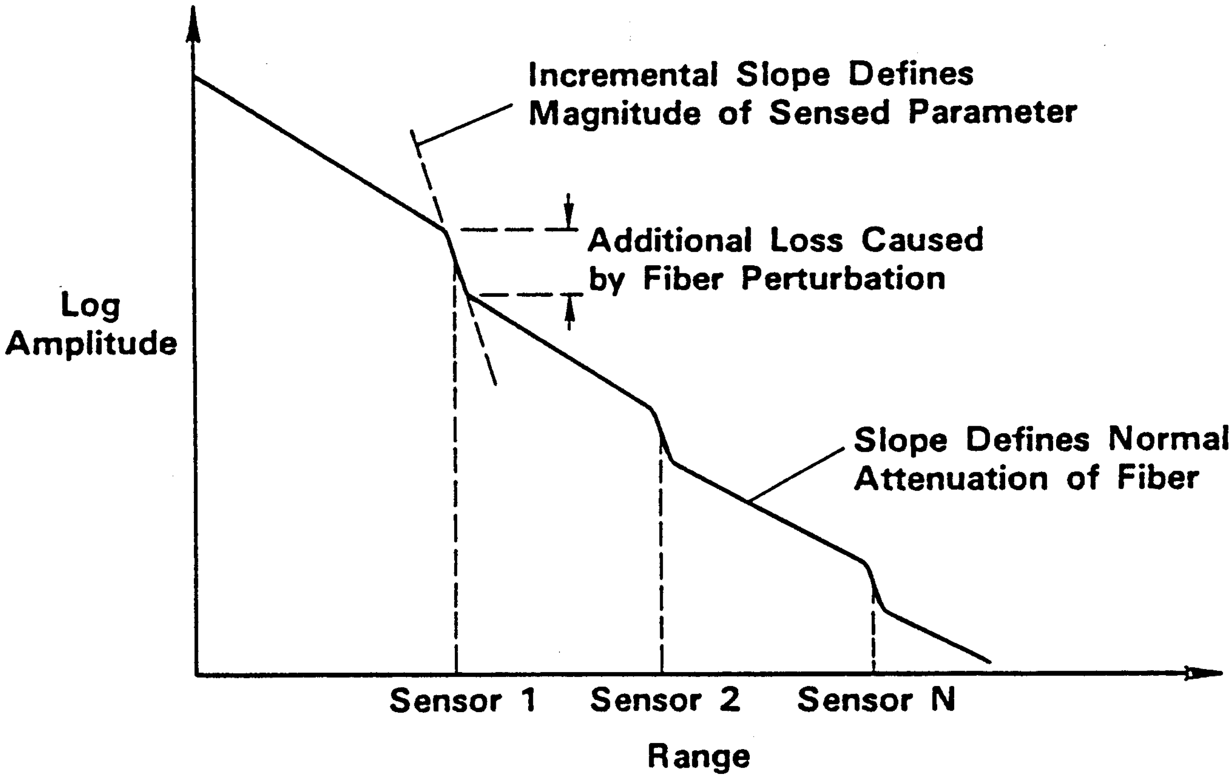

Figure 3-2
Typical Logarithmic Backscattering Signal Intensity versus Distance Measurement

To use the OTDR approach as the basis for a distributed fiber optic sensor, the fiber must be modified along its length. The modification causes a change in the loss and/or backscattering characteristics of the fiber when a particular parameter (e.g., temperature) changes. The change in some parameter is monitored by measuring the amount of change in the local backscattered light characteristics (local change in backscattered signal in Figure 3-2). Furthermore, the location (in time) of the OTDR signal change can be used to identify the location (in space) where the change in a given parameter occurred.

The most active area of distributed fiber optic sensing has been temperature measurement. In fact, several review articles on the subject appear in the literature [2,3]. In the current Distributed Fiber Optic Temperature Sensor DFOTS system, the Contractor used a special high-resolution OTDR instrument from Opto-Electronics, Inc. (Ontario, Canada). This OTDR (Model TDR30) uses multiple laser pulses that are orders of magnitude shorter than other instruments. A photo-counting-based detection system is used to provide 32 dB of dynamic range and a linearity of 0.08 dB/dB. The TDR30 provides selectable length resolution of 2, 8, and 30 cm. This high resolution is required for the DFOTS temperature measurement application to most electrical power systems.

Point Fiber Optic Sensing

In the current project effort, strain measurements are made using an approach called point fiber optic sensing. In most point sensing cases, the fiber is only a light transmitting device and does not take part in the sensing process. Figure 3-3 shows a typical fiber optic point sensor block diagram. Light from a source, remotely located at one end of the fiber, is transmitted to the transducer at the other end. Within the transducer, the light properties are modulated by the measurement parameter of interest. The light then returns to the remote readout device (usually using another fiber). At the readout, the modulated light signal is converted to an electrical signal and processed to display the parameter being measured at the *point* the transducer is located.

A special version of fiber optic point sensing, called a quasi-point approach, was used in the current project to measure strain in end-winding structures. The fiber itself is a distributed bending loss sensor that responds to pressure (force) along its entire length. The transducer used to convert strain into transverse force is, however, attached to the sensing fiber at only one point. The transducer could be moved to a different location along the fiber, but strain can only be measured at the point where the transducer is located. The special fiber is used to modulate the light, but the point transducer converts strain to force. As shown in Figure 3-3, the fiber optic point sensor provides a simpler instrument set-up than the distributed sensor variety, however, one transducer is required for each measurement location. The overall sensing system can be more complex because of the need to measure a given parameter at multiple points. Multi-point measurement requires multiple transducers, and usually multiple fibers. There are various ways to multiplex optical signals, so multiple source/readout devices will not likely be required. For end-winding strain monitoring, four transducers could be placed on four end-winding loops on the two ends of the machine. This multi-sensor system would mean that eight optical signals traveling in up to 16 fiber segments must be multiplexed to provide the strain measurements required for monitoring a given generator.

Another option for the pseudo point sensing approach, suggested herein, is to use the one distributed sensing fiber and a set of four or more transducers. These transducers are attached to the common fiber at various points along its length. In this case, the system measures a summation of strain from all the sensors attached to the one common bending-loss fiber. In the case of winding looseness monitoring, this integrated sensing approach may be sufficient since a large increase in summed strain would probably be sufficient for most generator monitoring applications. The various possible point-strain-sensing systems will be further discussed in more detail in Section 5.

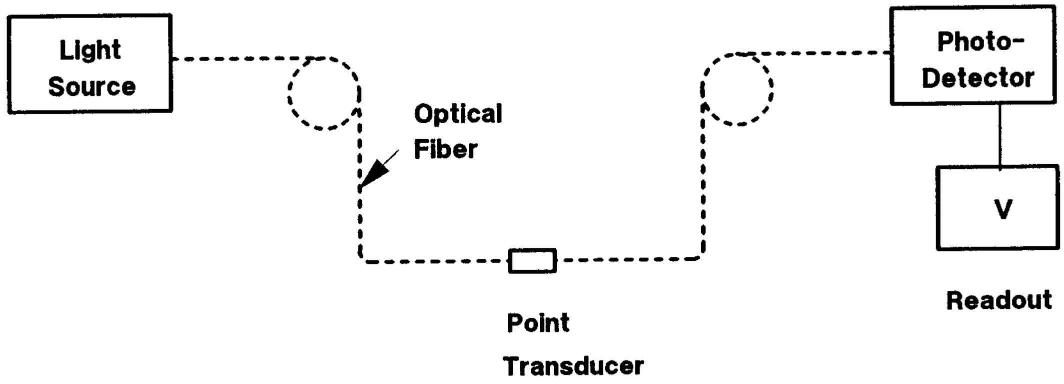

Figure 3-3
Block Diagram of Typical Fiber Optic Point Sensor System

4

TEMPERATURE MEASUREMENTS USING DFOTS APPROACH

The distributed fiber optic temperature sensor, DFOTS, system provides a method to monitor temperature at multiple points within an electrical power system. The approach uses Rayleigh backscattering from the fiber and an optical time domain reflectometer, OTDR, to provide the temperature data. Laboratory tests indicate that the DFOTS approach can measure temperature over a range from 0-150°C with an accuracy of ±5 % at 100°C. The sensor length is limited to approximately 100 meters, but spatial resolution is less than 0.1 meter. This is equivalent to having 1000 sensors that can be interrogated from one end of the fiber that is in contact with the electrical equipment of interest.

In this section, we discuss details of the DFOTS approach to temperature sensing. We first describe a theoretical model for the sensor. This model discussion serves to provide a theory on how the sensor works and also compares the Rayleigh backscattering approach to other distributed temperature sensing methods. Calibration methods and example calibration data are then provided for the two basic approaches to determine temperature from the backscattering signal. These calibration data also serve to confirm the theoretical model calculations. A new reference method is then discussed that simplifies data analysis procedures and we also describe other phenomena that can affect the temperature sensor's backscattering signal.

Methods of attaching the fiber sensor to electrical equipment and protecting it from damage are also discussed. We then provide a general description of the experimental set-up to obtain backscattering data from the fiber in a typical electrical system. We further describe specific modifications for use of the sensor in rotating machinery applications. Finally, data acquisition and analysis procedures are reviewed to provide the reader with the information necessary to use the equipment in a typical temperature measurement application.

Sensor Model Refinement

To use the OTDR approach as the basis for a distributed fiber optic sensor, the key is to modify an ordinary optical fiber along its length. This modification should result in a fiber where the local loss and/or backscattering characteristics are changed by changes in a particular parameter (e.g., temperature). By monitoring the amount of change in the local backscattered light characteristics using the OTDR methodology, temperature can be measured along the entire fiber length. Furthermore, the point (in time) of the maximum OTDR signal change can be used to identify location (in space) of the peak temperature.

The amount of backscattered light, $P_{bs}(\ell)$, from a given location l along the fiber, within the scattering element dx, can be written as

$$P_{bs}(\ell) \;=\; 1/2\;\; P_o\;\; \Delta t\;\; \upsilon_g\;\; C_s\;\; NA^2\;\; \exp\;(\textstyle\int_0^{\ell} -2\alpha\, dx)\quad , \tag{2}$$

where P_o is the launched power, Δt the source pulse width, and υ_g the pulse group velocity. The term NA in Equation (2) is the fiber's local numerical aperture (i.e., light capturing efficiency), which is dependent on the index of refraction of the core and clad materials. In (2), C_s and α are the scattering constant and the total loss coefficient, respectively. Equation (2) can be used to describe all distributed fiber optic temperature sensors. To use the backscattered light pulse intensity in a distributed temperature sensor, it is clear from (2) that α, C_s or NA must be dominant functions of temperature.

Based on the theory of Gloge[4], C_s and α can be approximated using the following:

$$C_s \;\; \cong (\alpha_R)_{co} \;+\; (\alpha_s)_{co} \;+\; P_c/P_t\;(\alpha_s)_{c\ell} \quad , \tag{3}$$

$$\alpha \;\; \cong \alpha_{co} \;+\; P_c/P_t\;(\alpha_{c\ell}) \quad . \tag{4}$$

In (3) and (4), α_R is the Raman scattering coefficient and α_s is the Rayleigh scattering coefficient. Subscripts co and $c\ell$ are associated with the core and cladding, respectively. The factor P_c/P_t is the fraction of propagating power that exists in the cladding due to evanescent wave effects. These equations reveal that there are many possible parameters which could be exploited to provide a distributed temperature sensor.

The first demonstration of a distributed fiber optic sensor used a special fiber having a liquid core[5]. In this case, increasing the fiber temperature causes an increase in the scattering coefficient of the liquid core, $(\alpha_s)_{co}$, by 0.02 dB/°C. Researchers at Southampton University[6] produced a distributed temperature sensor based on temperature-dependent attenuation of the core glass (i.e., $\alpha_{co} = \alpha_{co}(T)$).

The Raman effect originates from molecular and crystalline effects within the core glass. Initial Raman work, carried out by Plessey at the CEGB (UK), led to a practical Raman DFOTS device incorporating solid state components[5]. The Raman Stokes to anti-Stokes scattering intensity ratio was used to determine temperature along the sensor length independent of attenuation losses. York Technology measured the anti-Stokes backscattered light from the fiber and utilized a different referencing scheme to cancel attenuation effects[6]. Efforts have recently been made to lower the 7.5-m spatial resolution of the Raman DFOTS to 1 m using narrow pulsed laser sources[7]. However, Raman scattering produces such a weak signal that it will always have limited resolution capability. A key advantage to the system is that long lengths of ordinary communications grade fiber can be used as the distributed temperature sensor.

Clad Loss and Scattering Change Approach

The DFOTS approach, used by the Contractor, functions by temperature dependent changes in the fiber's clad scattering that dominate the backscattered light signal. These scattering changes are controlled by the amount of core transmitted light that is present in the cladding (due to the evanescent wave effect). Since this evanescent wave causes a small fraction of the guided light to reside in the cladding, a low-loss material is normally chosen to minimize overall fiber scattering and absorption losses. However, in the DFOTS fiber, scattering centers are purposely added to the cladding material to induce clad-dependent fiber loss and backscattering changes. The clad contribution to overall loss and backscattering is shown in (3) and (4) where P_c / P_t is the fraction of power traveling in the clad material. Based on the model for weakly guiding fibers[4], this fractional power can be estimated as:

$$P_c / P_t = 2\,\lambda / [3\pi a\,(2 n_{co}\,\Delta n(T))^{1/2}] \quad , \tag{5}$$

where

λ = wavelength of incident light source
a = radius of fiber core.

The index-difference term Δn(T) can be written as:

$$\Delta n(T) = n_{co} - n_{c\ell} \quad . \tag{6}$$

As the core or clad index changes with material temperature, this change alters the index-difference term Δn(T). More or less power will, therefore, be present in the cladding and more or less fiber transmission loss and backscattering change will occur.

A combined loss and scattering approach is used to describe changes in backscattered light intensity since both of these effects are present. For increasing temperatures it will be shown later that NA increases along the fiber are not important so equation (2) can be written:

$$P_{bs}(\ell,T) = C_o\;C_s(T)\;\exp\;-\left(\int_0^{\ell} 2\alpha(T)\,dx\right) \quad , \tag{7}$$

where C_o is a constant and $C_s(T)$ and $\alpha(T)$ are changes in the temperature-induced backscattering and attenuation coefficients, respectively. For the case where clad scattering effects dominate, these two coefficients are given by (3), (4), and (5) as:

$$C_s(T) = C_1(\alpha_s)_{c\ell} / [\Delta n(T)]^{1/2} \quad , \tag{8}$$

and

$$\alpha(T) = \alpha_{co} + C_2 \alpha_{c\ell} / [\Delta n(T)]^{1/2} \quad , \tag{9}$$

where C_1 and C_2 are constants. Assuming a constant core index, n_{co}, and a linear change in clad index, $n_{c\ell}$, with temperature, (6) becomes:

$$\Delta n(T) = \Delta n(25° C) + (dn_{c\ell} / dT)(T - 25) \quad , \tag{10}$$

where

$\Delta n(25°C)$ = constant index difference at 25°C

and

$dn_{c\ell} / dT$ = constant clad index temperature change.

In (8) and (9), the terms $(\alpha_s)_{c\ell}$, α_{co}, and $\alpha_{c\ell}$ are assumed to be constant. Therefore, the entire change in backscattered light intensity is controlled by the rate of change of the clad index ($dn_{c\ell} / dT$) with temperature. For most polymer materials $dn_{c\ell} / dT < 0$. Therefore, as temperature increases, the index of polymer materials usually decreases. From (10), $\Delta n(T)$ will, therefore, increase. Given this increase, (5) indicates that P_c / P_t will decrease (i.e., less light in clad) so C_s and α decrease. Further, the numerical aperture, NA, will increase with increasing temperature. This increased NA will not, however, change the backscattered light intensity. Given these facts, the OTDR's backscattered light intensity signal is predicted to initially decreases in a hot zone. Further, the slope of the backscattered light signal versus distance plot (i.e., the loss coefficient) also should decreases (hot fiber becomes less lossy). Following the hot zone, the local backscattered intensity and OTDR slope is predicted to return (increase) to values indicative of local conditions. There is no permanent intensity loss predicted across the hot zone. In fact, the signal should actually be greater after a hot zone than it would normally be if the hot zone was not present. This occurs because the lower loss coefficient in the hot zone causes less transmission loss through that zone. The fiber temperature profile is determined by measuring the change in backscattered light intensity along the fiber length and use of Equation (7).

Comparison of DFOTS to Other Distributed Temperature Sensing Approaches

Besides the clad-scattering-based DFOTS method used by the Contractor, the Raman approach turns out to be the only other practical method to accomplish distributed temperature sensing. The Raman method has the longest sensor length (1 to 2 km) and the highest accuracy (±1°C). However, because of the low backscattered intensity, the length resolution is approximately 3 m. The special Rayleigh clad-scattering method provides a medium sensor length (20 to 100 m), good accuracy (±5°C), and the best length resolution (≤10 cm). The clad-scattering method meets the length resolution requirements of most electrical power applications. On the other hand, the Raman approach would be most applicable to monitoring transmission lines.

Calibration Data

Figure 4-1 shows the typical OTDR backscattering signal obtained from both ends of a 40 meter long unheated (i.e., ambient temperature) sensing fiber. Note that after the typical reflection noise in the first five meters of the fiber, the back-scattered light signal is relatively smooth. The slope of the fiber signal in figure 4-1 indicates a sensing fiber two-way loss of 0.094 dB / meter for the particular fiber and ambient temperature associated with the particular test conditions. Also note the strong Fresnel reflection at the end of the fiber (i.e., at 40 meter position).

A sensing fiber is calibrated by placing a known length (e.g., 5 meters) of the fiber length into a standard oven using a random coil pattern. The sensing fiber is then heated to known temperature conditions from 20 to 100°C. A typical OTDR plot of the heated and unheated portions of a 30 meter sensing fiber is shown in Figure 4-2. Note that, as predicted by the theory, the back scattered intensity drops in the 5-meter heated zone by an amount dBs, which is a function of fiber temperature, T. Within the hot zone, the fiber loss coefficient (i.e., S(T) in Figure 4-2) also decreases. Following the hot zone, the loss value returns to its reference value, S(Tr) = - 0.080, where Tr is the reference (i.e., ambient) temperature of 23°C. Note also that the scattered light intensity also increases after the hot zone as the theory predicts. In fact, due to the reduced loss in the hot zone, the scattered light intensity is initially greater after the hot zone than it was just prior to the heated portion of fiber.

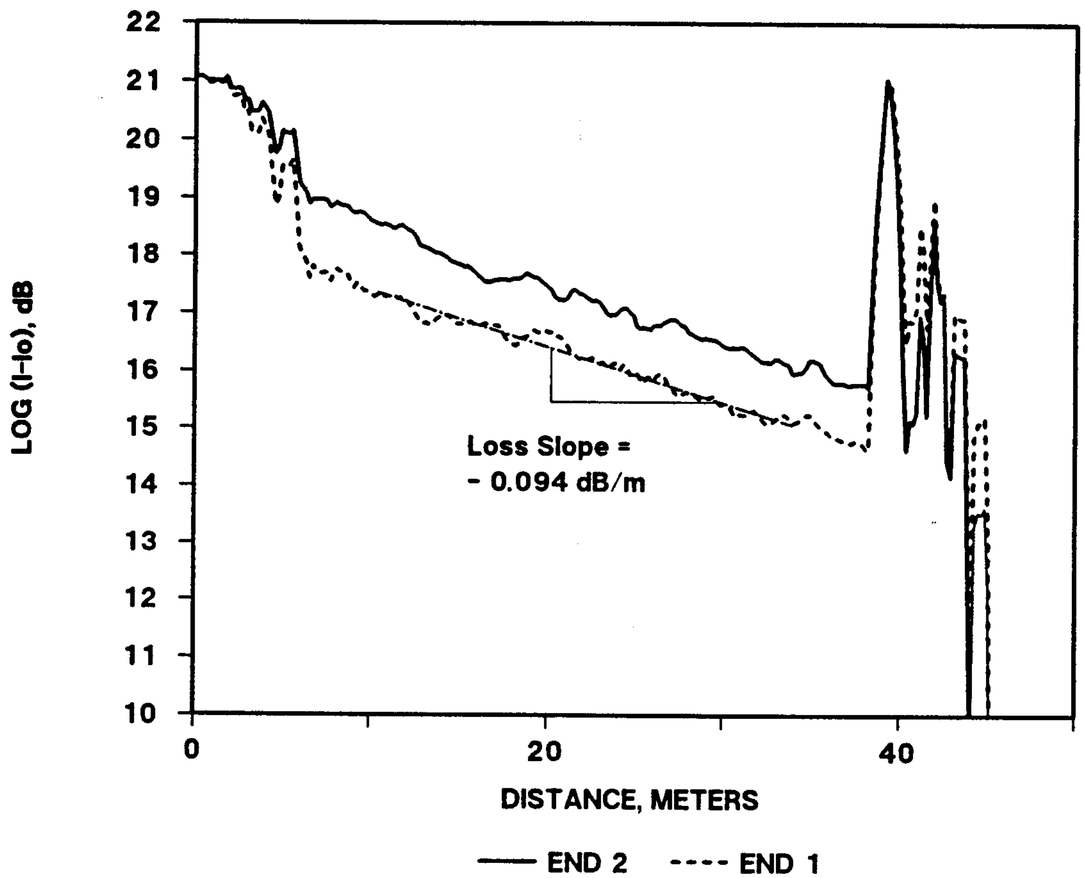

Figure 4-1
OTDR Plot of 40 m Sensing Fiber Prior to Installation (Ambient Conditions)

As predicted by the above model, both the fiber loss slope, S(T), and the scattering intensity change, dBs(T), are functions of temperature, T, so recording of these values, as a function of temperature, constitutes a calibration of the sensing fiber. Using these calibration data, unknown temperatures can be determined along the fiber length. The reader should consult EPRI TR-101950 (March 1993) for further details concerning how the sensing fiber responds to temperature variations along its length. Based on results in this report, one can write:

$$T/Tr = S(Tr)/S(T) \quad , \tag{11}$$

where T and Tr are measured and reference temperature respectively, and S(T) and S(Tr) are the slopes of the OTDR plot for both reference and measured temperature conditions. Therefore, by measuring the slope S(T) along the fiber length, temperature can be calculated from Equation (11), given the reference temperature and reference condition slope (Tr = 23°C, S(Tr) = - 0.080).

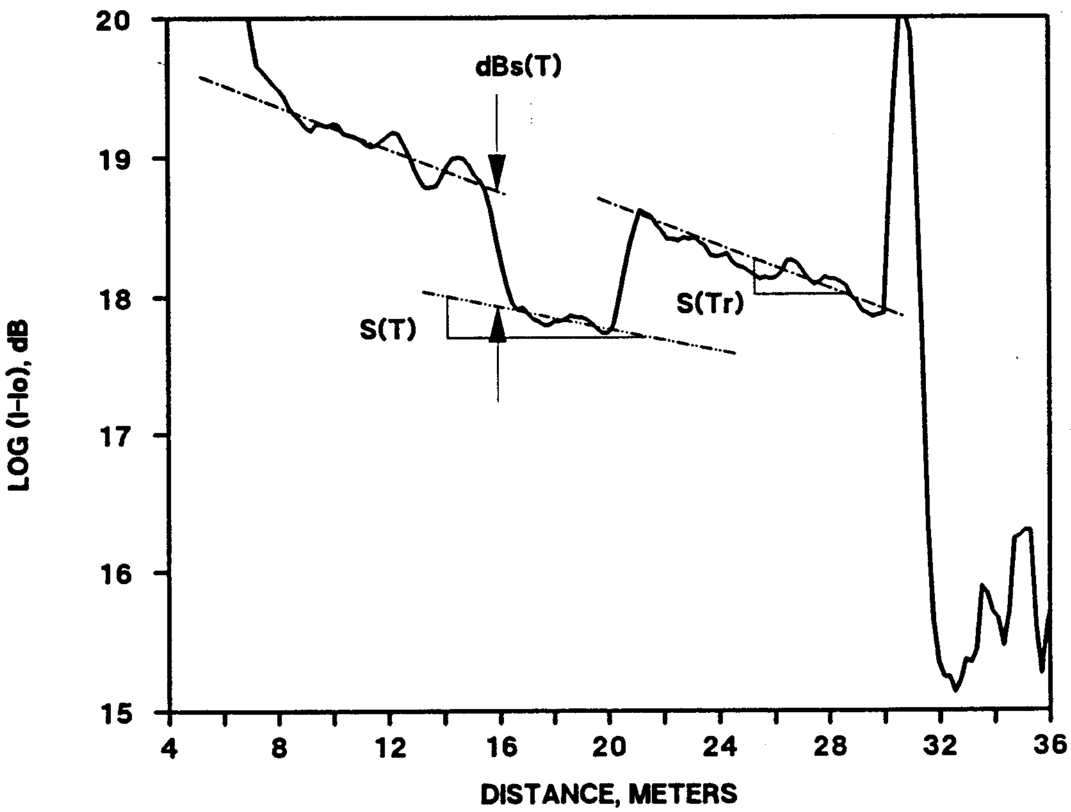

Figure 4-2
OTDR Plot of Sensing Fiber with 5 m Hot Zone Located at 16 Meters from Fiber End 2

Figure 4-3 shows results of the OTDR slope calibration for several types of sensing fibers. Note in Figure 4-3 that the measured slope ratio is linearly proportional to the temperature ratio as described in Equation (11). The theoretical line, using Equation (11), is also shown in this figure for comparison purposes. Note also in Figure 4-3, that the measurement error increases with temperature. This error increase occurs because the change in slope diminishes as temperature increases so the "slope-method" of DFOTS temperature measurement is not as sensitive to temperature changes above approximately 60°C.

Figure 4-4 shows results of the calibration for the backscattering change, dBs, which changes with temperature as shown in Figure 4-2. Also shown in this figure is a curve fit to the data. This curve fit indicates that:

$$dBs = A \ \mathrm{Ln}(T) + B \quad . \tag{12}$$

Given the data in Figure 4-4, the coefficients A and B were calculated and their values are as follows:

$$A = -0.96, \ B = 3.07 \quad . \tag{13}$$

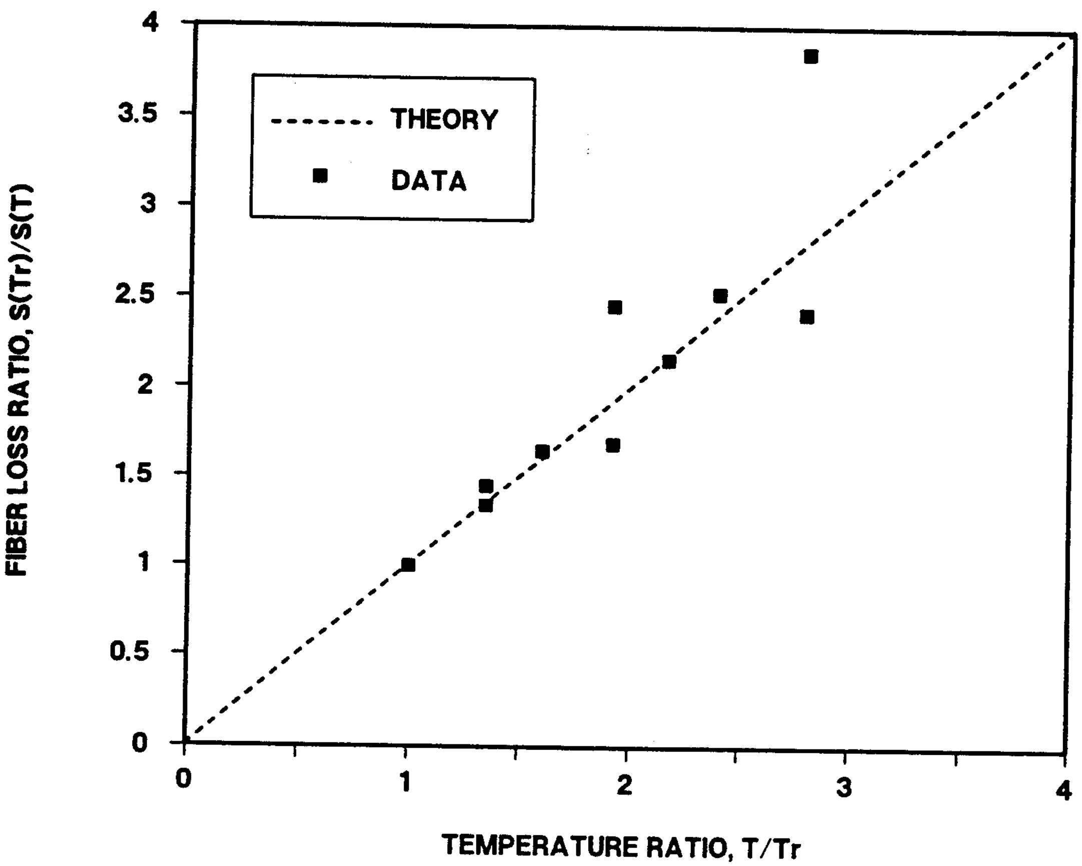

Figure 4-3
Calibration Results for Loss-Slope Method of DFOTS Temperature Measurement

Therefore, the calibration result, represented by Equation (12) and the constants given in Equation (13), can also be used to calculate temperature from the dBs data obtained along the fiber length. This second DFOTS temperature measuring technique could be called the "dBs-method" and either it or the above slope-method (or both) could be used to determine temperature along the fiber length.

Approaches used to Determine Temperature from Backscattering Signal

The calibration data in Figures 4-3 and 4-4 indicate that there are two general methods of determining temperature distribution along the fiber from the backscattering intensity profile measured by the OTDR, namely:

1. Loss-slope method involving measurement of the local slope (S) of the OTDR signal

2. Backscattering change (dBs) method involving changes in the OTDR signal intensity

These two approaches are discussed below.

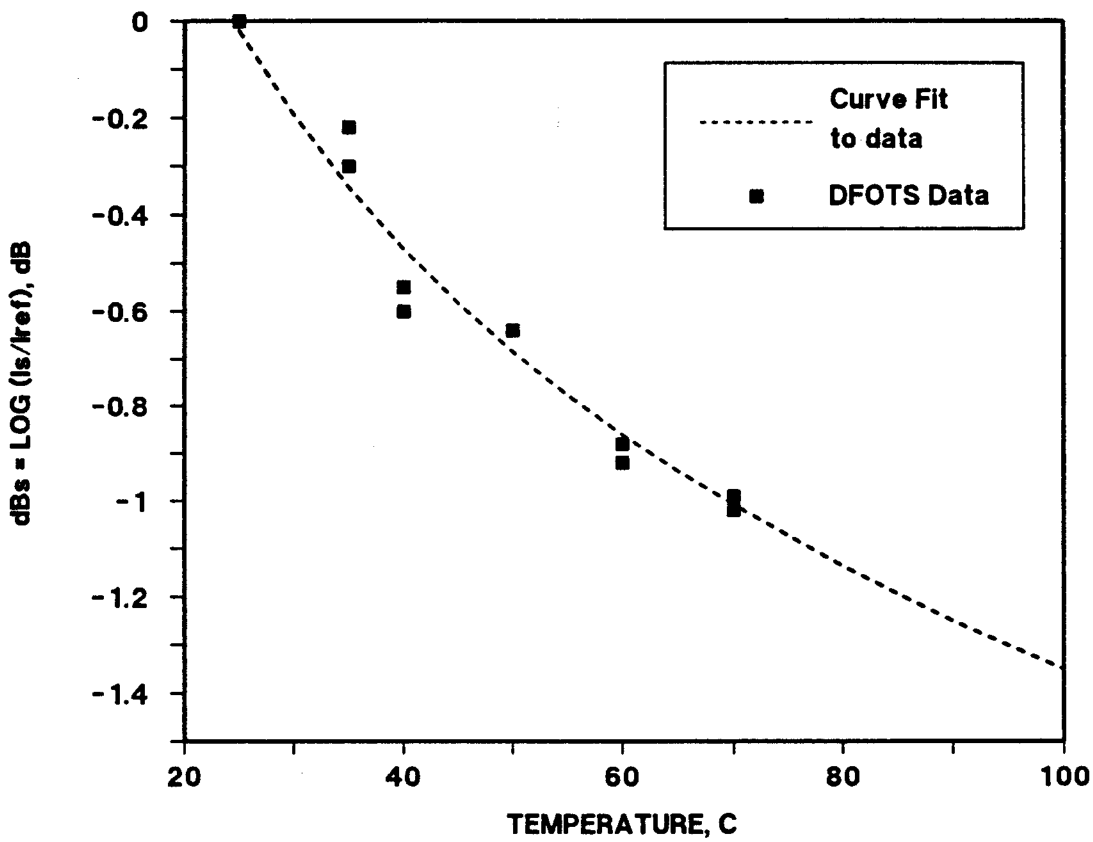

Figure 4-4
Calibration Results for OTDR Output Change (dBs-Method) of DFOTS Temperature Measurement

Loss-slope Approach to DFOTS Temperature Determination

The theoretical calculation in Equation (11) and data in Figure 4-3 indicate that temperature can be determined from a measurement of the local loss slope, S, where S is the local fiber loss per unit length. The loss slope is usually given in dB per meter and is determined from a linear regression analysis of the OTDR signal results using the log of backscattering intensity versus distance plot (see Figure 4-2). Rearranging Equation (11), the following formula is obtained:

$$T = Tr\,[S(Tr)/S(T)] \quad . \tag{14}$$

This equation indicates that measuring the loss slope, S(T), at the unknown temperature, T, can be used to calculate the unknown temperature provided the slope S(Tr) is also measured at some known reference temperature, Tr.

The key advantage to this approach is that discontinuities in the backscattering signal versus distance plot do not affect the temperature calculation. These discontinuities may be caused by local fiber effects such as an inadvertent sharp bends in the fiber resulting from installation in an electrical system. The major disadvantage with this "loss-slope" approach is that it takes signal from several meters of fiber to obtain an accurate loss slope value. This accuracy problem exists even for a high-resolution OTDR where intensity information is available every 0.1 meter. Noise on the OTDR signal requires that multiple intensity points be used, in a constant temperature zone, to accurately calculate the loss slope value. Therefore, the loss-slope method is most accurate when temperature changes are gradual. For example, measuring the temperature of hot spots along the fiber would be difficult for the loss-slope method because of large dBs changes that accompany large temperature changes (see Figure 4-2) and the difficulty of determining the slope value if the temperature rise occurs in a small length of fiber.

Another disadvantage with the loss-slope method is the fact that the slope does not change much at high temperatures (i.e., temperatures above 60°C). In fact, Equation (11) indicates that S(T) is proportional to T^{-1}. The change in S(T) with temperature (dS / dT) is proportional to T^{-2}, so this change is small at high temperatures. In summary, the loss slope method is usable when the temperature is less than 60°C and there are no hot spots (temperature nearly uniform in the region of interest).

Scattering Change (dBs) Method of DFOTS Temperature Measurement

Curve-fit data in Equations (12) and (13) plus results plotted in Figure 4-4 indicate that changes in the backscattering intensity (i.e., dBs values) can also be used to measure temperature variations along the fiber length. These intensity changes, within the heated fiber region, are obvious from the OTDR plot shown in Figure 4-2. In this case, the temperature can be calculated from a measurement of dBs along the fiber and use of the curve fit results shown in Figure 4-4. By rearranging Equation (12) we obtain:

$$T = \exp\ [(dBs - B)/A)] \quad . \tag{15}$$

Where A and B are the curve fit constants and dBs values are the measured intensity changes. The constants A and B can be approximated by solving for A and B using measured values of dBs obtained at temperatures T and Tr. The following equations are used to provide approximate values for A and B:

$$A = -dBs(T)/(\mathrm{Ln}(Tr) - \mathrm{Ln}(T)) \quad , \tag{16}$$

$$B = -ALn(Tr) \quad . \tag{17}$$

Equation (15) indicates a measurement of dBs can be used to determine temperature along the fiber provided that calibration data are available to determine the curve-fit constants A and B.

Figure 4-4 and Reference [1] show that the value of dBs is based on a scattering intensity difference (in dB) between the heated and unheated fiber, namely:

$$dBs = 10 \log ((I - Io) / (Ir - Io)) \quad , \tag{18}$$

where,

Io = Background intensity (noise level of OTDR)
I = Scattering intensity at unknown temperature, T
Ir = Scattering intensity at reference temperature, Tr

Therefore, dBs values along the fiber are measured by obtaining the OTDR data at the unknown and reference conditions. Besides providing dBs values along the fiber length for temperature calculation using Equation (18), this referencing approach is useful for removing some reflection noise in the OTDR intensity data.

A key advantage to the dBs approach for DFOTS temperature determination is that hot spots along the fiber can be measured without any of the problems noted above for the slope method. In fact, the dBs approach is ideally suited for measuring hot spots in an otherwise low to moderate temperature background. Hot spots smaller than 10 cm in length have been measured accurately with the DFOTS approach using the 2 cm OTDR resolution capability. There are also some disadvantages to using the dBs approach, namely:

1. Temperature-induced changes in loss slope along the fiber can complicate the data reduction process for complex temperature profile conditions, and

2. Regions of fiber damage (bending loss points) can corrupt the dBs measurements.

The first disadvantage is related to the fact that both loss-slope and dBs variations occur simultaneously for complex temperature profile conditions. This combined action is shown graphically in Figure 4-5 where dBs = Log (Signal / Reference) measurements are plotted as a function of distance along a heated fiber sensor. The data in Figure 4-5 are for the case of a 100°C, 1-meter wide hot spot near the middle of a 50°C, 7-meter wide hot zone. Note that the dBs value at approximately 6 and 13 meters changes by -0.7 then+0.7dB. This change occurs at the beginning and end of the hot zone and dBs value corresponds to the 50°C condition (see calibration plot in Figure 4-4). Note also that at 9.5 meters the hot spot results in an abrupt dBs spike that indicates an additional 0.6 dBs change. When the 0.6 dB is added to the 0.7 dB initial change, it results in an overall change of -1.3 dB. Note in Figure 4-4 that this corresponds to the 100°C condition.

Although the above observations can be made about the dBs profile in Figure 4-5, it is not obvious how to convert this dBs data into the desired temperature profile measurement. In effect, the loss-slope variations, due to the hot zone, tend to confuse matters and complicate the data reduction process. Only an iterative procedure can deconvolute the dBs data. This iterative process would involve assuming a temperature profile, then calculating the dBs profile and comparing it to the measured profile. Some type of residual error method could be used to determine that the iteration process was successful. Perhaps the loss-slope method could be used to provide a starting point (i.e., initial temperature distribution) for the iteration algorithm.

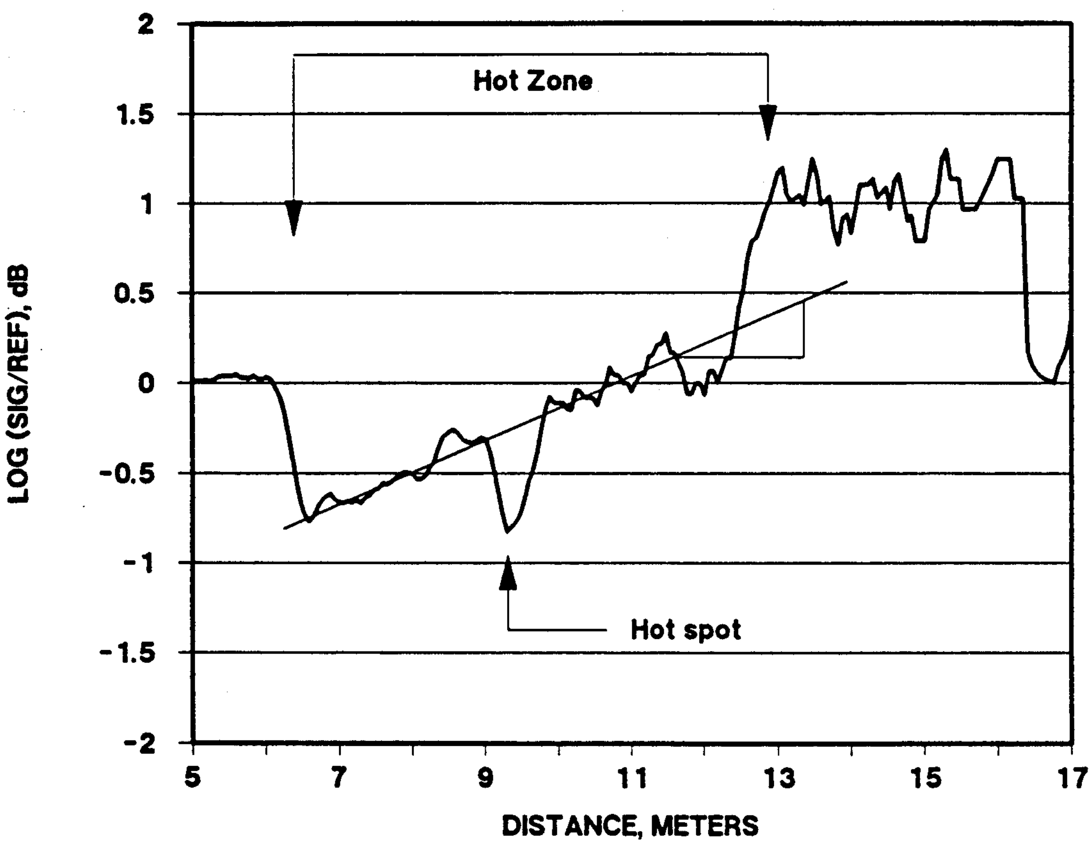

Figure 4-5
dBs Data for Hot Spot (100°C) in a Hot Zone (50°C) Using Ambient Temperature Referencing Approach

The second disadvantage, listed above, relates to the problem of damage to the fiber during installation. This damage results in abrupt decreases in the OTDR signal and these changes can be confused with intensity changes caused by increased temperature. This is a more serious disadvantage than the first because it can corrupt the dBs data and prevent temperature from being determined from the dBs measurements. Before the damaged area, accurate results are possible, however, beyond the damage zone the results are suspect. Absolute temperature measurements beyond the damage point are especially prone to error, but relative temperature changes may still be determined. A complicating factor is the case where the damage is due to a sharp bend in the fiber caused by rough handling or improper installation. A light loss occurs at this sharp bend, but this loss is not constant. As the temperature increases, the bend tends to transmit more light due to an increased fiber numerical aperture (NA in Equation (2)) at elevated temperatures. This change in light loss across a damaged area confounds the problem of determining an accurate temperature distribution beyond the damage point.

Comparison of DFOTS Measurement Methods

The dBs and loss-slope methods both can be used to determine an unknown temperature profile along the fiber sensor given a measured OTDR backscattering signal at known and unknown conditions. The loss-slope method is more suited to heated zones spanning a large spatial area where the temperature varies gradually (no hot spots). It is the only method that can be used in cases where fiber damage corrupts the dBs data. The dBs method is best suited for measuring hot spots that occur along an undamaged sensing fiber. For complex temperature scenarios (i.e., hot spots in hot zones), the dBs approach must be used, but deconvoluting the data can be time consuming. In the next section, a new referencing approach is introduced that attempts to simplify the process of using the dBs approach to provide a straight-forward method of extracting complex temperature distribution information from the dBs data.

New Reference Method

The referencing approach, discussed above, uses OTDR data collected at reference (usually the ambient) and unknown temperature conditions to calculate the changes in backscattering signal, dBs, caused by fiber temperature changes. This approach is valid, however, the resulting dBs data plot is not easily converted to temperature information (stated in the above discussion of disadvantages to the dBs temperature-measurement methodology). A different approach was required that simplified the dBs calculation by removing the effect of loss-slope variations with temperature. The new referencing method is described in this section of the report.

To remove the effect of loss-slope variations, OTDR data are obtained from both ends of the sensing fiber. The standard one-ended OTDR signal is called the forward signal (If). This standard OTDR data is collected first and stored in memory. The OTDR signal is then obtained from the opposite end of the sensing fiber and also stored. This backward intensity measurement is called (Ib). The backward signal is then mathematically inverted to obtain Ib(inv). The inversion process involves the following:

1. The last backward OTDR intensity value Ib(L), collected at the end of the fiber, is used as the first inverted value, $Ib(inv)_0 = Ib(L)$.

2. The next to last Iv value, Ib(L-δ), where δ is the distance along the fiber between OTDR data points, is used as the second inverted value, therefore, $Ib(inv)_1 = Ib(L-\delta)$.

3. The third from last backward OTDR intensity Ib(L-2δ) is used to obtain the second inverted value, $Ib(inv)_2 = Ib(L-2\delta)$.

4. This process continues along the fiber to generate the inverted array $Ib(inv)_i$ of intensity values.

Once the inversion is complete, the new dBs is calculated using the following:

$$dBs_i = [If_i + Ib(inv)_i]/2 \quad , \tag{19}$$

where

i = 0, 1, ... N (number of OTDR data points along the fiber length).

The new referencing process can be seen graphically in Figures 4-6 through 4-8. Results in these figures were calculated using a spreadsheet program based on the model outlined above. In these figures, we used fiber sensor calibration values as follows: A = -1.66 and B = 5.34. These values are somewhat different than the ones for data shown in Figure 4-4 (see Equation (13)).

Figure 4-6 (a) is the assumed temperature profile (i.e., 100°C hot spot in a 50°C hot zone). In Figure 4-6 (b) the calculated dBs profile is shown based on the old referencing method. Note the similarity in the theory shown in 4-6 (b) with fiber sensor data in Figure 4-5. Note also the difficulty in deconvoluting this data to determine the temperature profile. Figure 4-7 (a) shows the calculated OTDR signals obtained from both ends of the fiber, given the assumed temperature distribution in Figure 4-6 (a). Figure 4-7 (b) shows the calculated forward and backward inverse intensity distributions. Finally, Figure 4-8 (b) shows the results of using Equation (19) to calculate dBs using the new referencing approach. In Figure 4-8 (a) the assumed temperature distribution is replotted. Note in Figure 4-8 how much easier it is to deconvolute the new dBs values to obtain the temperature distribution. In fact, one can perform the deconvolution using the following equation:

$$T = \exp\left[-(dBs - 5.34)/1.66\right] \quad . \tag{20}$$

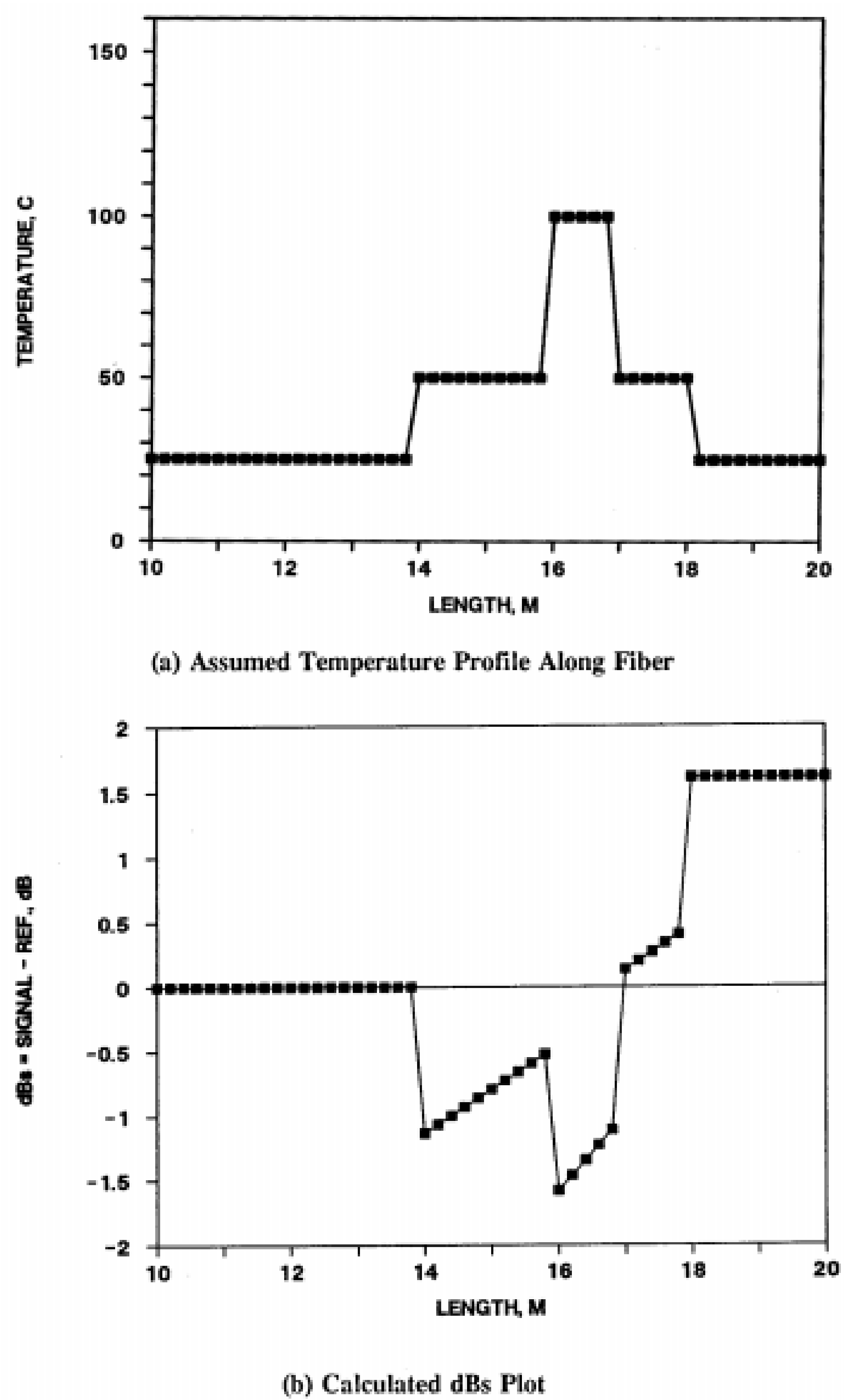

Figure 4-6
dBs Calculations based on Old (Ambient Temperature) Referencing Approach

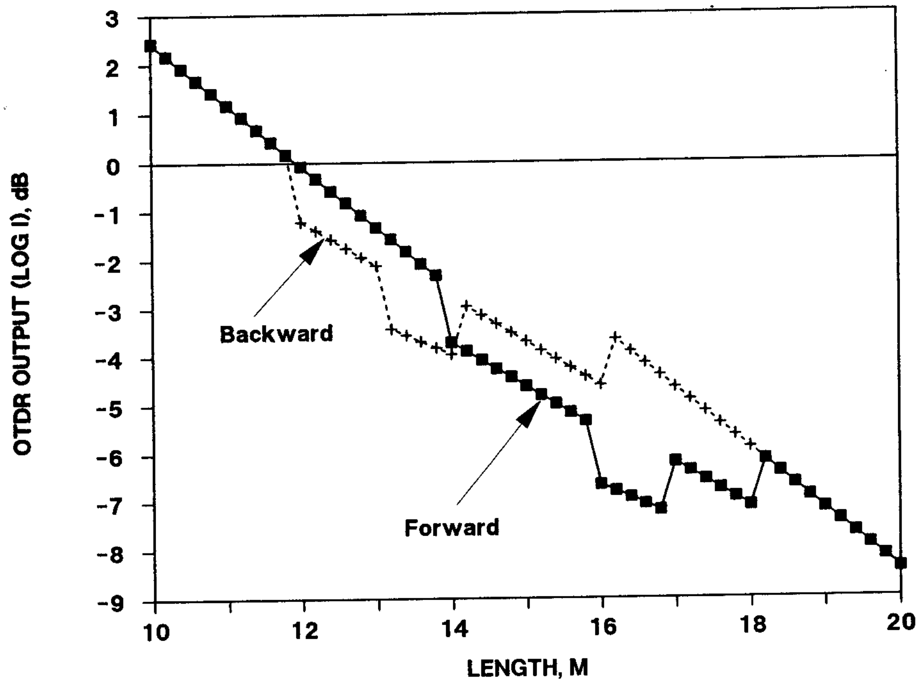

(a) Calculated OTDR Plots for Both Ends of Fiber

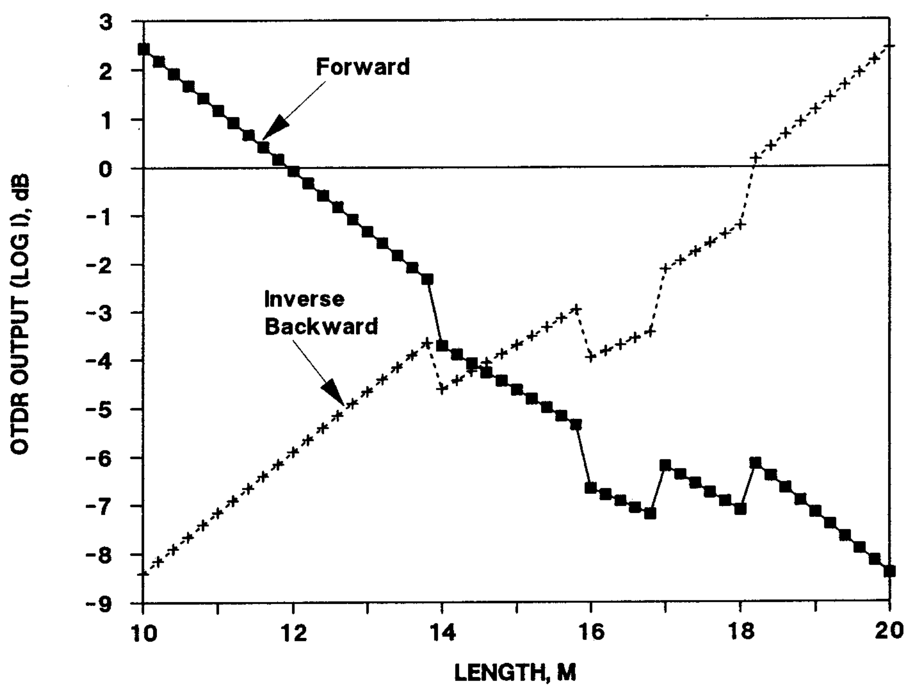

(b) Calculated Profiles used in New Referencing Approach

Figure 4-7
Intensity Profiles Calculated for Assumed Temperature Distribution

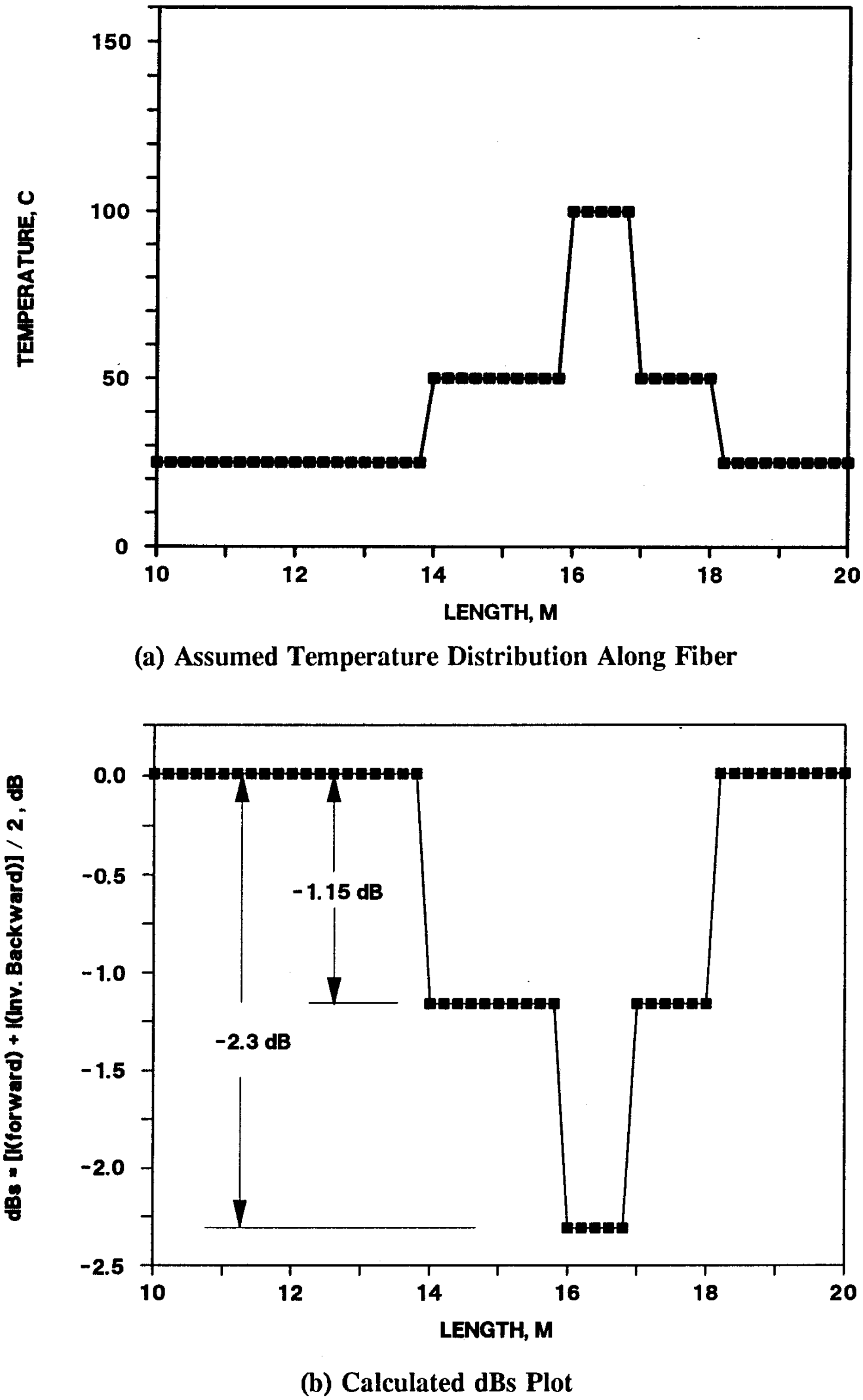

Figure 4-8
dBs Calculations Based on New Referencing Approach

In summary, the new referencing approach eliminates the main disadvantages of the dBs approach to DFOTS temperature measurement by eliminating the loss-slope change effect. The added complexity of taking data from both ends of the fiber is offset by the simplicity of data reduction (conversion of OTDR results to a measured temperature distribution). Another advantage to the new referencing approach is that no sensor data need be obtained at ambient temperature prior to a test. The only ambient temperature results that need to be obtained are during the sensor calibration process. In a field application, one only needs to take OTDR data from both ends of the fiber regardless of the previous temperature conditions.

Other Effects on Sensor Response

Temperature changes produce the major effect on the backscattered light signal from a DFOTS fiber, however, other parameters can also have a secondary effect, namely:

1. Fiber bending losses resulting from sharp bends and / or damage to the fiber at one or more points along its length, and

2. Force or pressure that is distributed over a length of fiber. This force per unit length causes a series of small bends (i.e., distributed bending loss effect).

Both these effects result in a decrease in the backscattered light intensity. These loss effects are discussed below.

Point Bending Loss

A protective tefzel™ (teflon™-based material) jacket surrounds the fiber to increase its ruggedness. This jacket material has an outer diameter of 0.5 mm. The fiber must be handled with care, however, to prevent point bending losses. These losses occur when the fiber is subjected to a sharp bend at one or more points along its length. A sharp bend results in a decrease in backscattered intensity that occurs over a short length and it is fairly easy to detect these point bending losses in the OTDR signal. Sharp bends can also increase reflection noise in the measured scattering intensity. The origin of these point losses is normally associated with fiber installation although rough handling of the fiber can also cause sharp bends to occur.

The fiber should not be bent beyond a minimum radius of approximately 2 cm at any time. If the fiber is installed in a serpentine fashion within an electrical system structure, then care must be taken to observe this minimum bend radius rule. Care must also be taken when the fiber is attached to a structure. The free fiber must be handled carefully or a sharp bend can be induced at the attachment point. Further, the fiber is especially vulnerable at points where it enters or exits the electrical system.

Some type of strain relief should be used to insure that the weight of the fiber itself or handling of a loop of fiber will not induce a sharp bend at these points.

The data acquisition / analysis process can sometimes canceled point bending loss effects if they are not too severe and if they don't occur in the wrong place along the fiber length. A key problem, however, arises because the loss is not constant. As temperature increases, the fiber NA increases (see equation 10). The fiber becomes a better light guide with increasing NA, so a bend will have less of an effect on light propagation in a heated fiber. The new referencing approach must be use to cancel this temperature-dependent point-bend-loss effect because the loss at elevated temperature is different than at ambient temperature.

No referencing approach will work, however, if the point loss occurs at the wrong position along the fiber. For example, if the point loss occurs too near the beginning or end of a fiber, then it will appear as a connector loss. It takes approximately 10 meters of fiber for entry noise to subside to the point where light scattering can be observed. If damage occurs within this 10-meter dead zone, and temperature changes occur within this region, no data can be gathered to allow the referencing approaches to work. In other words, light scattering data must be available on both sides of a point loss and be available from the signals obtained using both ends of the fiber to cancel the temperature-dependent point loss effect.

Distributed Bending Loss

Distributed bending loss occurs when force or pressure is applied to a fiber over an extended region of fiber length and is noted as a distinct increase in the OTDR loss-slope. The force does not cause a single sharp bend, but rather a series of small bends over the region where that force is applied. The force can come from a physical origin or be induced in other ways. A typical method of inducing a distributed bending loss is to attach the silicone-jacketed fiber to a structure using an epoxy that is hard when it dries. Epoxy contraction during the drying process can squeeze the silicone-jacketed fiber and cause distributed bending loss effects.

Another cause of distributed bending loss is even more subtle. During fiber installation, the fiber is sometimes placed in a series of loops or serpentine bends over a long length of fiber. These bends can be periodic or a periodic and can extend over the entire temperature measurement region. Experience shows that the installation geometry (pattern of bends and associated bending loss effects) can alter the way the sensing fiber responds to temperature changes within the installed fiber region. For this reason, it is wise to calibrate the fiber sensor using the approximate geometry to be used during installation.

For reasons outlined above, distributed bending loss can have a profound effect on the accuracy of the DFOTS technology especially if the loss-slope method is used to measure fiber temperature. For the dBs method, theory indicates that the new referencing approach can cancel this effect because it is a loss-slope type of phenomenon. It is still prudent, however, to calibrate the sensor using a fiber geometry and attachment procedure (epoxy, ...etc) similar to the actual measurement scenario.

Sensing Fiber Protection and Placement

Placement and protection of the fiber sensor are important considerations in applying this technology to operating power plant equipment. These aspects of the DFOTS sensing approach are discussed in this section of the report.

Fiber Placement

An optical fiber sensor can be placed along the surface of the electrical conductor to determine surface temperature or imbedded within the conductor to monitor internal temperature conditions. For the motor/generator winding application, Ontario Hydro suggested placing the fiber under the slot wedge and/or on the surface of the wedges within the slotted region. This placement would be particularly suitable for retrofit applications. Westinghouse also suggested placing the sensing fiber within the winding itself to obtain better thermal contact and to measure internal winding temperature. This second placement scenario is best suited for new windings since the sensor is placed inside the high-voltage (and thermal) insulation in direct contact with the conductors.

It is likely that the surface-attachment option will be chosen as the primary method for most fiber placements since retrofit is a larger part of the current electrical system sensing need. When placing the sensor is a surface location, several precautions must be taken, namely:

1. The fiber must be securely fastened to the conductor surface to prevent it from coming loose during operation. This is especially important for rotating machinery involving windage effects. Some type of flexible epoxy should be used to fasten the fiber in place at an appropriate number of points along the conductor.

2. The fiber should be attached so that it measures conductor temperature not the temperature of the surrounding air. Placing the fiber in good physical contact and insulating the side facing away from the surface can minimize any errors caused by this thermal conduction-based effect.

3. The fiber should be made electrically uniform by coating it with an appropriate dielectric paint to avoid variations in dielectric properties within the electrical environment.

Taking note of these attachment precautions will assure accurate and safe temperature monitoring using the DFOTS fiber in an electrical system.

Fiber Protection

As stated above, the fiber can be damaged during installation and handling, so some type of protection may be required. Protection is provided in the following fiber areas:

1. The fiber itself (along its length),
2. The optical connectors at the ends of the fiber, and
3. At places where the fiber enters and exits the electrical equipment (interface regions).

To further protect the fiber, an additional jacket was often added. One type of added protective jacket is called a bifurcation tube. This special tube has an outer sheath and a hollow inner tube that contains a loose piece of string. The sensing fiber can be attached to the string and "pulled" through the bifurcation tube. Placing some dry powder on the fiber can assist in the pulling process. Using the powder-assisted pulling technique, the Contractor routinely pulled 40 meter lengths of sensing fiber through a standard 1.04 mm I.D. inside tube. The bifurcation tube we currently use is made of a high-temperature material called hytrel™ (O.D. = 3 mm). This material can operate continuously at 150°C. Further, the current tube's walls are protected from physical abuse by adding an inner kevlar™ sheath as a strength member.

Optical connectors are placed on each end of the fiber / bifurcation tube to provide for a rugged connectorization. Communications-grade ST connectors are used by the Contractor to match the connectors on the OTDR. These connectors are crimped to the outer hytrel material using standard commercial fiber-connector attachment practices. Connector ferrule attachment to the fiber itself is, however, a customized procedure because of the soft silicone-based cladding. Basically, almost any attempt to remove the tefzel™ jacket, also removes the 140 μm cladding and leaves only the 100 μm core material.

To provide fiber / connector attachment, the 100 μm diameter sensing fiber is placed in a standard 125 μm diameter connector ferrule after stripping away the cladding. A low-index silicone adhesive is used to hold the fiber in place. Approximately 1 cm of fiber protrudes from the ferrule end-face after installation. The low index material essentially substitutes for the cladding in the bare-core region. The fiber can't be polished because of the soft silicone adhesive, therefore, it is cleaved as close as possible to the ferrule end-face after the adhesive cures. With practice, connector losses of 2 dB were achieved.

The final fiber protection approach involved strain relief at interface points where the fiber enters / exits the piece of electrical equipment. Several strain relief methods were used, namely:

1. Use of a bushing that allows to connectors to mate. The sensing fiber is kept inside the equipment, while a standard commercial fiber (with commercial strain-relief device) is outside the equipment.

2. Placement of a strain-relief device on the sensing fiber outer jacket. A rubber boot is one such device that prevents sharp bends from being induced in the fiber at the transition points.

Using all the above protective methods, the fiber damage could be minimized and even eliminated during installation and use in a power plant environment.

General Experimental Set-up and Data Acquisition Process

The general experimental set-up, used to obtain DFOTS data, is described in this section. This set-up consisted of the sensing fiber, a high-resolution OTDR (Opto-electronics Inc. TDR20) and a portable computer (Compaq Corp.). A block diagram of the system set-up is shown in Figure 4-9. A 1 X 2 fiber optic switch (latch-type from DiCon Fiberoptics Inc.) was used to provide simple access to either end of the sensing fiber using a simple control box. An electrical switch, battery, and push-button activation mechanism were located in the fiber optic switch control box. The single input fiber from the switch was connected to the OTDR while the two outputs from the switch were connected to both ends of the sensing fiber. Standard ST type fiber optic connectors (C in Figure 4-9) and bushings were used to connect the switch to the various system components.

In the current system, the data acquisition procedure was semi-automated. A Lotus 1-2-3 program called Lotus-measure was used to acquire OTDR data automatically by initiating a test using the computer key board. The OTDR and computer communicated using a standard (commercially available) RS232 interface board. Upon receiving the key-board command, the OTDR was activated and data was acquired based on particular OTDR settings. Following completion of the OTDR data acquisition, the backscattering signal versus distance results were transferred to a column in the Lotus spreadsheet.

Although the basic OTDR data acquisition was automatic, the switch operation was manual. Further, data from different ends of the fiber were manually stored in different spreadsheet columns for data analysis. The entire process of acquiring and analyzing data could be automated since the switch was capable of being controlled by the computer.

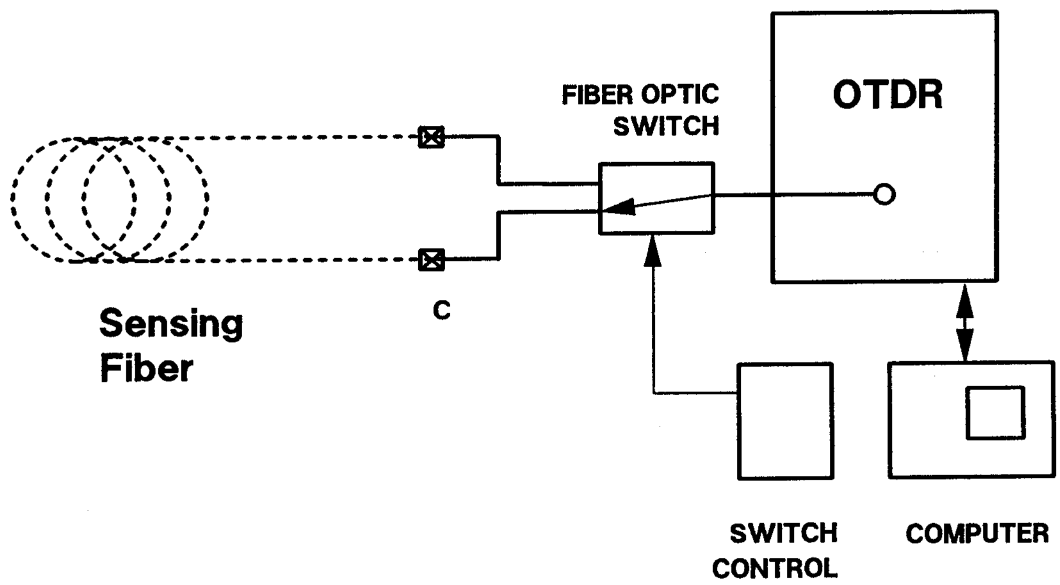

Figure 4-9
Block Diagram of General DFOTS Set-up for Temperature Measurement in Electrical System

OTDR Settings

The OTDR is a key component in the DFOTS system and its settings govern the data acquisition process. The most important OTDR settings are as follows:

> *DELAY* - There is an internal delay between OTDR laser pulse initiation and analysis of the returning scattering signal. The delay setting value, entered using the OTDR keypad, adjusts this internal delay value. Selecting an appropriate delay allows the experimenter to pick where along the fiber the data acquisition process starts. Equation (1) indicates that a delay value of 10 nsec must be added for every meter of fiber to ignore before starting the data acquisition process. There is an initial delay of 160 nsec within the OTDR and fiber optic switch, so the delay should be set at DELAY = 160 + Li X 10, where Li is length of fiber (in meters) that an experimenter desires to ignore.

> *T/D (Time per Division)* - This is an OTDR setting that controls the length of fiber that will be examined. For every 10 nsec increase in the T/D value, 10 more meters of fiber is interrogated by the OTDR. Choosing proper values of T/D and DELAY allows the experimenter to chose exactly what part and how much sensing fiber will be used to obtain temperature data.

> *SENSITIVITY* - The TDR20 provides three levels of sensitivity, namely: High, Medium, and Low, however, this parameter actually controls the measurement length resolution of the OTDR. On the High setting, the TDR20 collects scattering data from 30 cm of fiber, while on Medium and Low settings, 8 and

2 cm of fiber are respectively used. By choosing more fiber from which to collect light , the signal will increases (improved sensitivity), therefore, signal strength and length resolution are interrelated. Typically, Medium sensitivity (length resolution = 8 cm) has been used in the present report, however, High sensitivity settings have also been used to improve the signal to noise ratio of collected backscattering data.

FIXED LOSS - A special analog adjustment (knob on OTDR module) allows the experimenter to adjust the fixed loss of the TDR20's detection system. This fixed-loss adjustment is required to avoid saturation of the signal when the backscattering intensity is large. Proper adjustment assures that the collected data is valid. Validity depends on signal strength because too low of a collected intensity results in noisy data and too strong of a signal cause signal saturation effects.

Proper adjustment of all the above OTDR settings provides backscattering data that can be used to determine the temperature profile along the sensing fiber.

Data Acquisition Procedure

We briefly review the data acquisition procedure in this section. As stated above, the data acquisition process itself is semi-automated and uses several macro-based programs written for the overall Lotus 1-2-3 spreadsheet approach. The following procedure is used:

1. Adjust OTDR settings to initially examine the entire fiber from the fiber optic switch output through the sensing fiber and back to the switch. In fact, the T/D and DELAY adjustments should be selected to examine backscattering data beyond any actual fiber in the OTDR path. This allows one to obtain what is referred to as the background intensity, Io. The Io value is an input to the data analysis program (discussed below).

2. After Io is determined, readjust the OTDR settings to examine the sensing fiber region of interest. The settings should be adjusted to provide saturated conditions for the first few OTDR channels (beginning of fiber sensor). The OTDR goes through an auto-scaling process and having maximum (saturated) conditions at the beginning of the OTDR plot assists in keeping this auto-scaling process consistent throughout the data taking period.

3. Obtain and store data for reference (i.e., ambient) conditions.

4. Obtain and store data for unknown temperature conditions.

Obtaining and storing data is controlled by macro programs. For example, ALT-R causes the OTDR to operate, collect data and store it in the "reference" column of the spreadsheet. ALT-S performs an OTDR data sequence and stores the data in a "signal" column. Several other data acquisition macros are available to the experimenter. ALT-1 through ALT-10 obtains OTDR data and stores it in ten special columns designated in the spreadsheet. These columns can be labeled and the results examined later during an off-line data analysis. The OTDR data can also be analyzed as it is obtained and the reduced data appropriately stored.

OTDR Data Analysis

Data is analyzed with the same Lotus 1-2-3 program as used for data acquisition. Two inputs are required, namely: 1) Io is typed into the appropriate spreadsheet location as stated above, and 2) The length of fiber (plus length beyond the fiber) that is examined by the OTDR (T / D X 10) is typed into the appropriate spreadsheet program location. The forward OTDR scattering intensity data are then copied into the "signal" column and the backward scattering data are copied into the "reference" column. The spreadsheet automatically calculates all the required information necessary to convert the OTDR data in these columns into a desired temperature profile. The temperature profile result is viewed using an ALT-T macro command. Various other calculations are available for viewing by using other macro commands. Any of the computer screen-displayed results can be stored electronically on disk to provide hard-copy plots or archival information for future retrieval. Appendix A lists the various program macros and provides further details regarding the spreadsheet-based program.

Modifications for Rotor Measurements

Presently, temperature monitoring in rotating machinery is limited to the outside surfaces that can be viewed by an IR camera or other line-of-site measurement equipment. In this case, the DFOTS approach could provide unique, on-line thermal monitoring of internal temperature for this type of electrical equipment. For example, the internal temperature distribution could be obtained within the rotor of a motor or generator. In this case, the fiber would again be attached along the conductors, however, an optical commutator (see Figure 4-10) is now used to access one or more sensing fibers as the rotor spins on its axis. Two optical commutation schemes are possible:

1. Single fiber monitoring using a rotating fiber device on the rotational axis of the machine under test, and

2. Multiple fiber monitoring using a fixed fiber device that is located off the rotating axis of the machine. In essence, the rotor motion acts as an optical multiplexer so temperature information can be obtained for several fibers attached to the rotating piece of electrical machinery.

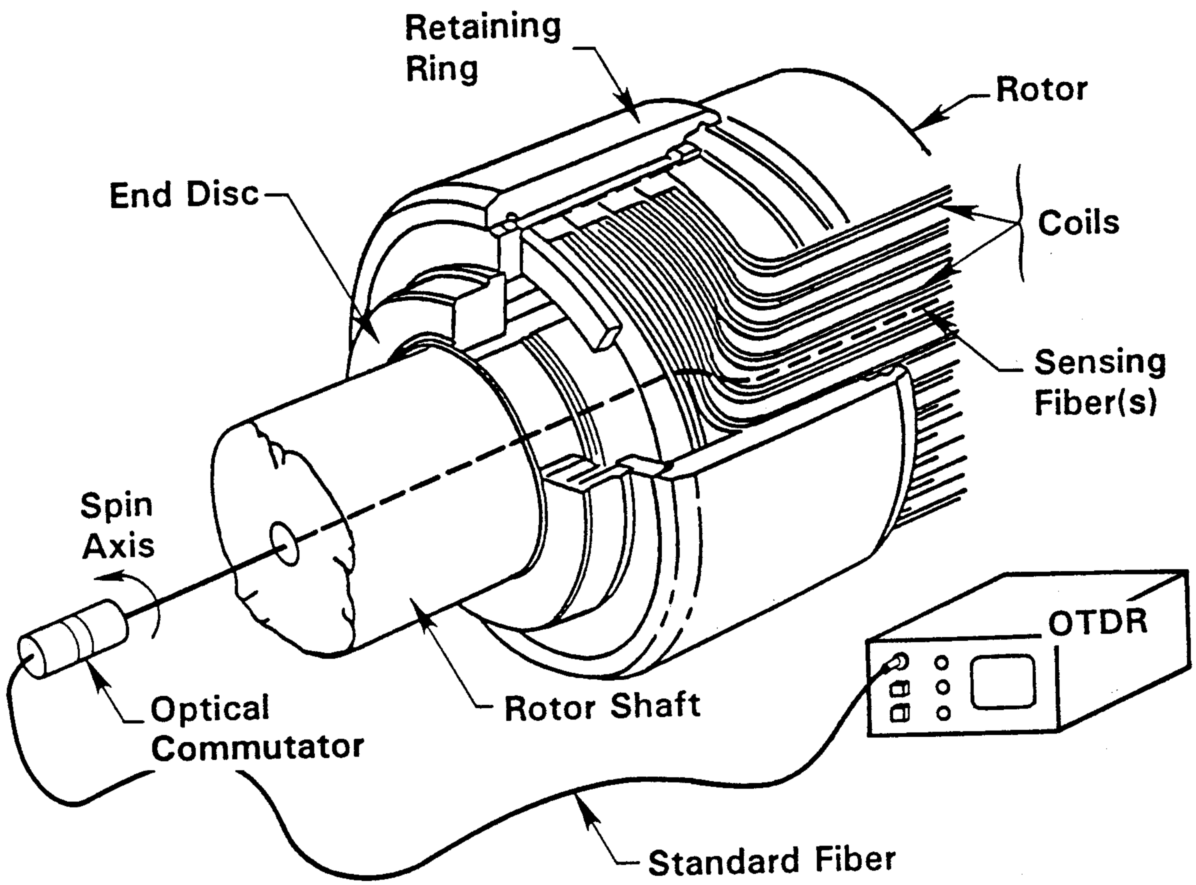

Figure 4-10
Schematic of DFOTS Approach Applied to Rotating Machinery

The first approach is straight-forward and uses existing equipment previously developed for examining a fiber optic cable while it is being unrolled from a large spool. The second method would be difficult to implement and requires a substantial development effort.

5

FIELD-TEST RESULTS FOR DFOTS SYSTEM

The DFOTS system, described in the previous section, was used to obtain temperature information in several electric power systems under field test conditions. In late 1992 through May of 1993, the DFOTS system was used to measure rotor winding temperature in a hydrogen-cooled synchronous condenser at PG&E's San Mateo Power Plant. These rotor measurements were part of an effort to validate model calculations aimed at predicting internal rotor temperature. From October 1993 through April 1994, temperature was then measured in the stator winding of a boiler feed pump motor. This motor was from Con Edison's Hudson Avenue Power Station. Field test results were also used to detect hot spots in a switch gear device at the R.E. Burger plant near Moundsville, West Virginia. These measurements were made in December of 1993. Several overheat conditions and a major fire had occurred in switch gear devices at the plant. The effect of cooling fans was also quantified. Finally, in June of 1995, the DFOTS approach was used to measure temperature in the stator winding of an air-cooled generator at Con Edison's Gowanus Power Station. The switch gear results are described in Reference [8]. Field test results, for the various winding temperature measurement applications, are discussed in the following text.

Application to Synchronous Motor Rotor Winding

The Contractor's first field-test of the DFOTS system involved assisting PG&E (Pacific Gas and Electric) in the testing of a hydrogen-cooled synchronous condenser at its substation in San Mateo, California. Details of the Synchronous motor are shown in Figure 5-1. PG&E wanted to instrument the rotor winding on the condenser to obtain temperature data that would verify thermal load models. The condenser's rotor coil was being rewound at Sytek/Benkiser Inc (S/B) across the bay in San Leandro. Following fiber installation at S/B, the rotor was sent, by barge, to the substation for installation in the condenser unit. Details of the rotor DFOTS application are provided below.

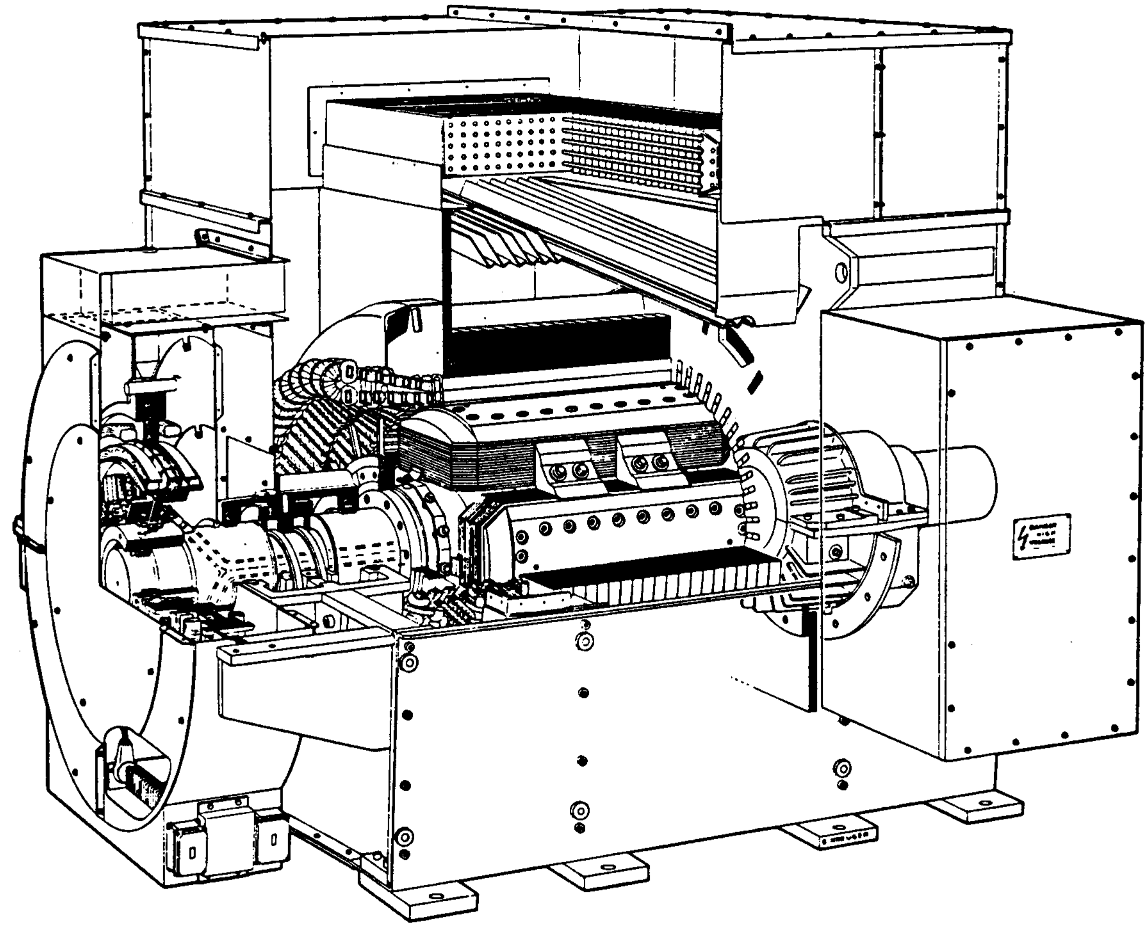

Figure 5-1
Synchronous Motor Details

Sensor Fabrication for Rotor Winding Application

The Contractor constructed five fiber sensors (20 meters long) for the rotor winding tests. An ST connector was placed on only one fiber end to allow for threading of the fiber through various parts of the rotor. A terminator (to reduce end reflections) was place on the other end of each fiber after installation in the rotor. To make the fiber easier to install, no protective jacketing was used in this rotor-temperature sensing application. Following construction, the fibers were tested at the Contractor's lab to insure proper function. The connector and terminator functioned properly and there were no breaks or damaged locations on any of the fibers. Four of the fiber sensors were sent to Sytek/Benkiser and one fiber was held as a spare.

Fiber Sensor Calibration for Rotor Application

S/B attached the sensing fiber in two different V-Block regions of the rotor coil using epoxy. Epoxy was used to minimize any vibration effects caused by centrifugal loads in the rotating winding. S/B had a choice of various epoxies that provided appropriate sensor bonding, however, it was not known if epoxy would degraded sensor performance. Further, the fiber was installed in a multiple S-shaped pattern within the V-Block region and bends can alter the sensor's response characteristics as described above. These effects were examined by testing the fibers as follows:

1. Approximately 1 meter of sensing fiber was placed in the multiple S-shaped pattern of groves on micarta pieces supplied by S/B. The pattern was identical to that used to install the fiber in the rotor.

2. Several typical epoxies (supplied by S/B) were placed over the fiber within the grove region to bond the fiber in place.

Sensor calibration tests were carried out at known temperature conditions from 20 to 150 °C using facilities at the Contractor's site. Typical data were obtained for the epoxied fiber (in the multiple S-shaped pattern) to show what effect epoxy and bends had on fiber temperature sensing performance. The results showed that silicone-based epoxies provided the best method of holding the fiber in place. Epoxies that "set-up" harder than silicone placed too much pressure on the unjacketed fiber and resulted in higher than acceptable distributed bending losses.

Results of the silicone epoxy calibration tests are shown in Figure 5-2 for a 1 meter length of fiber heated in the simulated V-Block region. In this figure, the term dBs is the measured parameter taken from the fiber backscattering signal for various temperatures. Therefore, Figure 5-2 serves to provide the sensor calibration required for extracting temperature information (using the dBs approach) from the fiber when it is installed in the rotor. Note the differences in calibration data from Figures 5-2 and 4-4 indicating the importance of calibrating the fiber using simulated test conditions.

Fiber installation in the Rotor Winding

Four fiber sensors were sent to S/B where they were installed (by S/B staff) in the rotor of a synchronous condenser from the PG&E San Mateo substation. Figure 5-3 shows the geometry of the fiber installation and Figure 5-4 shows how the fiber was physically placed in the rotor prior to the rewind operation. Two fibers were placed together (parallel to each other) in one path through the rotor and two others took a different path. This arrangement provided for redundant sensors and measurements for two different V-Block regions. In each case, a 5-meter loop of fiber was formed near the input end. After traversing a portion of the hollow rotor shaft, several bends were

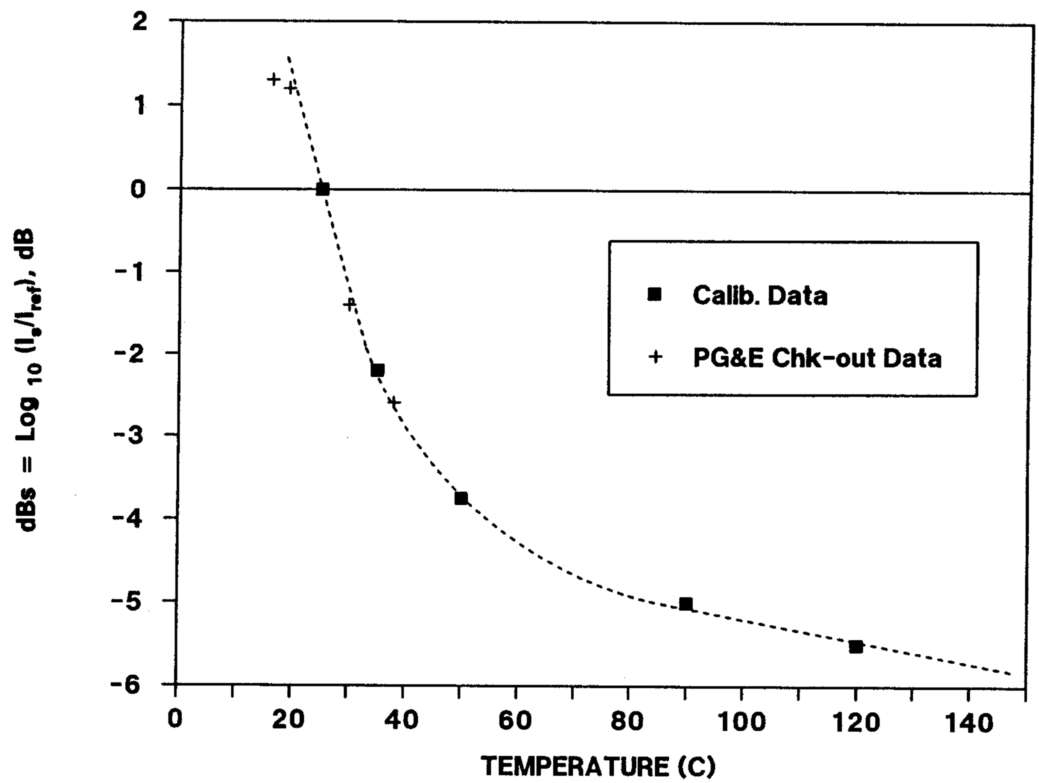

Figure 5-2
Backscattering Signal Change, dBs, for V-Block Pattern as a function of Fiber Temperature

provided to access a path to the V-Block regions. Following the V-Block, the fiber returned along its input route. The total fiber length was approximately 12 meters.

Within the V-Block region, the fiber was placed in the multiple S-shaped pattern and it was epoxied with a silicone-based material. An S-shaped pattern of sensing fiber was placed on each side of the V-Block to provide V1 and V2 regions as shown in Figure 5-3. The smallest radius of curvature in this S-shaped region was 1.91 cm (0.75 inches). Some protective sleeving and further silicone epoxy was used along the fiber path to help attach the fiber and maintain its integrity. A photograph of the V-Block (without the salient pole pieces) is shown in Figure 5-5 and Figure 5-6 shows a photograph of the sensor installed on the pole pieces in a position to receive the V-Block. The installation shown in these figures provided detailed temperature information in the vicinity of the V-Block and general temperature measurements in other regions of the rotor.

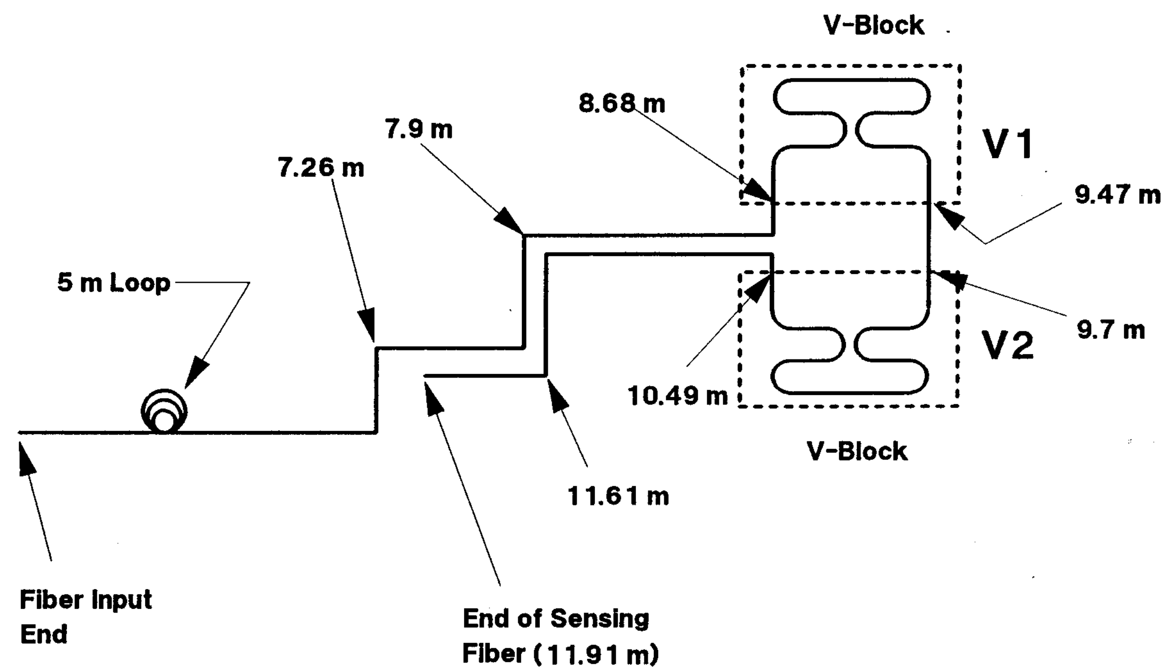

Figure 5-3
Geometry of Sensing Fiber in Rotor Winding

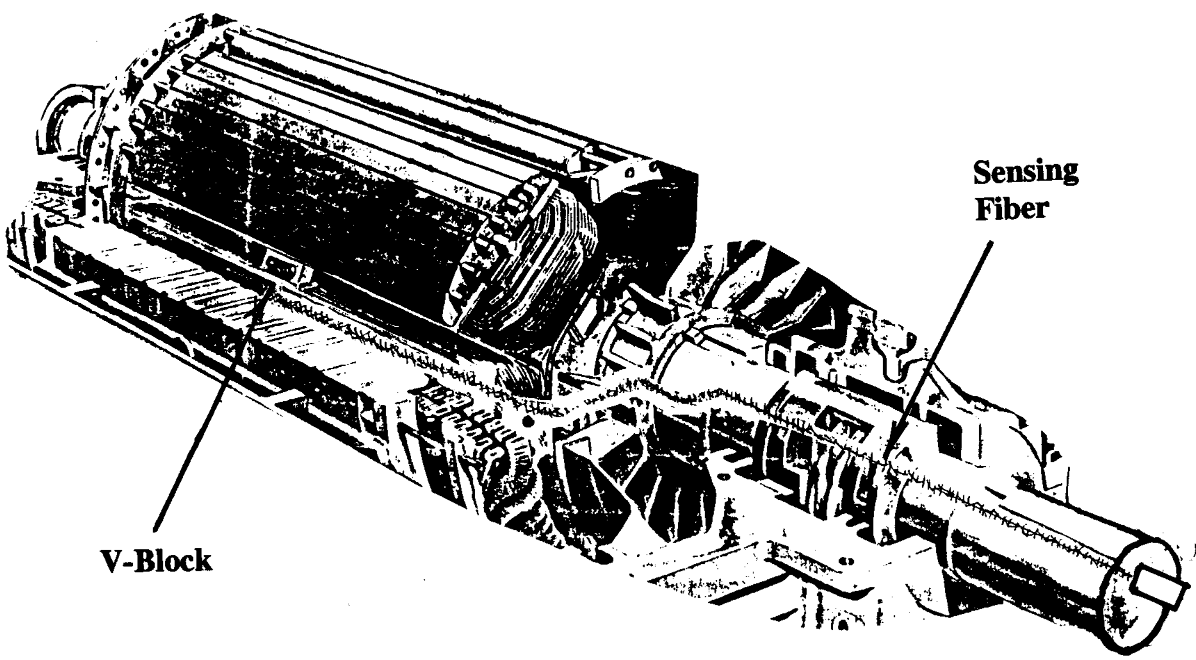

Figure 5-4
Physical Placement of Sensing Fiber in Rotor Winding

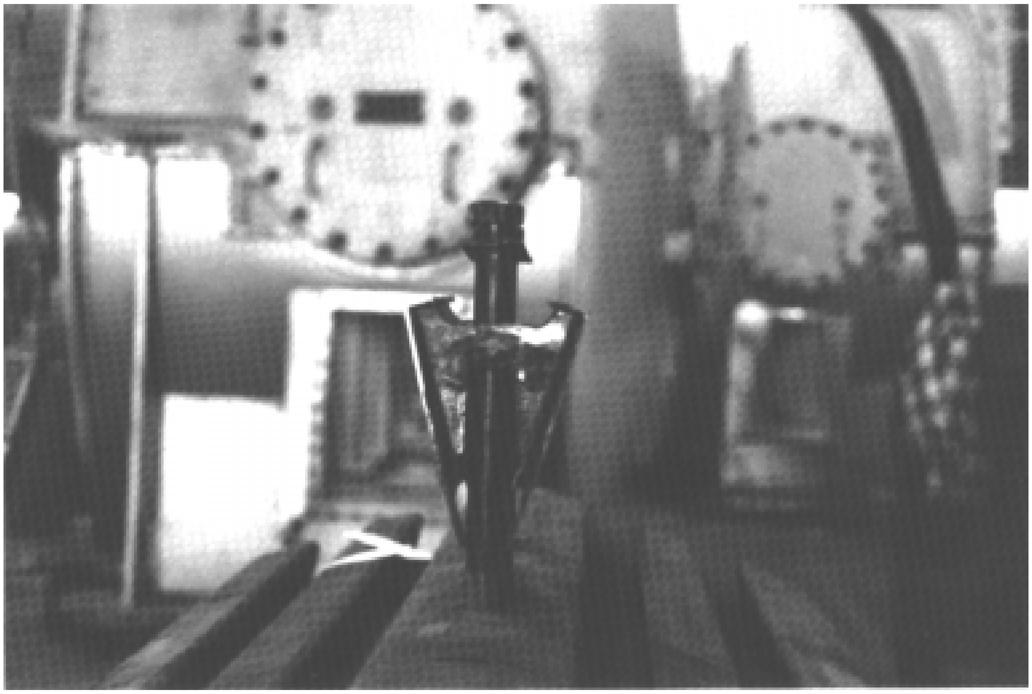

Figure 5-5
Photograph of V-Block Without Pole Pieces

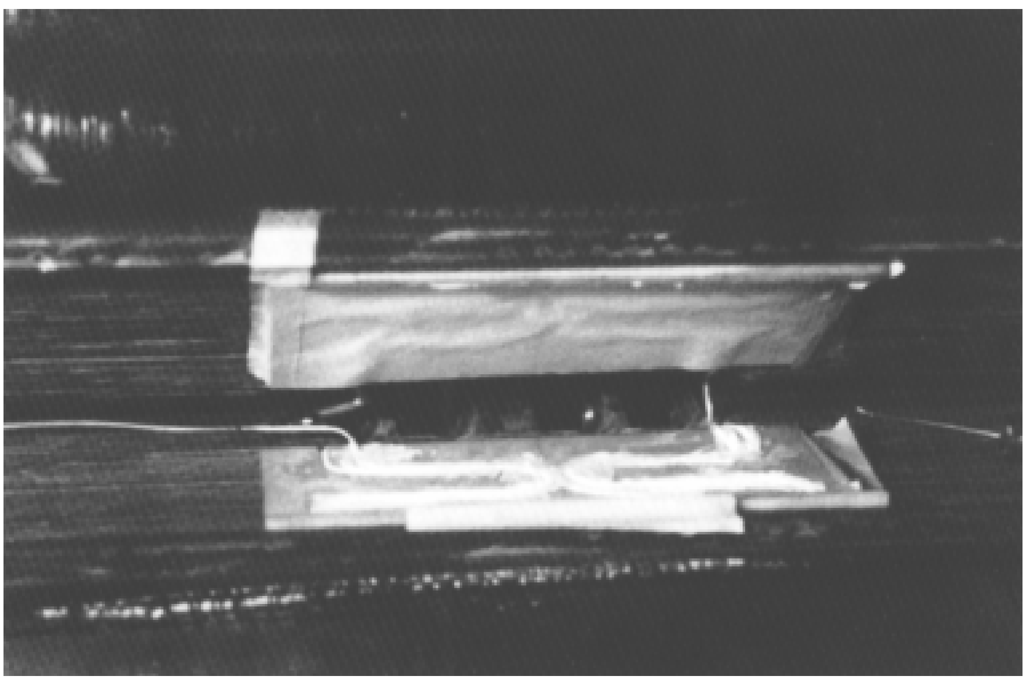

Figure 5-6
Photograph of Sensor Installed on Pole Pieces in Position to Receive V-Block

Fiber Check-out following Initial Installation

On January 22, 1993, the installed fibers were tested at S/B using the DFOTS opto-electronic readout system. These tests were performed after the rotor rewind was completed. Physical examination showed that two of the four fibers had lost their connectors (i.e., they were broken off). The other two fibers (with connectors) were tested and found to be properly functioning. However, the fibers must have been installed with several sharp bends because, the average light loss per unit length had tripled. Furthermore, a large light loss occurred in the fiber after the first part of the V-block region (V1) so no data was available from the second region (V2) along the fiber. In general, the signal-to-noise ratio also deteriorated considerably from 20 to 1 down to 4 to 1. Even with this signal-to-noise reduction, fiber temperature data were obtained (for one fiber) by heating the V-Block region with a gas-fired blower. A thermocouple on the V-Block recorded actual temperature. These fiber check-out results are also shown plotted in Figure 5-2. Note that the temperature data obtained at S/B agreed with the calibration data obtained in an oven at the Contractor's lab. Therefore, after the initial installation the sensing fiber was functioning, albeit not as well as desired.

Condenser Testing

To obtain rotor temperature data, the installed fiber sensors were connected (one at a time) to a rotary joint (RJ) device (e.g., Focal Technologies Inc.; NS, Canada). This device acted as an optical commutator (see Figures 4-10 and 5-7) allowing the optical signal to connect from a stationary to a rotating environment. The rotary joint can provide for optical interrogation of the sensing fiber during rotor motion up to 10,000 rpm. An optical feed through connector (Conax Corp.; Buffalo, NY), labeled FTC in Figure 5-7, was also required as a pressure seal for the fiber as it passed through the condenser housing. Outside the condenser, a 31 meter long jumper cable was used to optically connect the rotary joint to the OTDR, which was located in a van parked next to the condenser. A standard bushing connector (CBC in Figure 5-7) provided the main optical interconnect.

On May 20 through 22, 1993 DFOTS measurements were attempted at the San Mateo substation using the arrangement shown in Figure 5-7. Two PG&E personnel assisted a Contractor staff member during these tests. Physical examination showed that after rotor installation in the condenser, only one fiber remained connectorized and that connector was badly damaged. The Contractor, with assistance from a Fibertron Inc. staff member, attempted to splice the sensing fibers to the rotary joint fiber using a mechanical splice connection (MSP region in Figure 5-7). Three of the four sensing fibers could not be spliced because they were broken at a point near the fiber end and not enough fiber remained to accommodate the splice.

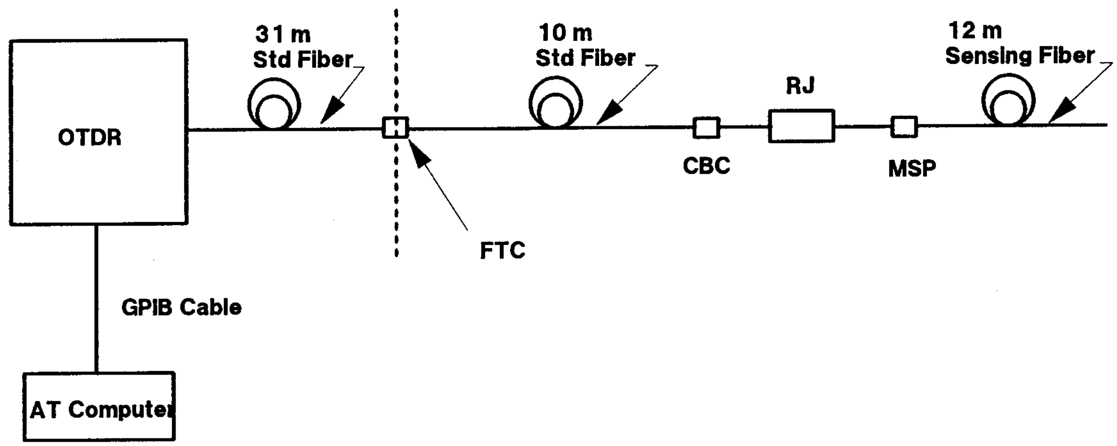

FTC - **Feed Through Connector**

CBC - **Standard Bushing Connector**

RJ - **Rotary Joint**

MSP - **Mechanical Splice Connection**

Figure 5-7
System Setup to Obtain DFOTS Data in Synchronous Condenser

A successful splice was made on one of the four fibers and OTDR data was attempted for static, rolling (no load) and load conditions (air and hydrogen). Examination of the OTDR plots showed that the first 6 meters of fiber were in tact. However, there was a break in the fiber near six meters so no data could be obtained in the V-Block region. Some OTDR output was available for the first 6 meters along the rotor shaft and this data showed that the temperature increased with load. Further, the DFOTS data for the shaft region indicated a lower temperature for the hydrogen test than for the air test (for identical load conditions). These shaft temperature results were consistent with what one would expect. The exact temperature values were not determined, because the setup was not optimized to measure temperature in the shaft area of the rotor.

Summary of Rotor Temperature Results

Four working sensing fibers were fabricated (i.e., bends, epoxies,...etc.) and successfully tested at known temperature conditions that would be encountered in the rotor winding tests. Both epoxy-induced distributed loss and fiber bends alter the temperature response of the fiber sensor. These variables were accounted for in the sensor calibration procedure. Installation of the fiber in the rotor winding caused its performance to deteriorate. Sharp bends introduced noise and light losses. Connectors attached to the sensing fiber itself were not rugged enough to withstand the handling associated with installation. The rotor winding forces in the V-Block region squeezed the fibers and introduced additional light losses. Although signal-to-noise and sensor performance were compromised, the sensing fibers were successfully installed in the rotor winding and V-Block. Calibration results taken on the installed fiber agreed with previous data taken at the Contractor's site. The rotating joint/optical commutator and optical feed through functioned properly providing a means for making DFOTS measurements in a hydrogen-cooled, rotating device (e.g., rotor in condenser unit). Shaft temperature data were obtained for a limited (6 meter) length of fiber during load and no-load conditions. These data agreed with expected trends. Results of shaft temperature for hydrogen charging were also as expected. No V-block temperature results could be obtained because fiber was broken during rotor transportation from S/B to San Mateo or during mounting of the rotor into the condenser unit. The fiber breakage problems indicate that some type of fiber protection is required.

Application of DFOTS to Boiler Feed-pump Motor Stator Windings

The DFOTS system was installed in a boiler feed-pump motor from the Hudson Avenue Power Station (Consolidated Edison Company of New York, Inc.). Initial experiments were performed at the Van Nest shop facility following a stator coil rewind. These shop tests were followed by field tests during actual pump operation at the Hudson avenue power station.

Sensor Installation in Motor Stator Winding

Based on early field experiences discussed above, the sensing fiber was jacketed with a hydtrel™ bifurcation tube that included kevlar™ strength members. The jacket protected the fiber, minimized sharp bends, and provided a rugged method of applying fiber optic connectors. A jacketed fiber sensor was sent to Con Edison and it was installed (by Con Edison staff) in the stator winding of a boiler feed-pump motor. The installation followed a stator-coil rewind coordinated at the Van Ness shop (Bronx, N.Y.), so it was a true retrofit sensor installation. Figures 5-8(a) and 5-8(b) show how the fibers were placed in the stator. Ten meters of fiber, on either end, were left outside the motor. Starting at the 10 meter point, End 1 was placed in slot 43 and the fiber was then laid in every third slot by looping back and forth throughout the winding as shown in Figure 5-8. The last slot instrumented with fiber was slot 40, then the fiber was brought out of the motor (see End 2 in Figure 5-8). The length of each slot (plus end loops) was approximately 1 meter, therefore, eighteen slots were instrumented with 20 meters of fiber placed throughout the stator winding. The fiber was held in place at several points (especially near the end of the slots) by tying it with standard polyester sleeve material and applying Sterling Epoxy. Within the slots, RTV adhesive was placed at several points to anchor the fiber. The fiber jacket was then painted with

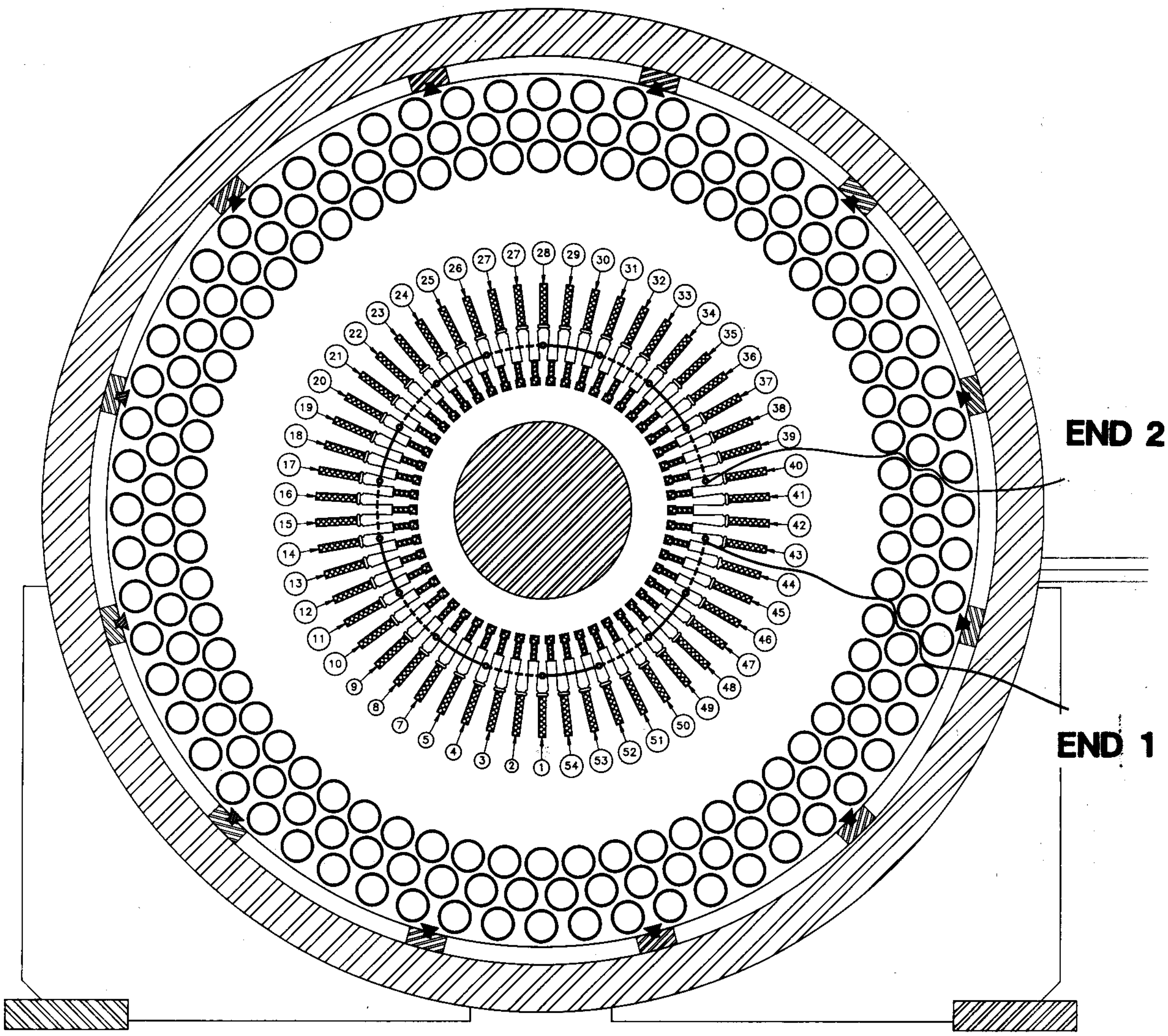

Figure 5-8 (a)
Sensing Fiber Installation Pattern in Pump Motor Stator Winding (Front View)

standard Dolph's ER41 insulating Paint. A photograph of the installed fiber is shown in Figure 5-9.

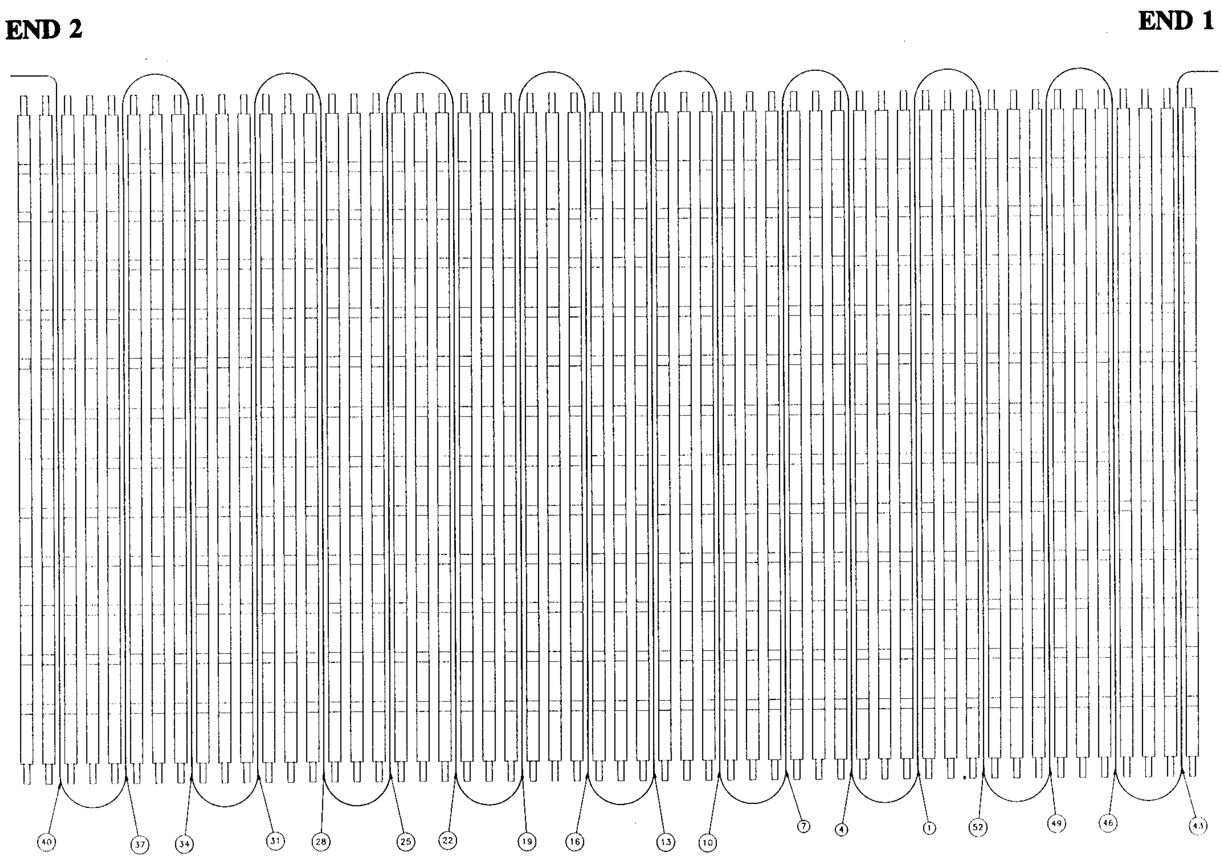

Figure 5-8 (b)
Sensing Fiber Installation Pattern in Pump Motor Stator Winding (Top View)

Check-out Tests using DFOTS System in Motor Winding

Following fiber installation, the Contractor's staff set-up the DFOTS readout system at the Van Ness shop. The DFOTS system set-up, shown in Figure 5-10, was first utilized to examine the installed sensing fiber at room temperature (i.e., ambient) conditions. In this case the ambient or reference temperature, Tr, was equal to 23°C. OTDR plots of the installed sensing fiber, for the reference condition, are shown in Figure 5-11 for both ends of the fiber. Comparing Figure 5-11 with the OTDR plot of a pre-installed fiber, it was obvious that some fiber damage (abrupt decrease in OTDR output) occurred. This loss in fiber transmission was located at the 10 and 30 meter points along the fiber length. These lengths represent positions where the sensing fiber entered and exited the motor housing. Physical examination of the fiber indicated the presence of kinks in the sensing fiber jacket caused by small radius bends in the jacket at these locations.

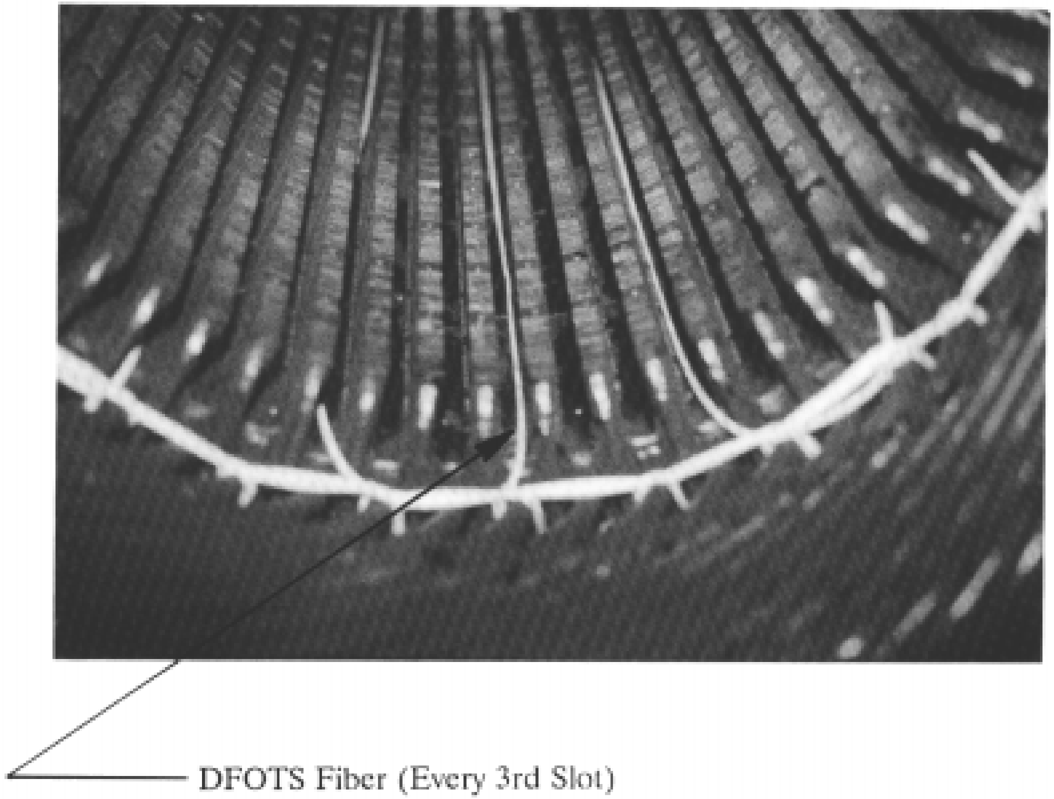

Figure 5-9
Photograph of Sensing Fiber Installed in Boiler Feed-Pump Motor

Transmission checks (using a source and detector approach) prior to OTDR testing indicated that the installed fiber had a 7 - 10 dB increase in one-way loss over what it had been prior to installation. OTDR data in Figure 5-11 indicate that most of this light loss was caused by damage which occurred near End 1 of the fiber as it entered the motor housing prior to being located in slot 43. The OTDR plots also indicate a small amount of damage near End 2 (approximately 1 - 2 dB) and additional points of fiber loss (i.e., damage) at 22 and 27 meters from End 2 caused by minor bends in the sensing fiber.

The ambient temperature results in Figure 5-11 show that the fiber was damaged somewhat during installation. Most of this damage did not occur within the stator winding, but was caused by excessive bending as the fiber entered and exited the motor case. The damage was minor near End 2, so data could still be obtained using End 2 of the sensing fiber, however, the dual-end reference approach could not be used.

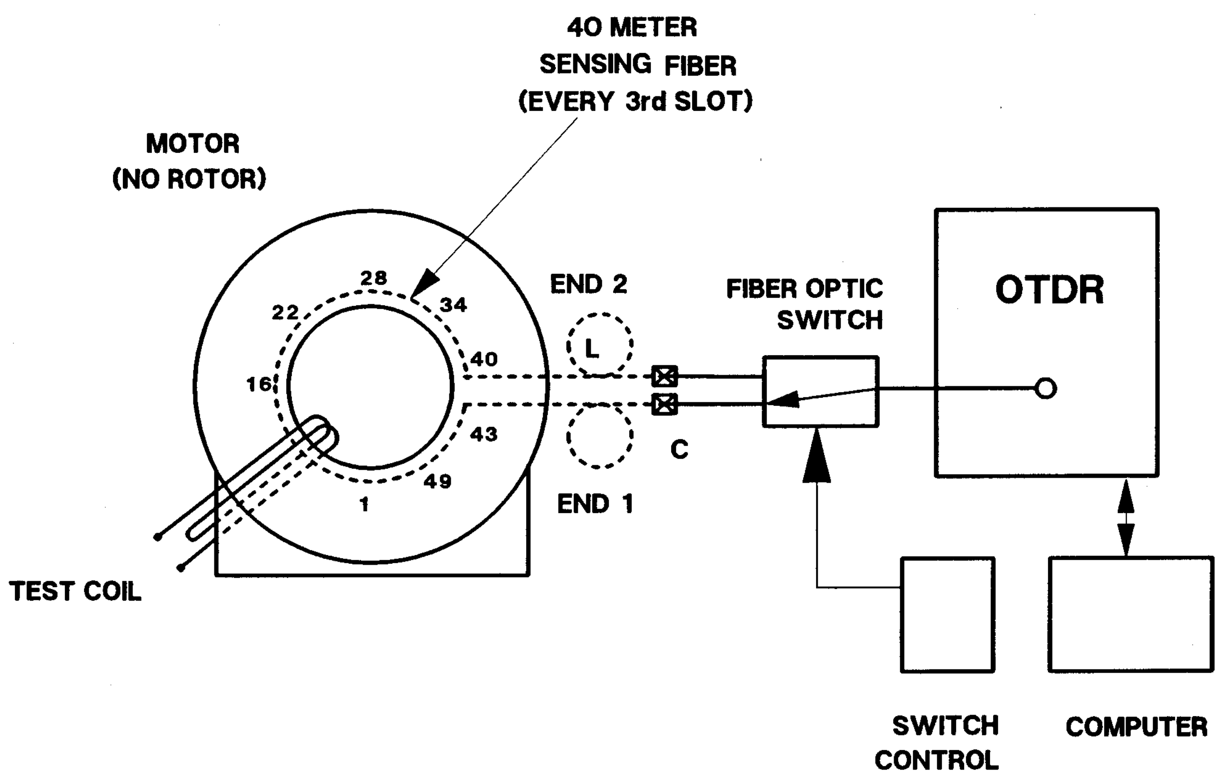

Figure 5-10
Block Diagram of DFOTS Set-up for Motor Temperature Measurement

Shop Temperature Tests of Stator Winding

For the shop testing, temperature conditions were generated in the motor's stator winding by looping a "test coil" several times through the core (no rotor present) as shown in Figure 5-10. Powering the test coil in the proper manner induced current in the stator winding, which heated the stator to various temperatures. RTD's in the stator coil were used to record temperature at known points within the winding.

DFOTS data were obtained at winding temperatures of 35 and 50°C. Variations in temperature within the motor were less than $\pm$1°C for these temperature conditions based on concurrent RTD measurements. To obtain the desired temperature levels, the test-coil power was started at 16 kW and raised as necessary. The temperature rose slowly with time and three RTDs (slot 42, 49, and 52) were used to monitor stator temperature during the heating process. OTDR plots (End 2) are shown in Figure 5-12 for reference temperature (Tr = 23°C) and the two test temperatures. Note that for the heated fiber region in the motor winding area, the loss slope decreased (as expected). Also note that the slope was approximately constant (i.e., temperature constant) throughout the motor. The constant slope is more evident in Figure 5-13, where the OTDR signal difference data are plotted. The difference data plot was obtained by

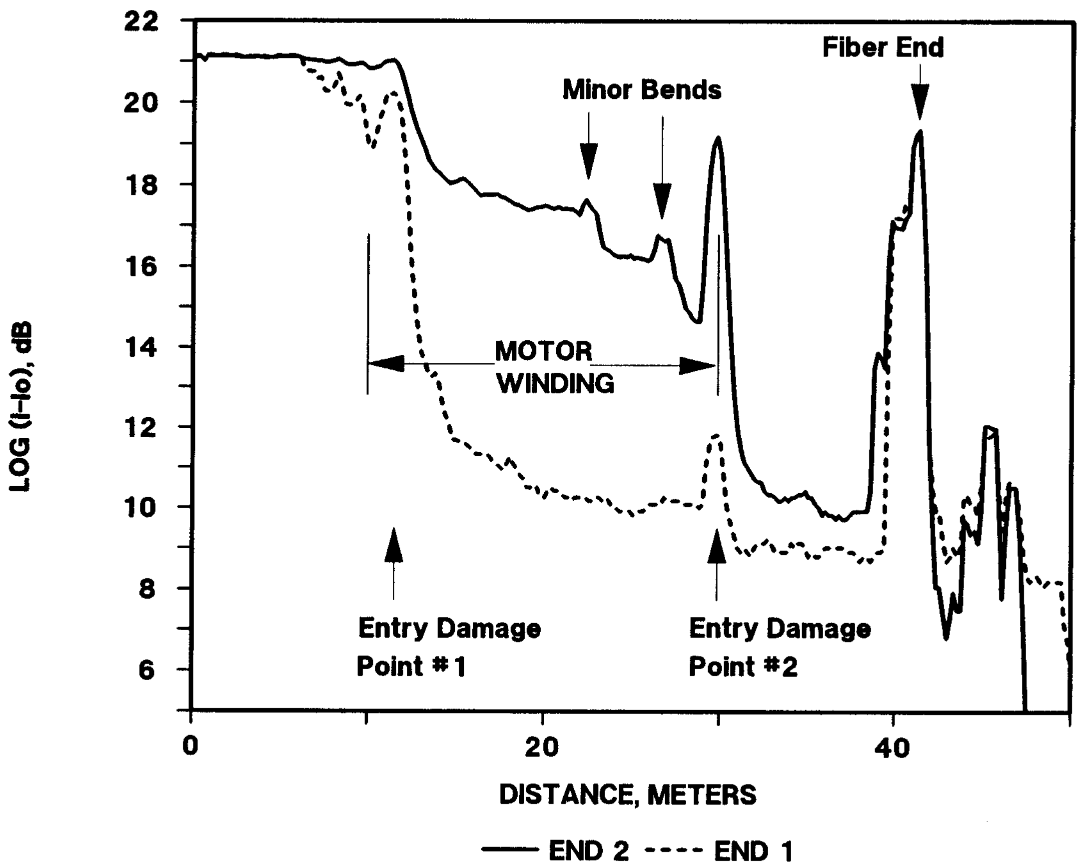

Figure 5-11
Reference OTDR Plot for Sensing Fiber Following Installation in Motor

subtracting the room temperature signal from the OTDR signal obtained at the two different test temperatures. In this case, the difference slope (loss(T) - loss(Tr)) is plotted and this slope is approximately constant throughout the motor. Therefore, slope data in Figures 5-12 and 5-13 indicate a constant temperature condition existed in the motor winding.

Also note in Figures 5-12 and 5-13 that besides the changes which occur at locations of fiber damage, no dBs changes exist in the OTDR signature. Again, the lack of dBs changes reflects a constant temperature environment within the motor. The dBs data in Figures 5-12 and 5-13 also indicate that dBs data alone cannot be used to determine the absolute temperature. The dBs data can't be used because the fiber damage occurred so close to the points of temperature increase and decrease. Therefore, it was not possible to measure the changes in dB from the room temperature reference condition. In essence, the region of fiber damage corrupted the dBs data. Since dBs data were corrupted by fiber damage at the points where the fiber entered and exited the motor, only slope date could be used to determine the DFOTS measured temperature in the motor. The results of the data reduction process are listed in Table 5-1.

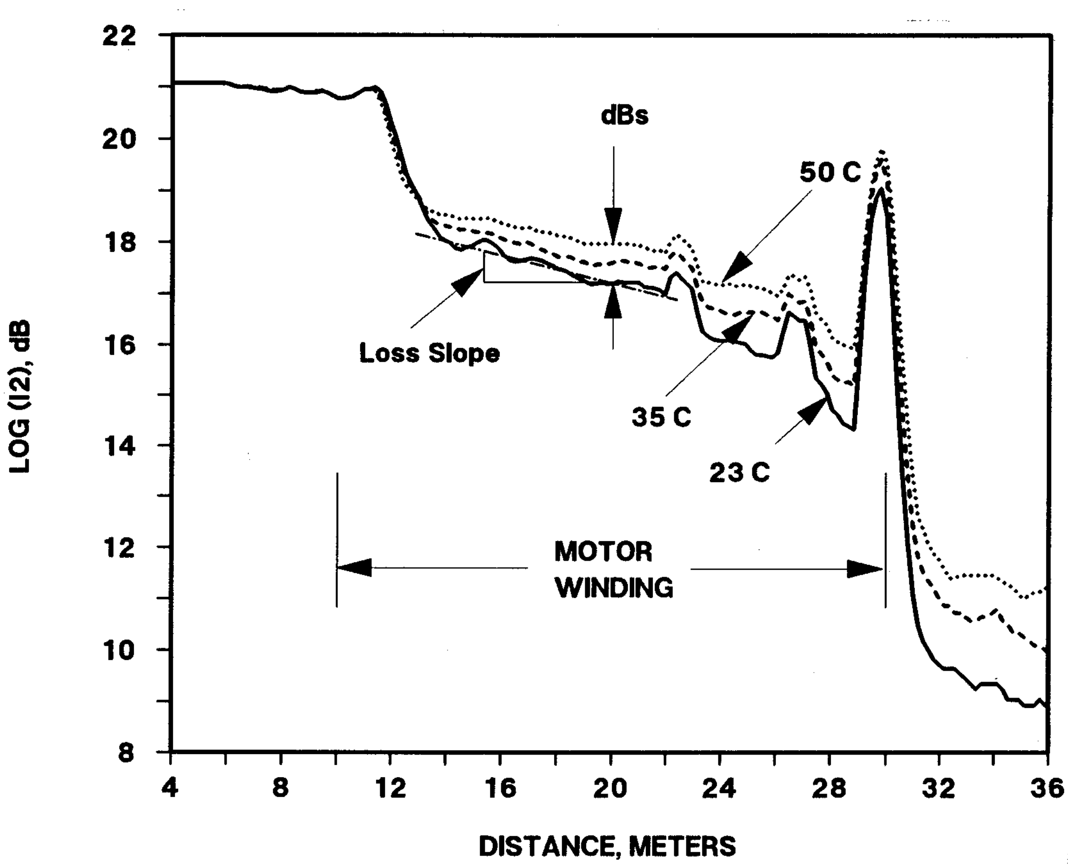

Figure 5-12
OTDR Plots (End 2) Obtained During Motor Testing

Table 5-1
Results of Slope-Method for Determining DFOTS Temperature of Motor Winding

Difference Slope S(T) - S(Tr), (dB/m)	Loss Slope, S(T) (dB/m)	Loss Slope Ratio S(Tr)/S(T)	Temperature, DFOTS T=Tr*S(Tr)/S(T) (°C)	Temperature, RTD (°C)	Temperature, Error (%)
0.0	- 0.080	1.00	23	23.0	0.0
0.029	- 0.051	1.57	36.1	35.2	+ 0.9
0.044	- 0.036	2.22	51.1	50.0	+ 1.1

Column 1 of Table 5-1 is the difference slope shown in Figure 5-13. In column 2, the actual slope of the OTDR plot is provided. This slope was determined by subtracting

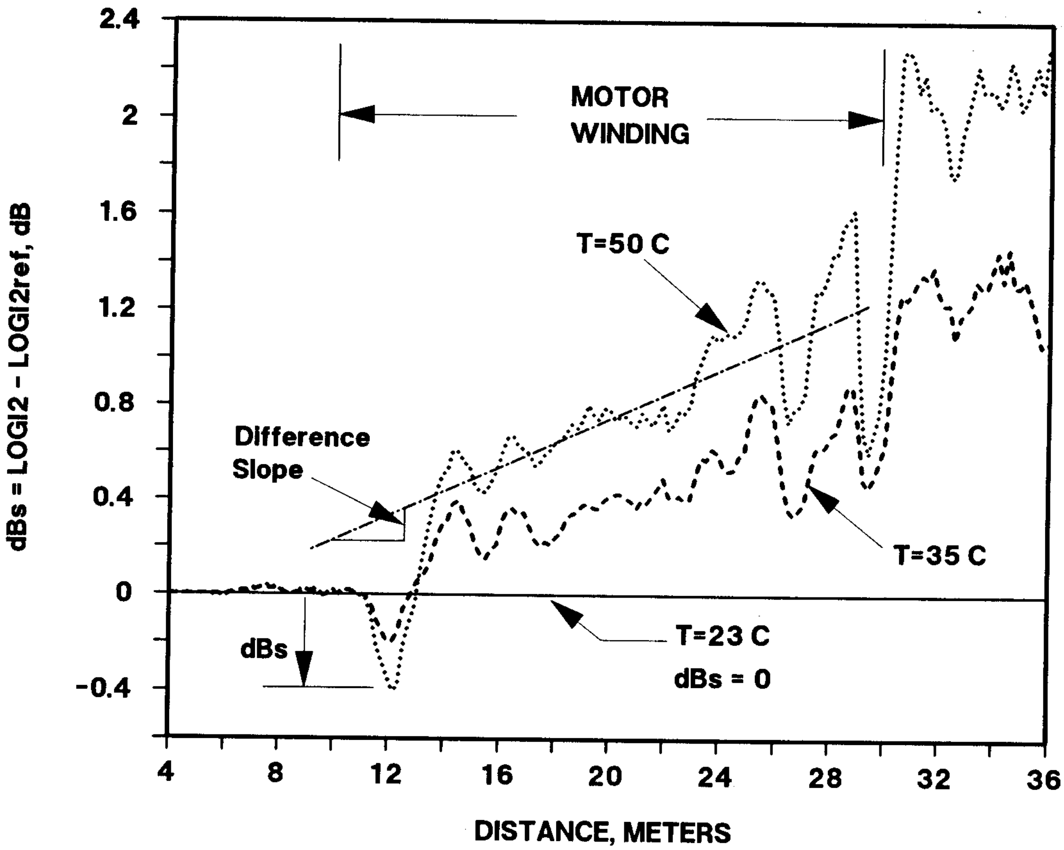

Figure 5-13
Difference Plot Used to Determine Difference Slope During Motor Testing

the reference temperature slope (i.e., -0.080) from the difference slope values in column 1. The loss slope ratio, S(Tr) / S(T) is a simple calculation using values in column 2.

DFOTS temperature (column 4 of Table 5-1) was determined using Equation (11) and the loss slope ratio values in column 3. These values compare favorably to the RTD temperature measurements listed in column 5 of this table. The temperature measurement error is approximately 2 percent, therefore, accuracy of the DFOTS approach appears quite acceptable. The temperature results represented in Table 5-1 look encouraging, however, there is room for improvement. For example, the slope method used in the above analysis requires that at least 4 meters of fiber be averaged in order to determine an accurate slope value (see Figure 5-13). Even with this rather large spatial resolution, the data in Figure 5-13 is fairly noisy and it would be difficult to determine an accurate slope value except over a fairly large portion of the motor winding area. Most of the noise was associated with fiber damage, therefore, improved measurement results will result once fiber damage is reduced or eliminated.

Field-test Data at the Hudson River Power Station

Following the stator coil and DFOTS system check-out tests at the Van Nest shop, the rotor was refitted and the boiler feed-pump motor was installed at Con Edison's Hudson River Station. DFOTS temperature results were then obtained for conditions of no pump load (i.e., motor free turning) and at near maximum pump load. A uniform OTDR slope (i.e., constant S(T) with no dBs (T) changes) was measured throughout the motor, indicating a uniform temperature (no hot spots). This slope was used to determine the DFOTS temperature using a least-squares-fit data analysis process. Figure 5-14 shows a temperature versus time plot measured by the DFOTS fiber for no pump load. Note that the DFOTS measured temperature increased, then leveled off to a value that was 18°C above ambient conditions after approximately 50 minutes of motor operation.

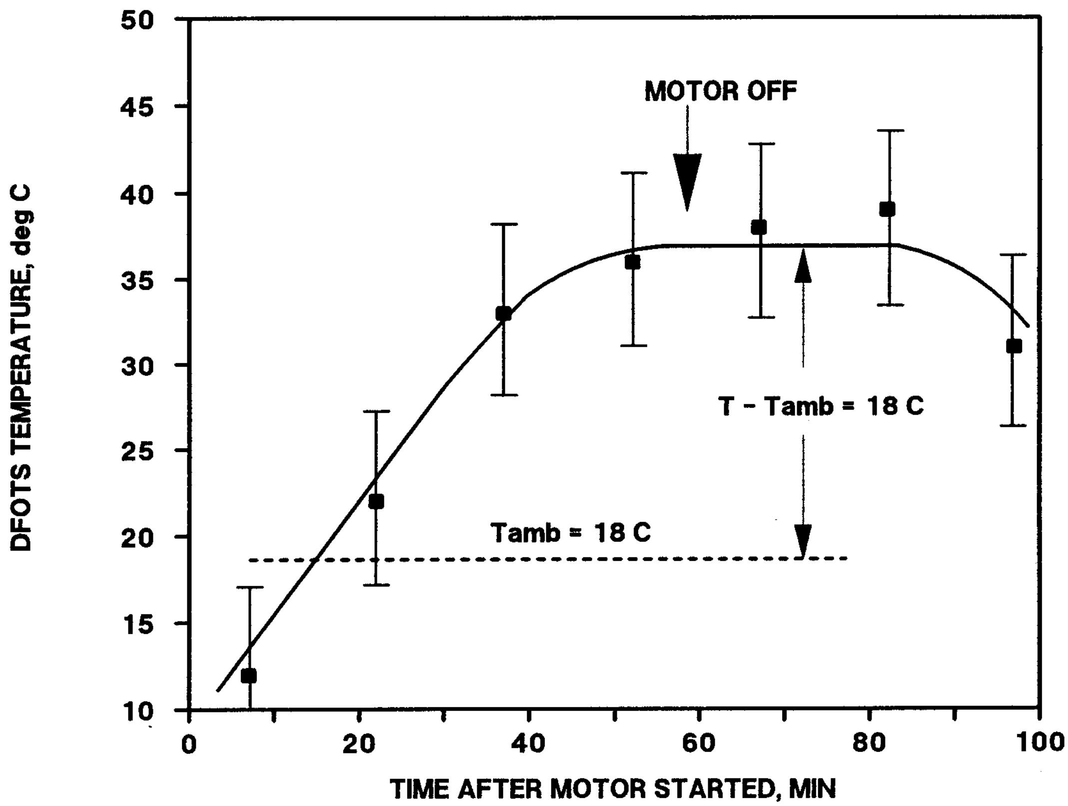

Figure 5-14
DFOTS-determined Motor Winding Temperature versus Time for No Pump Load (i = 320 A)

Figure 5-15 shows the DFOTS determined maximum temperature difference from ambient (i.e., T-Tamb) as a function of motor current. Only two conditions (no-pump load and near maximum pump load) were examined. An RTD was used to measure air

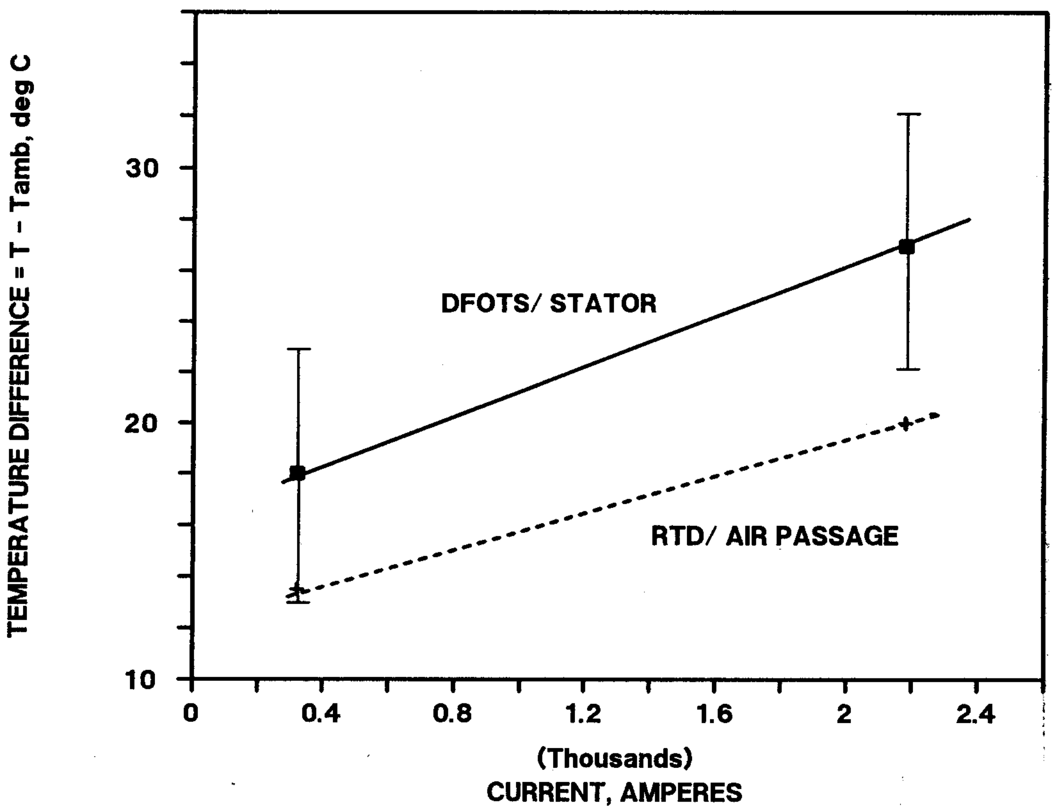

Figure 5-15
Measured Winding and Air-passage Temperature in Pump Motor as a Function of Motor Current

passage temperature. These data are also plotted in Figure 5-12. Note that the stator temperature increase (above ambient) is higher for higher motor current (as expected). Further note that the stator is approximately 5 to 7°C hotter than the air passage temperature over the operating range of interest.

Summary of Boiler Feed-Pump Motor Test Results

In summary, the DFOTS system successfully measured temperature in a motor/stator winding. These measurements were successful even though some fiber damage occurred. The damage was mainly limited to regions where the fiber entered and exited the motor housing. The OTDR slope-method was used to determine temperature along the fiber because the OTDR output change approach (i.e., dBs method) was corrupted by the damaged fiber. To avoid damage to the fiber in future tests, it is recommended that some type of strain relief be used where the fiber enters and exits the motor housing. This strain-relief member could be a simple length of rubber tubing around the fiber(s) at the fiber/housing interface. RTV silicone cement could be used to seal the fibers to the tubing and the tubing to the motor housing. This strain-relief arrangement should help reduce damage by preventing sharp fiber bends.

Application to Air-cooled Turbine Generator Stator Winding

The DFOTS approach was also used to make temperature measurements in an air-cooled generator at the Gowanus Power Station (Con Edison) near Manhattan, N.Y. These measurements were limited in nature, but served to demonstrate use of this fiber optic sensing approach in a generator monitoring application. In this case, the sensing fiber was installed (retro-fitted) into the stator of an air-cooled generator on Barge no. 4 (i.e., stator no.4-5).

Sensor Installation in Generator Stator Winding

The sensor was installed on-site (at the Gowanus station) by Con Edison staff after the rotor was removed for a rotor coil rewind. During installation, the sensing fiber was placed along the surface of the top half of the coil in every third slot. Seven out of 36 slots were instrumented with sensing fiber that was held in place with silicone adhesive and coated with insulating paint as mentioned above. During this installation, the fiber placement geometry, near the ends of the slot, was changed. In this case the fiber was not looped outside the slot and not lashed to the end-windings as in the case of the boiler feed pump motor. Instead the fiber was turned 90 degrees, at a point near the end of each 2.4 meter long slot, and threaded through an air cooling passage to the next instrumented slot. Figure 5-16 shows a diagram of the fiber installation geometry. The installation scenario resulted in placing approximately 17 meters of the 40 meter sensing fiber in contact with the stators outer surface in the gap between the rotor and stator coils. OTDR backscattering results were obtained every 10 cm along the sensing fiber length to provide high-resolution DFOTS temperature information.

The diagram in Figure 5-16 shows that two 10-meter coils were formed (one at each end) in the 40 meter long sensing fiber. These sensing fiber coils were placed inside the generator's frame assembly so they were exposed to air cooling passage temperatures rather than ambient conditions. Only a short piece of sensing fiber existed outside the generator and the fiber was strain-relieved at the fiber-frame interface. This installation procedure provided maximum protection for the sensing fiber following installation. Note in Figure 5-16 that two 40 m lengths of standard (commercial communication grade) optical fiber were used to provide for remote location of the DFOTS readout system within the generator control room. The forty meter length value was selected to match the length of the sensing fiber. This length match resulted in minimum noise due to light reflections from fiber-to-fiber connections. As before, a fiber optic switch (FOS) was located near the OTDR and used to remotely interrogate both ends of the sensing fiber.

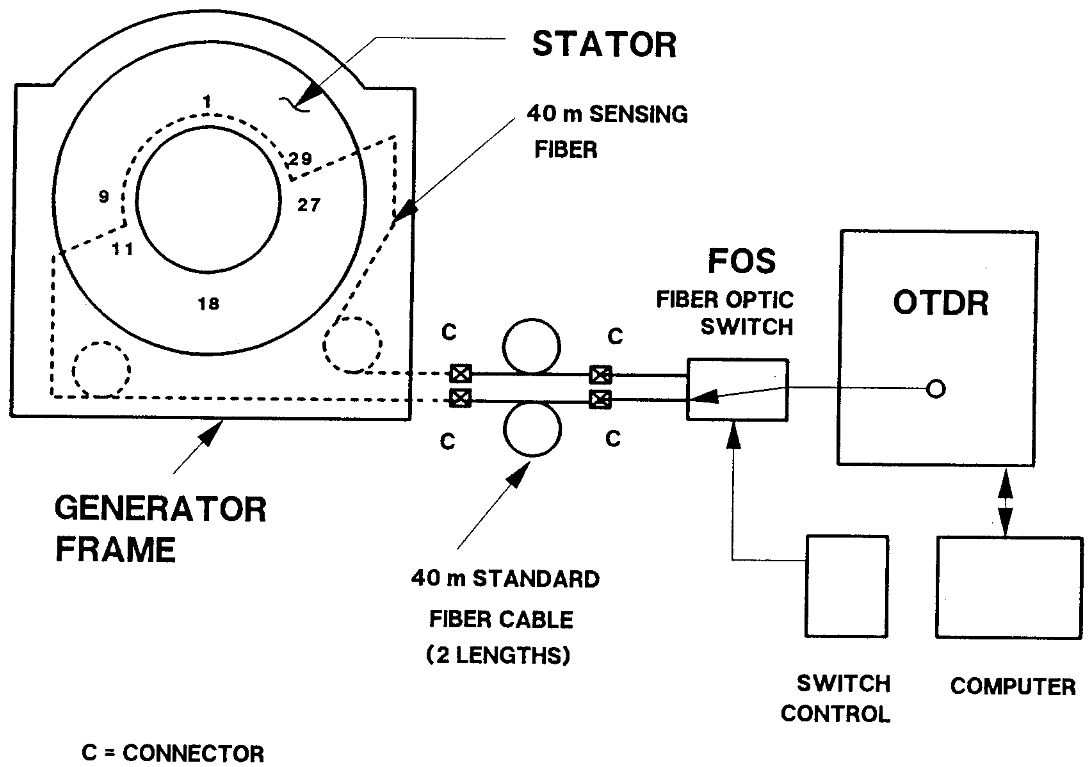

Figure 5-16
Block Diagram of Sensing Fiber and DFOTS System Installation for Generator Application

Check-out Tests in Generator Winding

OTDR check-out tests indicated that only minor light losses were introduced in the fiber during the installation process. These minor decreases in the backscattered light signal occurred at points where the sensing fiber entered and exited the stator coil. Within the stator coil, and throughout the remainder of the fiber, no light loss (i.e., no damage) occurred. Therefore, the setup shown in Figure 5-15 represents the best fiber installation procedure (i.e., one that minimizes fiber bending loss effects).

Field Testing at Gowanus Power Station

After obtaining some reference data prior to generator start-up, DFOTS data were recorded periodically over a nine hour period as the generator was brought on line. Two generator starts were attempted. During the first start-up, a circuit breaker failed to close properly so the generator was taken off-line almost immediately. After 3 hours, the generator went back on-line, without problems, and DFOTS data were obtained over a two hour test period. Generator output was 15 Megawatts (3 Megavars).

A combination of slope-and dBs-methods provided temperature results from the backscattering data. Both the frame assembly and stator temperatures could be determined because the central portion of the sensing fiber was attached to the stator surface and the two end loops were located in the frame assembly housing. The loss slope, S(T), was nearly uniform throughout the sensing fiber indicating that the frame assembly was approximately the same temperature as the stator coil. Small dBs changes did occur at the entrance and exit of the stator. These dBs changes indicate that the stator was slightly hotter (2 - 5°C) than the environment within the frame assembly. The nearly uniform loss slope and the lack of dBs changes within the stator also indicate that no hot spots existed in the upper portion of the coil.

Figure 5-17 shows the uniform DFOTS-determined stator temperature results plotted as a function of time after the reference data acquisition. Note that upon start-up, the coil temperature rose quickly from the ambient value of approximately 25 - 27°C to a maximum value approaching 45°C.

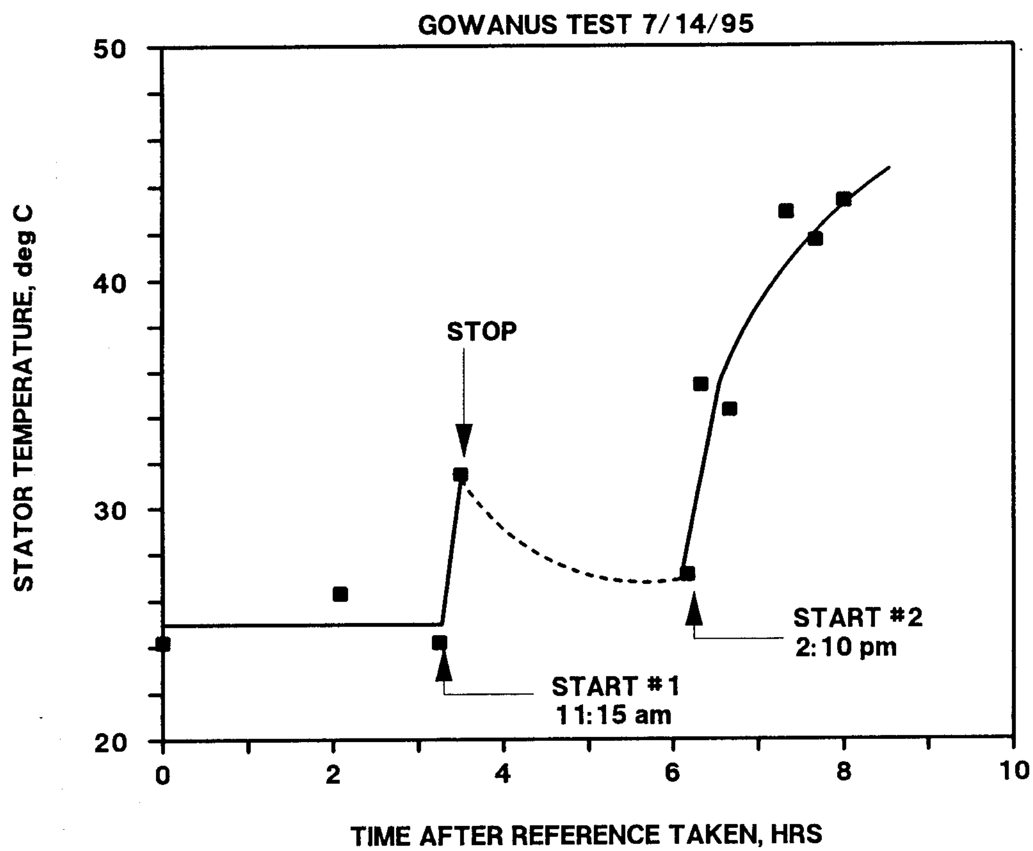

Figure 5-17
Stator Temperature Results as a Function of Time During Generator Test Period

After 2 hours, the temperature had not reached an equilibrium value, but data acquisition had to be terminated due to scheduling constraints.

Summary of Air-cooled Generator Test Results

In summary, the DFOTS system was successful in measuring temperature within the stator winding of the air-cooled generator. The location for measuring temperature was limited to the stator's inner surface on the top half of the coil in close proximity to the air gap. Temperatures were uniform throughout the coil region measured (no hot spots) and the coil temperatures were similar to the air cooling passage values. The fiber installation procedure was the best to date resulting in only minor light loss effects in areas where the fiber entered and exited the coil. Looping the sensing fiber inside the generator frame prevented damage due to handling the fiber ends. Air cooling passage temperatures could also be measured using this particular fiber-coil placement scheme.

6

END-WINDING STRAIN SENSOR APPLICATION

Besides temperature, stress-induced strain is another basic parameter that is measured in many mechanical systems. The strain measurements provide a check for abnormal conditions that may damage system components. Measurement of strain can also indicate abnormal component vibrations. The literature, however, does not indicate that any strain measurements have been made in power generation equipment. The lack of strain measurement data is undoubtedly caused by the strong electromagnetic interferences associated with this environment and the difficulty of obtaining a direct measurement of strain in electrical structures. One focus area for strain measurement is the end-winding area of stator components in rotating power generation equipment. Wedges can loosen and this defect can cause vibrations in the stator end-windings. If these vibration conditions are not detected rapidly and corrected, mechanical wear of the insulation can occur that could result in a forced outage. Measurement of end-winding vibration using fiber optic accelerometers have been reported [9, 10]. Westinghouse Corporation also supplies a system that measures vibrational amplitude using eight fiber optic accelerometers mounted on eight end winding coils.

In this section, we discuss the development and laboratory testing of a fiber optic strain sensor (FOSS) that could possibly be applied to electrical power generation systems. The general areas of stress-induced strain and strain related vibration measurements in stator windings are discussed in the following text. Various fiber optic strain measurement devices are described and a new fiber optic strain gauge is introduced for obtaining stress-induced strain measurements in electrical equipment. This new device was tested at the Contractor's site under laboratory conditions. The experimental set-up and the results of static and dynamic tests are described in this section.

Strain Sensing in Electrical Equipment

The Contractor's staff first investigated the requirements for sensing strain in electrical equipment (especially end-windings). The following list of key specifications resulted from this investigation:

- Sensitivity (lowest strain detectable): ≤ 10 micro-strain
- Range: -500 to +500 micro-strain
- Gauge length: ≤ 2 cm
- Frequency Response: 20 - 360 Hz
- System cost (readout and 8 sensors): ≤ $30,000

These specifications were used to guide our efforts at locating or developing, and testing a suitable sensor for the end-winding strain measurement application.

Researchers have exerted a good deal of effort investigating the general area of fiber optic strain sensing. A literature review revealed at least twelve different approaches to fabricating a strain sensor using fiber optic technology. Several literature reviews exist on the subject [11, 12] and one commercial device was recently introduced by Fiber & Sensor Technologies (Blacksburg, VA). The Contractor gathered information on all the approaches discussed in the literature before and during this project effort. We then evaluated the approaches based on the above specifications. Two approaches satisfied the specifications. These approaches are listed in Table 6-1 along with the performance parameters of interest.

Table 6-1
Performance parameters of Several Key Strain Sensing Technologies

Approach	Sensitivity, micro-strain	Range, micro-strain	Gauge Length, cm	Frequency Response, Hz	System Cost (8 sensors)
Micro-bending loss	5	-1000 to 1000	2	0 to 360	$ 5,000
Fabrey-Perot gap-Interfer.	0.03	-10,000 to +10,000	0.5 - 2	0 to 1000	$29,200

Both the approaches in Table 6-1 satisfy the specifications. Note, however, that the micro-bending approach is less expensive. Further, both these systems are considered less expensive than the Westinghouse vibration monitoring system. The second approach was not commercialized at the time the sensor technology was selected. Based on the above analysis of sensing technology and the lack of a commercial sensor, the Contractor elected to develop a micro-bending loss approach for strain sensing in end-windings.

Micro-bending Loss Strain Sensor

Fiber optic sensor have been developed based on the fact that light losses occur in an optical fiber when fiber bends are introduced. The term micro-bending loss applies because the fiber bends have a small radius, are generated in a periodic fashion, and the bends are produced at many points in a small fiber length. A strain sensor based on the principle of micro-bending of an optical fiber [13] was developed for measuring beam deflection, however, this device did not mount on the beam as does the standard electrical-based strain gauges. Instead, the device actually was mounted to a fixed structure below the beam and really measured beam deflection caused by loading. The deflecting beam applied force to a transducer that introduced micro-bending in the fiber. The Contractor developed a transducer that mounts directly to the structure under test. This device is described below.

Basic Transducer Function

Battelle used a commercially available bending loss fiber, from Herga Ltd (Suffolk, UK), that produces bending loss when the fiber is subjected to transverse force (i.e., force perpendicular to the fiber axis). Herga incorporates the micro-bending loss fiber in its optical switches for consumer safety applications. Micro-bending losses can be measured for very small bend radii [13], therefore, this approach can provide a highly sensitive strain measurement device when a transducer is used to convert structural strain to a transverse force on the fiber.

Figure 6-1 shows how light losses occur in the Herga fiber. As shown in this figure, the bending loss fiber consists of a deformable cylindrical sleeve, a helical coil and a silicone-jacketed optical fiber. The coil is wrapped around the silicone-jacketed fiber in a helix to provide fulcrum points for bending. Figure 6-1 shows a square-cross-section coil. The Herga fiber actually uses a coil with a circular cross-section. In Figure 6-1(a), no transverse force is placed on the fiber, so it remains relatively straight (only large radius bends occur). A straight fiber transmits the maximum amount of light from one end to the other. Over a short fiber length, ΔL, the intensity, I_o, traveling in the unbent fiber remains constant.

Figure 6-1(b) indicates that exerting a transverse force (compression) on the Herga fiber causes fiber bends in many places and in a periodic fashion along the compressed fiber length. The number of bends per unit length depends on the pitch of the coil wrap. The force-induced micro-bending along the fiber length, dL, causes an amount of light, dI, to be lost over that length. The amount of loss per unit length, Λ, can be written as:

$$\Lambda = dI/dL \quad . \tag{21}$$

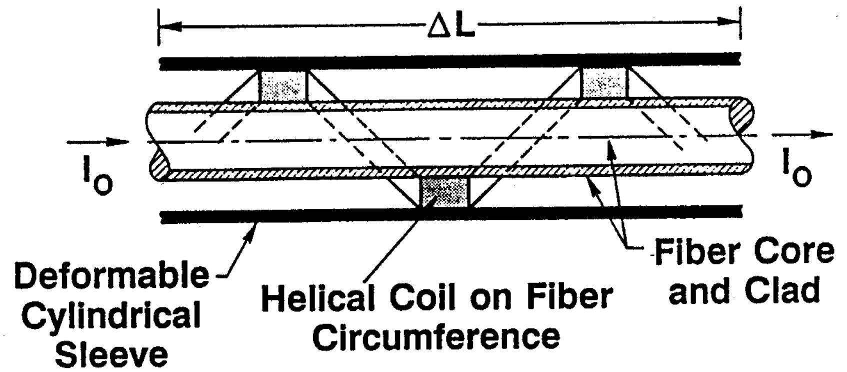

(a) No Transverse Force

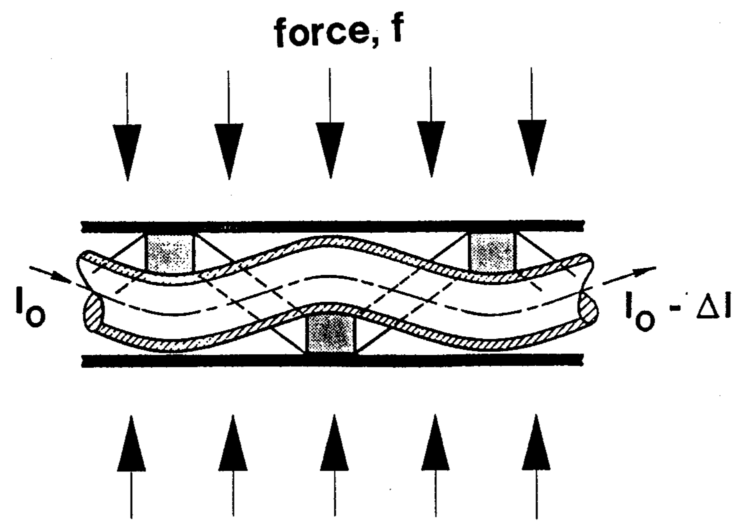

(b) Transverse Force Applied

Figure 6-1
Mechanism for Creating Micro-bending Loss in the Herga Fiber

Further, the loss factor Λ is proportional to the amount of force exerted on the fiber. Therefore, the total light loss, ΔI, is dependent on the transverse force, f, and the length of fiber, Lc, that is compressed as follows:

$$\Delta I(f) = \Lambda(f) * Lc \quad . \tag{22}$$

To create a strain sensor, using the Herga fiber, the task is to convert strain forces within a structure into transverse forces on the fiber. If this is accomplished, then the force related light-loss term in Equation (22) becomes a function of strain.

Herga Fiber

The bending loss fiber, manufactured by Herga, uses a standard silica clad - silica core commercial fiber as the main light-transmission device. This standard fiber has a 50 and 125 μm core/clad diameter respectively and has a low intrinsic light loss. This small diameter glass fiber is surrounded by a 2.74 mm diameter flexible silicone jacket material that allows the fiber to bend easily. The silicone material is wrapped in a helical fashion with an 88 μm diameter polymer coil. The coil has a small pitch resulting in 10 coil wraps every 1 cm of fiber length. Finally, the coil is held in place with a protective polymer jacket that gives the fiber a rectangular shape that resembles a piece of tape (i.e., 5 mm wide with a variable thickness from 0.1 to 0.4 mm). The Herga fiber can be ordered in various lengths and usually comes connectorized using standard, commercially available connectors.

Point Strain Measurement Transducer

The Herga fiber was mounted in a special transducer, as shown in Figure 6-2, to produce a point fiber optic strain sensor. The small transducer can be mounted at any point along the fiber length and has nominal dimensions of 18 x 18 x 12 mm. A three-dimensional view of this transducer is provided in Figure 6-3. The transducer is made of various materials. Initially, non-conductive materials were selected, but this choice proved impractical for the prototype design shown in Figure 6-2. Instead, the top portions were made of non-conductors (i.e., phenolic) while the strength members are made of conducting material (brass or aluminum).

The transducer itself is attached to a structure's surface to measure stresses in that structure (e.g., end-winding coil). As shown in Figures 6-2 and 6-3, the transducer resembles a small jack used to raise and lower objects. The device basically converts horizontal motion of the base elements into vertical motion of the top using four slotted and pinned bars (two on each side of the device) that link the top with the two base elements. The transducer's gauge length (Lo in Figure 6-2) is nominally equal to 11 mm.

Tensile stress at a structure's surface, that is parallel to the Herga fiber axis, produces tensile strain that increases the distance between the two bases by a small amount δLo. Under these tensile conditions, the transducer is designed to cause the top to move downward by an amount approximately equal to $\delta Lo / 2$. The downward motion of the top exerts an axial force on the Herga fiber located between the top and two bases. Conversely, the component of compressive stress in the structure that is parallel to the fiber axis, results in the bases moving together a distance equal to δLo. In this case, the

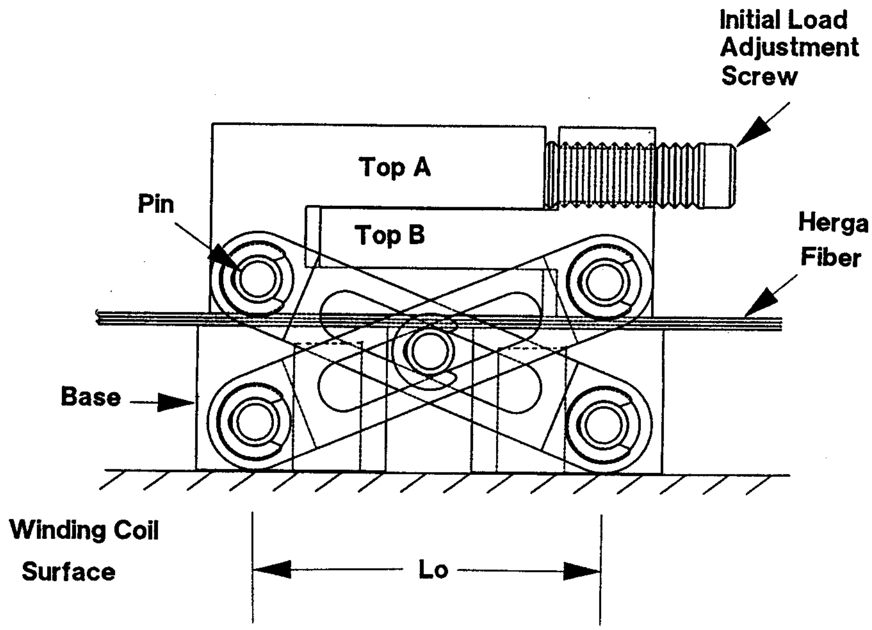

Figure 6-2
Assembly Drawing Showing Key Elements of Fiber Optic Strain Sensor

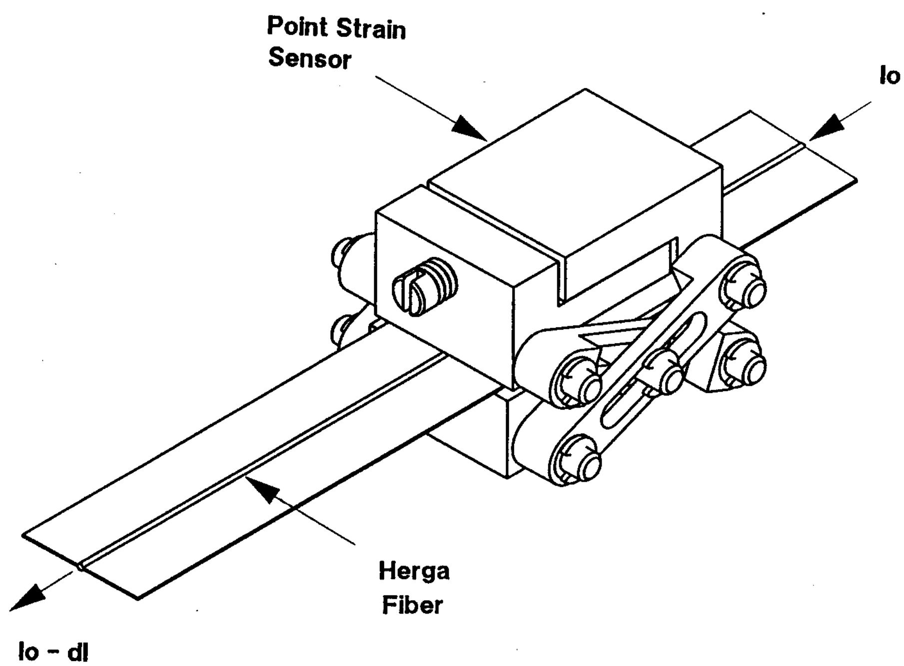

Figure 6-3
Three-dimensional View of Fiber Optic Strain Sensor

top of the transducer rises an amount δLo / 2. The top's upward motion increases the distance between the top and bottom and reduces the axial force on the Herga fiber.

The transducer device can measure both tensile and compressive components of strain by introducing a pre-set axial force on the Herga fiber (i.e., a pre-set loss value). This pre-set axial force is introduced by adjusting the initial load screw shown in Figure 6-2. Adjustment of this screw causes the top to change dimensions as the A-part of the top (Top A in Figure 6-2) moves relative to the Top B part. This motion changes the distance between the top pins, which changes the initial distance between the top and base elements. Given this initial axial force, tensile strain in the structure will increase the force and compressive strain in the structure will reduce the axial force on the Herga fiber. As stated above, these axial force changes will cause corresponding light loss changes in the Herga fiber.

Transducer Attachment Process

The transducer must be in intimate mechanical contact with the structure in which strain will be monitored to transmit structural strain into transducer motion. Further, the axis of the transducer (Herga fiber axis) must be placed in the correct direction to measure the desired strain component. Several attachment scenarios are possible, namely:

1. Direct mechanical attachment of two transducer bases to the structure using screws. The structure must be either drilled and tapped or the bases drilled and tapped and a through hole drilled in the structure.

2. Cement bases to structure using appropriate material.

3. Mechanically attach two bases of transducer to a thin plate and cement plate to structure.

4. Attach transducer to a plate that mechanically clamps onto end-winding and moves with it. Motion of end-winding induces motion in plate that induces strain in plate (plate could be cantilevered). Measure this plate strain and use the measured value to indicate levels of strain in end- winding. Two transducers could be mounted to a single plate providing multi-directional strain vector components.

The first attachment method requires physical alteration of the structure that could affect its performance. This method does, however, allow one to remove the transducer for future use. Cementing the transducer provides for minimal modification to the structure. Standard electrical strain gauges are attached using a special cement. Cementing is, however, a permanent attachment method and the transducer would need to be taken apart (several pins removed) to allow for partial transducer removal and reuse. The third method is a combination of the first two. The structure is left unmodified (no holes drilled) yet the basic transducer components can be removed from the cemented plate.

The first three approaches would also require that the coil have a flat region on its surface to which the transducer or plate can be properly attached. The flat region ensures good contact and accurate initial alignment of the sensor components. Larger end-windings likely have larger flat regions, however, small coils may not provide adequate flat mounting space to correctly mount the sensor. Grinding of the coil surface can provide a flat area for transducer mounting, but the grinding process may alter coil performance.

Finally, the fourth attachment approach is the easiest to install on an end-winding and easiest to move from one winding to another. This final approach also does not require a flat region on the coil for sensor attachment. On the other hand, the third approach provides only an indirect measurement of strain. Relative strain could still be obtained using this approach and careful calibration could provide information concerning strains in the actual structure.

In summary, the actual test scenario will dictate the specific attachment procedure. If possible, cementing the transducer itself (or a plate to which the transducer is attached) to the end-winding will likely be the method of choice for permanent transducer installation.

Laboratory Static Strain Testing

In this section, basic fiber optic strain sensor (FOSS) data are discussed. These data were obtained for static strain conditions.

Static Test Set-up

The fiber optic strain sensor was tested using a static strain setup-up as shown in Figure 6-4. A light emitting diode (LED) source was used to introduce light into the fiber. The particular LED source was a Fotec model S310 which operated at an 820 nm wavelength. Approximately 1 milliwatt (mW) of light exited the source but only approximately 3 microwatts (μW) was actually launched into the 50 μm diameter core of the Herga fiber. For the static testing, a Fotec model C detector (silicon photo-diode) was used to convert light that exited the Herga fiber into an electronic signal. This device had a light intensity-to-voltage conversion factor of 1 volt/μW of input light power. A standard digital voltmeter was used to read the voltage output of the Fotec C.

The FOSS transducer was mounted in the center on an aluminum bar that was 30.5 cm long and had a cross-section of 25.4 x 6.4 mm. A photograph of the FOSS sensor

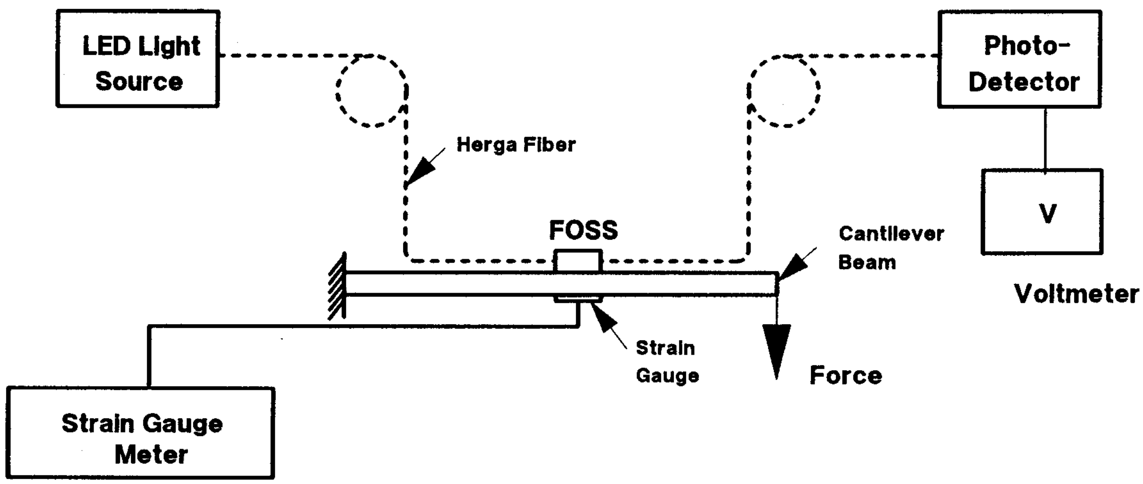

Figure 6-4
Experimental Set-up Used to Obtain Static Strain Data

mounted to the bar is shown in Figure 6-5. Sensor mounting was accomplished by drilling and tapping threads for two screws in the beam surface under the sensor. Flat-head screws were used to attach the two base elements to the surface of the bar. The bar was clamped in a cantilever arrangement that provided for introduction of compressive or tensile strains in the sensor by turning the bar to place the sensor on the top or bottom and applying a downward force at the tip. Values of strain from zero to ±1000 $\mu m / m$ (i.e., 1000 micro strain) could be easily generated in this static cantilever beam arrangement. A standard strain gauge was attached to the opposite side of the bar to record the applied strain values.

Static Strain Results

Fiber optic strain sensor (FOSS) output, V(FOSS), for various initial sensor pre-load voltage settings, V0i, are shown in Figure 6-6 as a function of the strain gauge reading. The data points in these figures are actual sensor voltage values from the digital voltmeter. The solid lines are a linear curve-fit of the FOSS output data points. The various initial sensor pre-load voltage settings (y-intercepts in Figure 6-6) were selected by changing the initial load adjustment screw and monitoring the sensor output for zero strain (zero force on the beam). For no initial pre-load on the Herga fiber, the FOSS voltage was V0o = 3.21 volts. Initial values from V0i = 0.97 to 2.62 volts were set using the load screw, therefore, the fraction of initial transmission, V0i / V0o , varied from 0.30 to 0.82. Data in Figure 6-6 indicate that the FOSS sensor output is linearly proportional to the strain gauge output over the range of ±1000 micro-strain. Some non-linear behavior is evident at the least amount of pre-loading because the fiber is no longer under load at the highest compressive strain levels (i.e., -800 to -1000 micro-strain). The pre-load must, therefore, be large enough to encompass maximum levels of

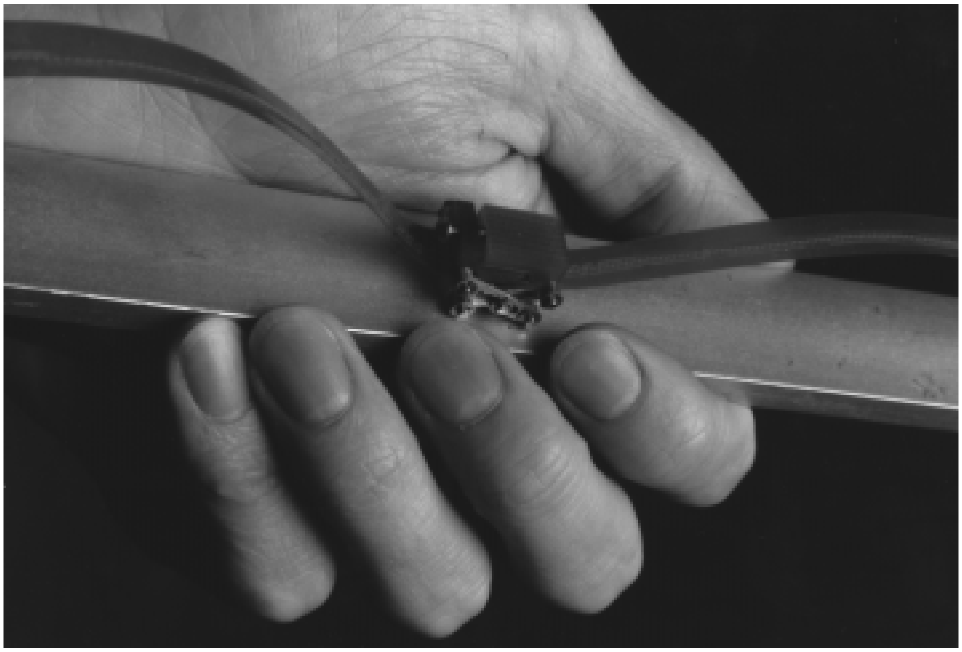

Figure 6-5
Photograph of Fiber Optic Strain Sensor Attached to Bar for Testing

compressive strain. Of course, pre-loads can't be so large that the fiber is completely compressed for the largest tensile strains (i.e., light completely extinguished).

The slope of the data in Figure 6-6 is the effective gauge factor, GF, for the FOSS sensor and the negative of measured GF values are shown plotted in Figure 6-7 for the various pre-load transmission fractions. Note that the gauge factor is nominally -0.55 volts / 1000 micro-strain and it is increases for higher initial transmission fractions (minimum pre-load values). Note also in Figure 6-7 that the gauge factor is approximately constant above an initial pre-load transmission fraction value of 0.7. Given the FOSS sensor gauge factor, GF, the FOSS determined strain is given by the following equation:

$$Strain\ (FOSS) = [V(FOSS) - V0i] * 1000 / GF \quad , \qquad (23)$$

where,

$$\text{Fraction of initial transmission} = V0i / V0o \quad . \qquad (24)$$

Knowing the value of V0o and setting a value for V0i (using the initial load adjustment screw), one can calculate the fraction of initial pre-load transmission using Equation (24). From this fraction and Figure 6-7, the gauge factor, GF, can be determined. Given the GF value and Equation(23), strain can be calculated using the FOSS sensor voltage output.

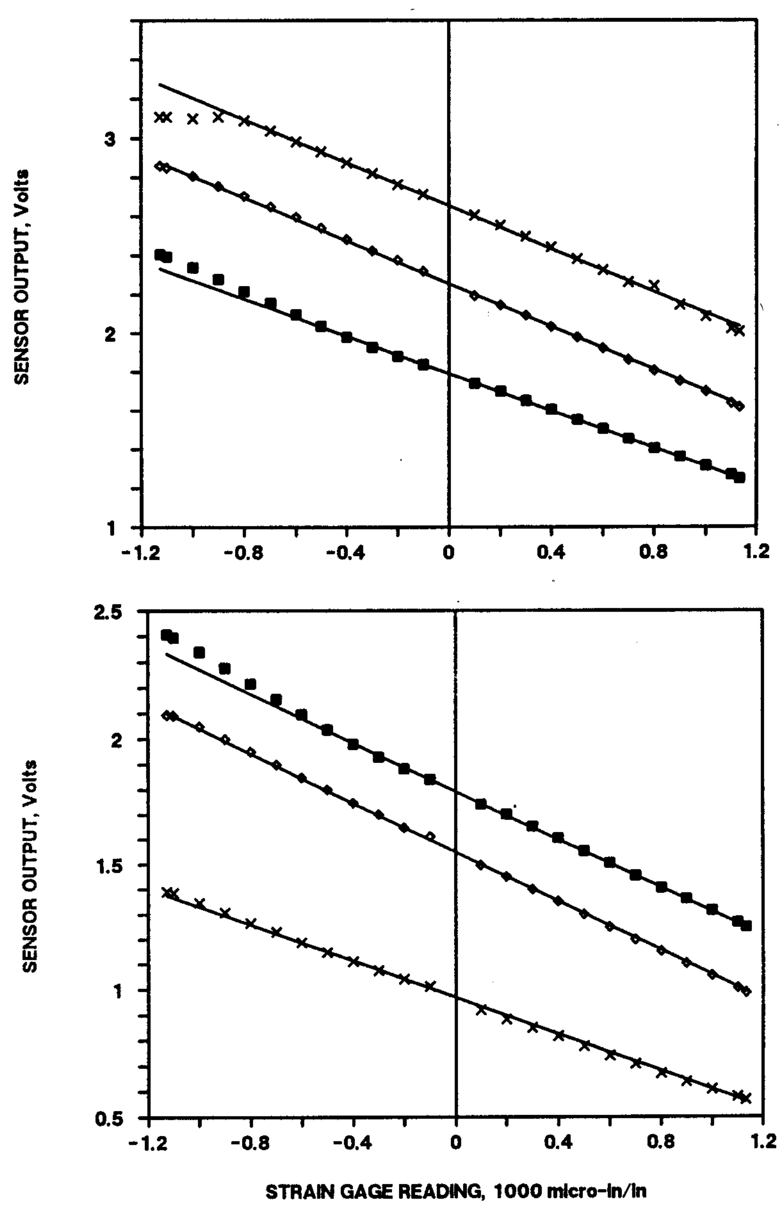

Figure 6-6
Fiber Optic Sensor Output as a Function of Strain in Structure for Various Sensor Pre-load Conditions

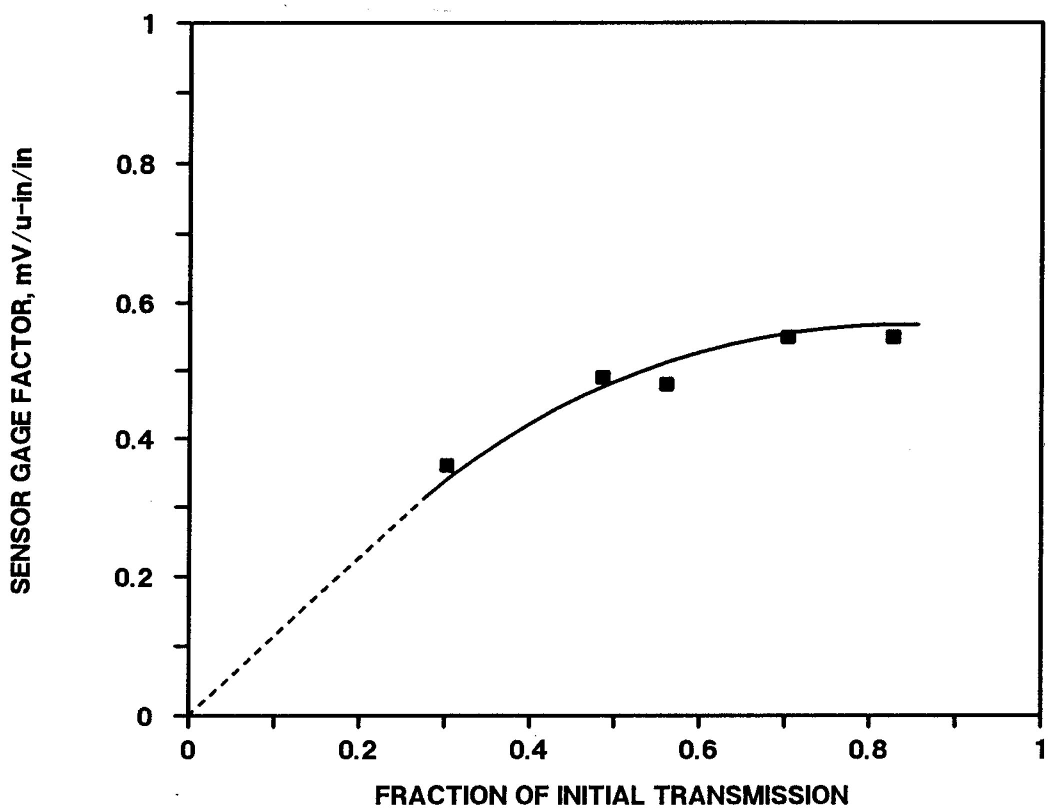

Figure 6-7
Sensor Gauge Factor as a Function of Sensor Pre-load

Laboratory Dynamic Strain Testing

Following the basic sensor experimental efforts involving static strain, dynamic tests were performed to determine the frequency response of the fiber optic strain sensor.

Dynamic Test Set-up

Dynamic strain data were obtained using an experimental set-up shown in Figure 6-8. The light source remained the same as the source used in the static experiments. The detector, however, was a Thorlabs Model DET1-SI silicon photo-detector that had a better than 1 Megahertz frequency response. Output of the photo-detector was used as the input to an amplifier with a 10X gain. An offset feature was built-into the amplifier to provide for zero voltage for zero strain (V0i = 0). The same aluminum beam (with FOSS device attached in the center) was used in the dynamic experiments. This beam was mounted in a dynamic load cell in the Contractor's materials testing lab. The load cell held the beam vertically and generated compressive loads. The strain gauge used in the static testing was also used during the dynamic tests. The load cell was set until a

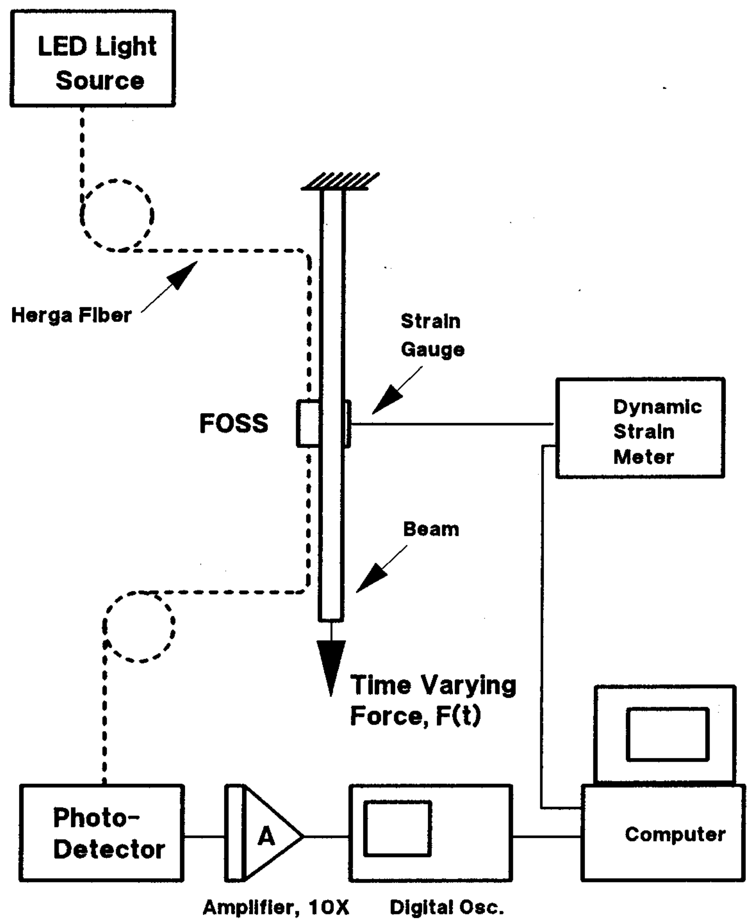

Figure 6-8
Experimental Set-up used for Dynamic Sensor Testing

maximum of 200 micro-strain was produced at maximum compression. The load cell thereby provided 0 to -200 micro-strain in a periodic fashion for a range of sinusoidal frequencies.

Output of the amplifier was used as input to a digital oscilloscope (Tektronix Model 2230). This oscilloscope had a digital storage and digital data transfer capability using a standard RS232 interface. A standard software package allowed the data to be transferred to a personal computer as a LOTUS 123 file. Within the LOTUS software, the file was further processed and/or displayed.

Dynamic Strain Results

The FOSS initial load adjustment screw was set to provide a fraction of initial transmission value of 0.7. For this setting, the Thorlabs photo-detector, coupled with the amplifier, provided a gauge factor of -2 volts per 1000 micro-strain, so the nominal sensor output varied from 0 to 0.4 volts for the 0 to -200 micro-strain induced by the dynamic load cell. Therefore, the dynamic FOSS device output is given by the following:

$$Strain(FOSS) = -V(FOSS) * 500 \quad , \tag{25}$$

where, V(FOSS) is the measured sensor output in volts.

Figure 6-9 shows the FOSS dynamic output response for load cell frequencies of 80 and 120 Hz. Note that some noise existed on the voltage output plot. This noise had a high frequency (approximately 1000 Hz) so digital filtering or smoothing could be used to improve voltage measurement resolution. Based on the initial signal-to-noise ratio in Figure 6-9, it is estimated that a voltage measurement resolution of 10 millivolts (or 5 micro-strain) could be achieved after appropriate filtering and / or signal processing. The peak-to-peak output values of dV = 0.42 and 0.39 volts evident in Figure 6-8 indicate that the sensor output is constant to approximately 100 Hz. The measured dV values for frequencies up to 140 Hz are shown in Figure 6-10. Note that the peak-to-peak sensor output starts to decrease around 100 Hz and is eighty percent of the static output at 140 Hz. These results show that the FOSS frequency response is adequate for generator applications.

Dynamic voltage output of the FOSS device, compared to the dynamic strain gauge output, is shown in Figure 6-11 for a 20 Hz load cell oscillation frequency. Note that the FOSS transducer's output indicates the same frequency as the strain gauge and has a zero phase lag compared to the standard strain gauge (SG) device output. Comparison data for frequencies up to 140 Hz show that the FOSS sensor follows the strain gauge sensor output frequency with no noticeable frequency measurement error and without any apparent phase lag. Some FOSS transducer output voltage ringing (variation if peak-to-peak output) is, however, noted in Figure 6-11. The amount of variation is the same for frequencies from 20 to 140 Hz and amounts to ten percent of the peak-to-peak sensor output value. The source of this ringing is not known at this time. Further experiments are necessary for various peak strain levels and other pre-load values to investigate the ringing effect.

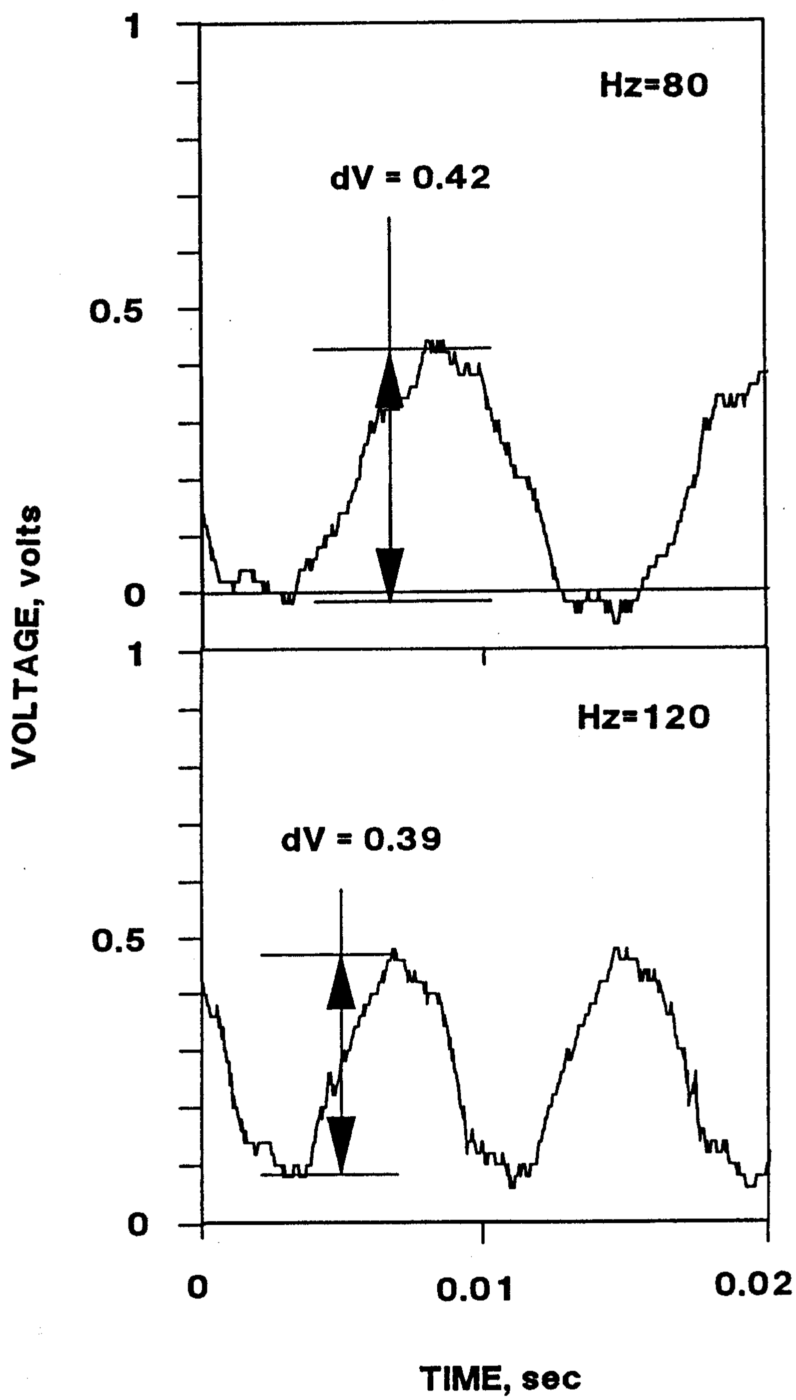

Figure 6-9
Sensor Output for Oscillating Strain (0 - 200 micro-strain) at 80 and 120 Hz

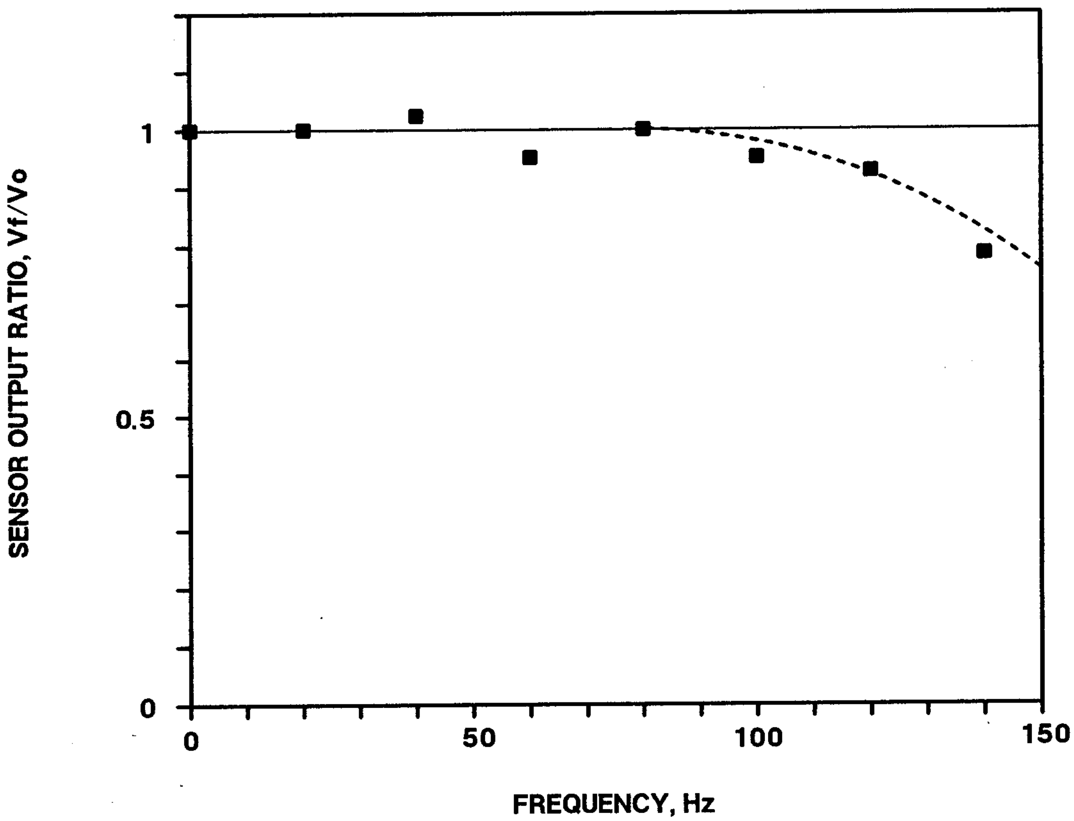

Figure 6-10
Sensor Peak Output Response as a Function of Oscillation Frequency

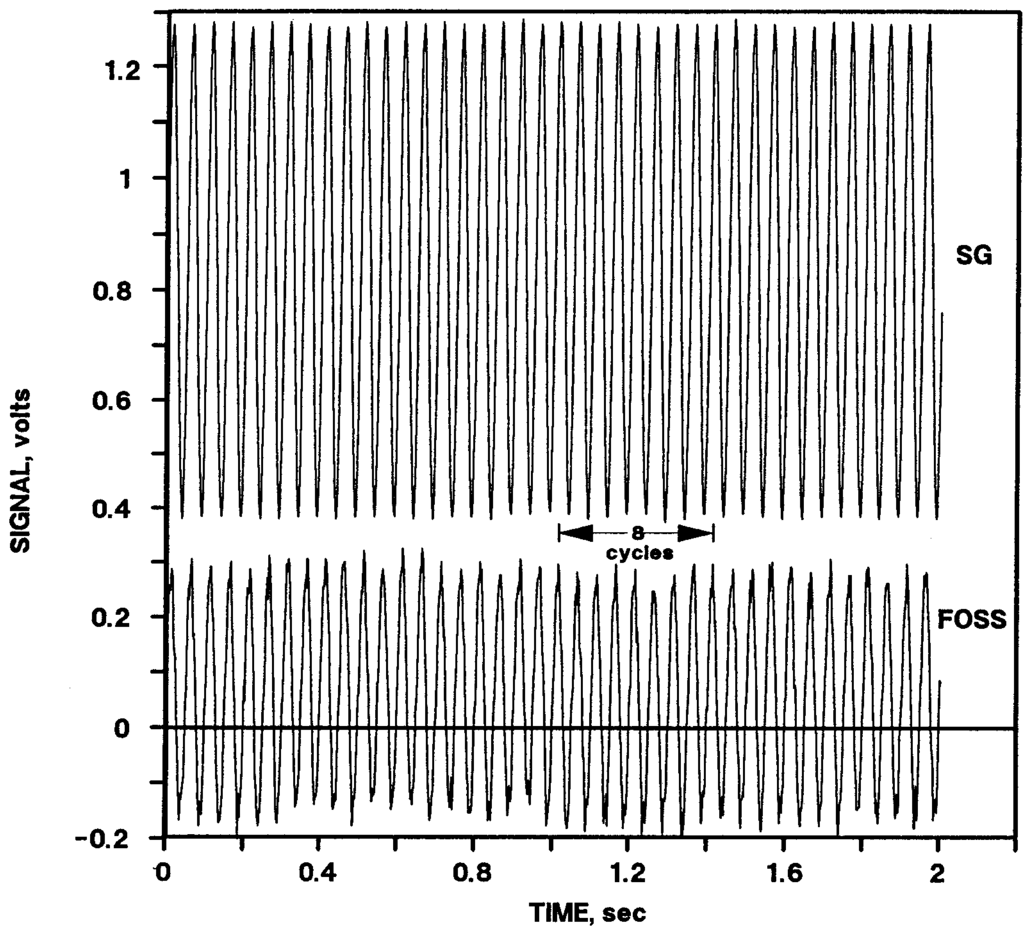

Figure 6-11
Fiber Optic Sensor Response Compared to Standard Strain Gauge Output for 20 Hz Oscillation

7

CONCLUSIONS

The results given in this report lead to the following conclusions regarding the application of fiber optic sensors to monitor temperature and end-winding strain in motors and generators:

1. The Distributed Fiber Optic Temperature Sensor (DFOTS), based on Rayleigh scattering in the fiber cladding, can monitor the temperature environment at multiple points within motor and generator windings under field test conditions. Both stator and rotor windings conditions can be examined.

2. The data reduction process to convert DFOTS results to temperature data was simplified using a new referencing scheme involving recording backscattering intensities from both ends of the sensing fiber.

3. The temperature sensing fiber can be retro-fit into stator windings during a rewind operation by attaching it within the stator slots.

4. The DFOTS fiber sensor can also be installed within a rotor during rotor-coil rewind operations. Access to the rotor's rotational axis (e.g., hollow rotor shaft) is required for installing the fiber and the rotating coupler. Also, rotating couplers can operate at 10,000 RPM, but no life-time data is available to indicate the joint will survive for the long periods of time required by the electric power industry.

5. The temperature sensing fiber is subject to damage and must be protected using a loose-tube jacket with a strength member. This jacket also provides a rugged means of adding optical connectors to the fiber ends.

6. Some type of fiber strain relief must be provided for the temperature sensing fiber at points where the fiber interfaces with electrical machinery to prevent damage due to sharp bends.

7. A fiber optic strain sensor (FOSS), designed and developed by the Contractor, provided point measurements of strain and the frequency of vibration-induced strain in a test structure (rectangular cross-section bar) under static and dynamic test conditions in a laboratory environment.

8. A suitable commercial fiber optic strain sensor was also identified near the end of the project effort.

9. Laboratory test results indicate that the Contractor's device and the commercial strain sensor met the required specifications for the end-winding strain monitoring application.

8

RECOMMENDATIONS

Based on the above conclusions and positive results obtained in this project effort, the following is recommended:

1. The DFOTS system should be further developed to provide a "turn-key" device capable of automated data acquisition, analysis and display of winding temperature for use by untrained personnel.

2. The modified and improved DFOTS system should be used to gather extensive monitoring data on several motors / generators in an operating power plant.

3. A lower-cost (lower spatial resolution) version of the DFOTS opto-electronics system should be developed for specific applications.

4. Further attempts should be made to obtain temperature data in rotating machinery using a jacketed fiber to aviod fiber damage problems.

5. The Contractor-developed fiber optic strain sensor should be installed and tested in an operating motor / generator to obtain start-up and operating system strain data for the end-winding monitoring application.

6. The commercial fiber optic strain sensor, identified in this project, should also be installed and tested, along with the Contractor's device, to compare each sensor's performance in operating power generation equipment.

9

REFERENCES

1. A.A. Boiarski, *Fiber Optic Distributed Temperature Sensor*, EPRI TR-101950, March 1993.

2. M. Twerdochlib, F.T. Emery, and G.B. Brandt, *Improved Temperature Sensors for Large Generators*, EPRI Report 2487-1 (GS-6338), April 1989.

3. A.J. Rogers, "Distributed Optical-Fibre Sensors", J. Phys. D: Appl. Phys. Vol 19, 2237-55, 1986.

4. D. Gloge, "Weakly Guiding Fibers", Appl. Optics, Vol. 10, 2252-58, 1971.

5. J.P. Dakin, et.al., "Distributed Optical Fiber Raman Temperature Sensor Using a Semiconductor Light Source and Detector", Elect. Lett., Vol. 21, No. 13, 569-570, 1985.

6. A.H. Hartog, et.al., "Distributed Temperature Sensing in Solid Core Fibres", Elect. Lett., Vol. 21, No. 32, 1061-1062, 1985.

7. K. Ogawa, et.al., "A Fiber-Optic Distributed Temperature Sensor with High-Distance Resolution", Springer Proc. in Physia, Vol. 44, Optical Fiber Sensors, Springer-Verlag Berlin, 1989.

8. A.A. Boiarski, et.al., "Temperature Measurements in Power Plant Equipment Using Distributed Fiber Optic Sensing", IEEE Transactions on Power Delivery, Vol. 10, No. 4, 1771-1778, 1995.

9. C. Mariottini, et.al., "On-Line Vibration Monitoring of End-Windings by Means of a Fiber-Optic Accelerometric System", Utility Motor and Generator Predictive Maintenance and Refurbishment, Nov. 28-30, Orlando, FL, 1995.

10. D. Bouilleret, et.al., "Fiber Optic Measurement Sensors—Recent Experiences in the Electrical Equipment Field", GEC Alsthom Technical Rev., No. 14-1994, 49-60, 1994.

11. A.J. Rodgers, "Distributed Optical-Fibre Sensors for the Measurement of Pressure, Strain and Temperature", Journ. of the Inst. of Electronic and Radio Engineers, Vol. 58, No. 5, 5113-5122, 1988.

12. J.P. Dakin, "Distributed Optical Fiber Sensors", SPIE Vol. 1797, Distributed and Multiplexed Fiber Optic Sensors II, 76-108, 1992.

13. J.S. Schoenwald, et.al., "Evaluation of an OTDR Microbend Distributed Sensor", SPIE Vol. 986, Fiber Optic Smart Structures and Skins, 150-156, 1988.

A

LOTUS 1-2-3 PROGRAM

In this appendix, the Lotus 1-2-3 program used to acquire and analyze OTDR data is briefly described. The program macros are listed along with a sample spreadsheet. The program is quite general and various types of calculations are provided so that the experimenter can try several different methods of data analysis.

Description of Macros

Figures A1 and A2 provide a portion of the spreadsheet. All the columns (i.e., A through Z) are shown, but only 80 of the 261 rows. The number of rows was selected to allow room to list all the macros. These macros are listed along the left side of Figure A1 and the macro name is given in column A. For example, the \R macro is listed in the B14 to D28 area of the spreadsheet. Each macro is run using the ALT key (e.g. ALT key with R key runs the \R macro). An explanation of each macro is provided below:

1. \B Macro - Must be run each time the OTDR and computer are turned off. This macro will initialize the system and activate the GBIB interface. The \B macro is run before several of the following macros can be used to acquire data. To analyze stored data, \B is not needed.

2. \R Macro - The \R macro results in the OTDR instrument acquiring standard reference intensity, Ir, data or backward intensity measurements, Ib, for the advanced referencing approach. These measured intensities are placed in the H5 ....H305 locations of the spreadsheet.

3. \S Macro - The \S macro is similar to the \R macro except the OTDR instrument acquires standard signal intensity, I, or forward intensity, If, data and places these data in the L5...L305 spreadsheet locations.

4. \T Macro - Causes the computer to calculate the temperature along the fiber (e.g., using Equation (15) in text of report) and display the temperature versus length measurements on the computer screen. The program uses newly acquired data or stored data, which is copied into the correct spreadsheet column, to make the temperature calculation.

	A	B	C	D	E	F	G	H	I	J	K	L	M
1	CON ED TEST 3 / 9/94-11/94												
2							DISTANCE	REF	SMOREF	Ir-Io	LOGR	SIGNAL	SMOSIG
3								(I1)			(L1)	(I2)	
4	L: 40 m						---------	--------	---------	-------	-------	---------	---------
5	SENSITIVITY: HI/MD	WAVE=		850 nm									
6	DELAY: 180, 560 ns						0.00	179	179.0	98.0	19.91	179	179.0
7	T/DIV:	50 ns					0.20	179	179.0	98.0	19.91	179	179.0
8	Lo:	0 m					0.39	179	179.3	98.3	19.93	179	179.3
9	Io:	81					0.59	180	179.7	98.7	19.94	180	179.7
10	dBo:	0	dB				0.78	180	180.0	99.0	19.96	180	180.0
11							0.98	180	180.0	99.0	19.96	180	180.0
12							1.18	180	179.3	98.3	19.93	180	179.7
13							1.37	178	176.3	95.3	19.79	179	178.3
14	\R	{INIT}					1.57	171	176.0	95.0	19.78	176	178.0
15		{REMOTE OTDR}					1.76	179	170.3	89.3	19.51	179	171.7
16		{OUTPUT OTDR,"CLEAR"}					1.96	161	163.3	82.3	19.16	160	164.0
17		{OUTPUT OTDR,"CALC S"}					2.16	150	157.0	76.0	18.81	153	160.7
18		{OUTPUT OTDR,"SEND CM"}					2.35	160	162.0	81.0	19.08	169	166.3
19		{LREAD OTDR,F38}					2.55	176	165.7	84.7	19.28	177	168.7
20		{OUTPUT OTDR,"RRET N"}					2.75	161	162.0	81.0	19.08	160	160.3
21		{OUTPUT OTDR,"SEND RR"}					2.94	149	159.7	78.7	18.96	144	158.3
22		{LREAD OTDR,F41}					3.14	169	156.3	75.3	18.77	171	152.3
23		{OUTPUT OTDR,"MSIG"}					3.33	151	155.7	74.7	18.73	142	148.3
24		{OUTPUT OTDR,"SEND M8"}					3.53	147	159.3	78.3	18.94	132	151.0
25		{BREAD OTDR,1U,H5..H305,256}					3.73	180	168.7	87.7	19.43	179	163.7
26		{CALC}					3.92	179	170.0	89.0	19.49	180	165.7
27		{BEEP}					4.12	151	160.7	79.7	19.01	138	153.0
28		{QUIT}					4.31	152	150.0	69.0	18.39	141	138.3
29							4.51	147	157.3	76.3	18.83	136	150.7
30							4.71	173	166.7	85.7	19.33	175	163.7
31							4.90	180	177.3	96.3	19.84	180	178.0
32							5.10	179	166.7	85.7	19.33	179	162.0
33							5.29	141	153.0	72.0	18.57	127	144.3
34	\S	{INIT}					5.49	139	140.3	59.3	17.73	127	127.3
35		{REMOTE OTDR}					5.69	141	149.7	68.7	18.37	128	142.7
36		{OUTPUT OTDR,"CLEAR"}					5.88	169	162.0	81.0	19.08	173	159.3
37		{OUTPUT OTDR,"CALC S"}					6.08	176	174.7	93.7	19.72	177	176.3
38		{OUTPUT OTDR,"SEND CM"}					6.27	179	168.3	87.3	19.41	179	162.3
39		{LREAD OTDR,F38}					6.47	150	157.7	76.7	18.85	131	146.0
40		{OUTPUT OTDR,"RRET N"}					6.67	144	145.0	64.0	18.06	128	128.0
41		{OUTPUT OTDR,"SEND RR"}					6.86	141	143.0	62.0	17.92	125	125.7
42		{LREAD OTDR,F41}					7.06	144	142.7	61.7	17.90	124	123.3
43		{OUTPUT OTDR,"MSIG"}					7.25	143	139.3	58.3	17.66	121	122.0
44		{OUTPUT OTDR,"SEND M8"}					7.45	131	133.3	52.3	17.19	121	122.0
45		{BREAD OTDR,1U,L5..L305,256}					7.65	126	129.0	48.0	16.81	124	122.3
46		{CALC}					7.84	130	132.0	51.0	17.08	122	125.3
47		{BEEP}					8.04	140	134.7	53.7	17.30	130	126.0
48		{QUIT}					8.24	134	134.7	53.7	17.30	126	126.0
49							8.43	130	131.7	50.7	17.05	122	123.3
50							8.63	131	130.0	49.0	16.90	122	122.0
51							8.82	129	130.7	49.7	16.96	122	121.7
52	\T	{M}G1NU					9.02	132	131.3	50.3	17.02	121	122.7
53		TEMP~					9.22	133	131.7	50.7	17.05	125	122.7
54		QP					9.41	130	132.0	51.0	17.08	122	121.3
55							9.61	133	131.3	50.3	17.02	117	118.3
56	\D	{M}G1NU					9.80	131	132.0	51.0	17.08	116	116.3
57		LOGREF~					10.00	132	131.3	50.3	17.02	116	117.7
58		QP					10.20	131	131.7	50.7	17.05	121	119.7
59							10.39	132	132.7	51.7	17.13	122	121.7
60	\L	{M}G1NU					10.59	135	131.0	50.0	16.99	122	118.0
61		LOGI~					10.78	126	130.3	49.3	16.93	110	114.0
62		QP					10.98	130	127.7	46.7	16.69	110	109.3
63							11.18	127	129.7	48.7	16.87	108	108.3
64	\I	{M}G1NU					11.37	132	127.7	46.7	16.69	107	108.0
65		SIGNAL~					11.57	124	124.0	43.0	16.33	109	106.7
66		QP					11.76	116	118.0	37.0	15.68	104	105.0
67							11.96	114	114.3	33.3	15.23	102	104.3
68							12.16	113	114.7	33.7	15.27	107	103.0
69	\B	{S}AA					12.35	117	113.7	32.7	15.14	100	101.7
70		GPIB-PC.APP~					12.55	111	113.0	32.0	15.05	98	99.7
71		I					12.75	111	111.3	30.3	14.82	101	99.7
72		GPIB-PC~					12.94	112	111.7	30.7	14.87	100	100.3
73		S					13.14	112	112.7	31.7	15.01	100	99.3
74		DEVICE1~					13.33	114	114.0	33.0	15.19	98	98.3
75		NR					13.53	116	115.3	34.3	15.36	97	98.0
76		OTDR.DCF~					13.73	116	116.0	35.0	15.44	99	98.3
77		T					13.92	116	114.7	33.7	15.27	99	98.3
78		100~					14.12	112	114.3	33.3	15.23	97	98.3
79		QQQ					14.31	115	113.7	32.7	15.14	99	98.7
80							14.51	114	114.0	33.0	15.19	100	98.7

Figure A-1
Columns A through M of Spreadsheet

	N	O	P	Q	R	S	T	U	V	W	X	Y	Z
1													
2	Is-Io	LOGS	LOGRI	dBs1	dBs2	dBs	TEMP	TEMP	dBs1I	dBs	TEMP		
3		(L2)	1INV	RT REF	RT REF	1I REF	RT REF	1I REF		IRT REF	IRT REF	LOGIR1	LOGIR2
4	------	------	------	------	------	------	------	------	------	------	------	------	------
5													
6	98.0	19.91	13.921	0.000	0.000	1.874	24.5	3.5	0.249	-0.475	27.6	20.00	20.00
7	98.0	19.91	16.902	0.099	0.040	3.364	23.5	0.7	0.528	-0.315	25.6	20.00	20.00
8	98.3	19.93	18.808	0.099	0.040	4.325	23.5	0.3	0.331	-0.413	26.8	20.01	20.01
9	98.7	19.94	19.883	0.100	0.041	4.869	23.5	0.2	0.246	-0.456	27.4	20.03	20.03
10	99.0	19.96	19.927	0.100	0.041	4.899	23.5	0.1	0.085	-0.536	28.4	20.04	20.04
11	99.0	19.96	18.513	0.100	0.041	4.191	23.5	0.3	0.113	-0.522	28.2	20.04	20.04
12	98.7	19.94	16.435	0.099	0.041	3.145	23.5	0.9	0.254	-0.452	27.3	20.01	20.03
13	97.3	19.88	12.553	0.051	0.024	1.175	23.9	7.2	0.909	-0.132	23.4	19.93	19.99
14	97.0	19.87	12.711	0.050	0.024	1.246	23.9	6.7	0.880	-0.147	23.6	19.91	19.97
15	90.7	19.57	13.291	0.024	-0.000	1.390	24.5	5.8	1.111	-0.044	22.5	19.67	19.70
16	83.0	19.19	13.741	0.058	-0.031	1.423	25.3	5.6	1.082	-0.074	22.8	19.28	19.34
17	79.7	19.01	13.554	-0.065	-0.021	1.240	25.0	6.7	1.128	-0.046	22.5	19.05	19.16
18	85.3	19.31	12.788	-0.014	0.007	1.006	24.3	8.6	0.777	-0.208	24.3	19.28	19.43
19	87.7	19.43	12.041	0.013	0.027	0.692	23.8	11.9	0.797	-0.187	24.1	19.44	19.53
20	79.3	18.99	12.041	0.143	-0.022	0.475	25.0	14.9	0.797	-0.211	24.3	19.12	19.14
21	77.3	18.88	12.304	0.123	-0.008	0.551	24.7	13.8	1.063	-0.072	22.8	19.01	19.01
22	71.3	18.53	12.304	0.100	-0.099	0.376	27.1	16.6	1.170	-0.064	22.7	18.85	18.75
23	67.3	18.28	12.389	0.061	-0.113	0.293	27.5	18.1	1.365	0.027	21.7	18.85	18.51
24	70.0	18.45	12.553	0.068	-0.143	0.459	28.4	15.2	1.314	-0.014	22.1	19.05	18.71
25	82.7	19.17	12.632	0.084	0.002	0.860	24.4	10.0	1.394	0.099	21.0	19.53	19.29
26	84.7	19.28	12.553	0.039	0.005	0.872	24.3	9.9	1.209	0.008	21.9	19.64	19.40
27	72.0	18.57	12.131	0.000	0.000	0.309	24.5	17.7	1.218	0.010	21.9	19.19	18.69
28	57.3	17.58	12.131	-0.092	-0.036	-0.186	25.4	29.7	1.105	-0.065	22.7	18.65	17.73
29	69.7	18.43	12.041	-0.081	-0.045	0.193	25.7	20.0	1.127	-0.058	22.6	19.08	18.59
30	82.7	19.17	12.131	-0.033	-0.015	0.609	24.9	13.0	0.995	-0.109	23.2	19.54	19.31
31	97.0	19.87	12.041	0.038	-0.019	0.911	25.0	9.5	0.797	-0.210	24.3	19.99	20.01
32	81.0	19.08	12.389	0.064	-0.053	0.694	25.9	11.9	0.842	-0.205	24.3	19.44	19.26
33	63.3	18.02	12.553	-0.023	-0.107	0.242	27.4	19.0	0.909	-0.198	24.2	18.77	18.24
34	46.3	16.66	12.711	-0.071	-0.166	-0.358	29.1	35.6	1.069	-0.148	23.6	17.97	16.93
35	61.7	17.90	12.711	-0.114	-0.069	0.263	26.3	18.6	0.973	-0.147	23.6	18.65	18.08
36	78.3	18.94	12.788	-0.014	-0.024	0.821	25.1	10.4	0.957	-0.132	23.4	19.28	19.08
37	95.3	19.79	12.788	0.018	0.007	1.247	24.3	6.7	0.957	-0.117	23.3	19.88	19.91
38	81.3	19.10	12.863	0.116	-0.120	0.940	27.7	9.2	1.127	-0.096	23.0	19.48	19.34
39	65.0	18.13	12.937	0.083	-0.143	0.490	28.4	14.7	1.202	-0.070	22.7	18.94	18.39
40	47.0	16.72	12.937	0.057	-0.248	-0.214	31.7	30.6	1.298	-0.074	22.8	18.17	17.08
41	44.7	16.50	12.937	0.007	-0.022	-0.324	25.0	34.3	1.495	0.137	20.6	18.08	16.63
42	42.3	16.27	12.863	0.052	-0.096	-0.478	27.1	40.3	1.420	0.063	21.3	18.02	16.47
43	41.0	16.13	12.863	-0.005	-0.137	-0.548	28.2	43.3	1.127	-0.104	23.1	17.83	16.37
44	41.0	16.13	12.937	-0.055	-0.036	-0.510	25.4	41.7	0.928	-0.153	23.7	17.40	16.27
45	41.3	16.16	13.222	-0.106	-0.135	-0.350	28.2	35.3	1.128	-0.103	23.1	17.08	16.40
46	44.3	16.47	13.358	-0.034	-0.117	-0.130	27.7	28.0	1.352	0.018	21.8	17.27	16.69
47	45.0	16.53	13.554	-0.049	-0.264	0.000	32.2	24.5	1.462	0.000	22.0	17.51	16.90
48	45.0	16.53	13.617	-0.074	-0.204	0.032	30.3	23.7	1.192	-0.105	23.1	17.53	16.84
49	42.3	16.27	13.979	-0.117	-0.193	0.080	29.9	22.5	1.173	-0.109	23.2	17.32	16.56
50	41.0	16.13	14.037	-0.100	-0.137	0.039	28.2	23.5	1.158	-0.089	23.0	17.16	16.37
51	40.7	16.09	14.094	-0.123	-0.173	0.050	29.3	23.2	1.215	-0.078	22.8	17.24	16.37
52	41.7	16.20	14.037	-0.119	-0.166	0.074	29.1	22.7	1.231	-0.066	22.7	17.30	16.47
53	41.7	16.20	14.094	-0.144	-0.230	0.103	31.1	22.0	1.144	-0.143	23.6	17.35	16.53
54	40.3	16.06	14.037	-0.115	-0.175	0.004	29.4	24.4	1.016	-0.179	24.0	17.35	16.33
55	37.3	15.72	13.979	-0.092	-0.271	-0.193	32.5	29.9	1.028	-0.220	24.4	17.27	16.09
56	35.3	15.48	13.921	-0.088	-0.255	-0.342	31.9	34.9	1.188	-0.132	23.4	17.32	15.84
57	36.7	15.64	14.420	-0.146	-0.241	-0.012	31.5	24.8	1.332	-0.054	22.6	17.32	15.98
58	38.7	15.87	14.624	-0.090	-0.153	0.206	28.7	19.8	1.337	-0.007	22.1	17.30	16.13
59	40.7	16.09	14.624	-0.031	-0.071	0.315	26.4	17.6	1.144	-0.063	22.7	17.32	16.27
60	37.0	15.68	14.314	-0.011	-0.091	-0.045	26.9	25.7	1.090	-0.100	23.1	17.16	15.87
61	33.0	15.19	14.205	-0.070	-0.158	-0.348	28.9	35.2	1.047	-0.155	23.7	17.16	15.44
62	28.3	14.52	14.205	-0.143	-0.298	-0.679	33.4	49.7	1.116	-0.190	24.1	16.99	14.91
63	27.3	14.37	14.037	-0.130	-0.501	-0.841	41.3	58.8	0.744	-0.478	27.6	17.16	14.96
64	27.0	14.31	13.802	-0.369	-0.823	-0.985	57.7	68.3	0.190	-0.916	34.1	17.22	15.23
65	25.7	14.09	13.617	-0.728	-1.379	-1.188	103.0	84.3	-0.515	-1.546	46.1	17.22	15.56
66	24.0	13.80	13.490	-1.247	-1.830	-1.397	164.8	104.9	-0.907	-1.968	56.4	17.08	15.72
67	23.3	13.68	13.680	-1.560	-2.106	-1.363	219.6	101.3	-1.011	-2.158	61.8	16.93	15.87
68	22.0	13.42	13.490	-1.516	-2.132	-1.586	225.7	127.8	-0.804	-2.067	59.1	16.93	15.64
69	20.7	13.15	13.222	-1.530	-2.162	-1.856	232.8	169.1	-0.804	-2.082	59.6	16.81	15.40
70	18.7	12.71	13.010	-1.590	-2.214	-2.183	245.7	237.8	-0.730	-2.071	59.3	16.78	15.01
71	18.7	12.71	13.222	-1.732	-2.168	-2.077	234.2	212.9	-0.691	-2.029	58.1	16.69	14.96
72	19.3	12.86	13.291	-1.622	-1.968	-1.966	190.2	189.8	-0.622	-1.894	54.4	16.63	14.91
73	18.3	12.63	13.010	-1.636	-1.911	-2.222	179.1	247.7	-0.730	-1.919	55.1	16.78	14.62
74	17.3	12.39	12.788	-1.604	-1.899	-2.455	176.9	315.8	-0.895	-1.996	57.2	16.93	14.37
75	17.0	12.30	12.863	-1.518	-1.822	-2.459	163.3	317.2	-0.819	-1.919	55.1	17.02	14.21
76	17.3	12.39	12.937	-1.346	-1.791	-2.380	158.2	292.1	-0.744	-1.867	53.7	16.93	14.26
77	17.3	12.39	12.863	-1.275	-1.845	-2.417	167.4	303.6	-0.938	-1.991	57.0	16.69	14.31
78	17.3	12.39	12.937	-1.288	-1.791	-2.380	158.2	292.1	-0.804	-1.897	54.5	16.66	14.26
79	17.7	12.47	13.010	-1.217	-1.762	-2.302	153.5	269.3	-1.018	-1.989	57.0	16.50	14.31
80	17.7	12.47	13.082	-1.237	-1.815	-2.266	162.2	259.4	-1.000	-2.007	57.5	16.56	14.37

Figure A-2
Columns N through Z of Spreadsheet

5. \D Macro - Calculates and displays the variable dBs using equation (18) in report text. An example plot is shown in Figure 4-5.

6. \L Macro - Usually displays the dB values 10 * Log_{10} (I-Io) and 10*Log10 (Ir-Io) versus length. Further, the forward and backward dB values can be displayed instead. This macro provides a typical OTDR plot and an example is shown in Figure 4-1.

7. \I Macro - Displays the measured values I and Ir or Ib and If versus length.

Brief Description of Program

The following text provides a brief description of the LOTUS 1-2-3 program. The description is based on explaining the calculations occurring in each row and column.

1. Column G is the distance, L_f, along the fiber, therefore, Row 80 provides data for L_f = 14.51 meters. The remaining rows list similar data for other distances up to the maximum distance of 50 meters. The program requires several numerical inputs to calculate the correct length information, namely:

   Lo =<u>0</u> meters (entered in spreadsheet position B8) is the initial length, and

   Li = <u>50</u> meters is the length of fiber examined (entered in B7).

   Other values of Lo and Li (i.e., other than 0 and 50) are used depending on the specific fiber geometry and measurement scenario. To perform the distance calculation in Column G, the following cell equations are used:

   G6 = B8

   G7 = G6 + (B7 / 255)

   G(i) = G(i-1) + (B7 / 255)

   for row i = 8, 9, 10, ... 261.

2. Column H contains the reference intensity data, Ir. For the advanced referencing approach, the backwards intensity values, Ib, are stored in Column H.

3. Column I is a running 3 point average of the reference intensity data in Column H, where:

   Ir(i) = (Ir(i-1) + Ir(i) + Ir(i+1)) / 3.

Using this data averaging procedure can smooth out electronic noise in the OTDR signal.

4. Column J contains the relative reference intensity value, Ir - Io, where Io is the background intensity, such that:

   J(i) = H(i) - B9

   The background intensity, Io = 81, is entered in B9. The Io intensity value varies (i.e., not always equal to 81) with the particular experimental conditions and it is determined by examining the last entries in column H to determine the intensity beyond the Fresnell end reflection. Io must be entered in speradsheet location B9 to provide accurate intensity data.

5. In Column K the relative reference Intensity is converted to dB, so the quantity 10 Log_{10} (Ir - Io) is calculated, where:

   K(i) = 10 * @LOG(J(i)).

6. Column L contains the signal intensity data, I. For the advanced referencing approach, the forward intensity values, If, are stored in Column L.

7. Column M is the running 3 point average of the signal intensity data in Column L, Hence:

   I(i) = (I(i-1) + I(i) + I(i+1))/3.

8. In Column N, the relative signal intensity values, I - Io, such that:

   N(i) = M(i) - B9.

9. Column O contains the signal intensity (or forward intensity) data converted to dB values, so the quantity 10 Log10 (I-Io) is calculated:

   O(i) = 10*@LOG(N(i)).

10. Column P contains the inverted backward intensity, Ib(inv), data (in dB form) that is required for the advanced referencing approach, where:

    P(6) = K215,

    P(7) = K214. ...etc.

    The K column data must usually be shifted vertically in the P column to provide a proper match-up of the forward and inverted backward length locations. Note that the inversion process (in this case) starts at row 215. An improved version of the code would use a macro to provide a more automated method for inverting and matching the forward and inverted backward intensities.

11. In Column Q, the dBs values are calculated for the backward direction in the fiber using the *standard* referencing approach. To perform these calculations, the Log_{10} (Ir-Io) values needed to be stored in the spreadsheet at locations (i.e., Column Y) that were not affected by any data acquisition procedures (especially ones associated with the new referencing method). The room temperature dB intensity values for the backward reference, dB = 10*Log_{10}(Ib), are also stored in Column Y, therefore :

    $$Q(i) = K(i) - Y(i) ,$$

    which is a form of Equation (18).

12. In a similar manner, Column R contains the dBs values calculated for the forward direction in the fiber. Again using the standard referencing approach, the values of Log_{10}(I-Io) are stored in Column Z, therefore:

    $$R(i) = O(i) - Z(i).$$

13. In column S, dBs is calculated using the new referencing approach. Equation (19) is used to obtain these dBs values, therefore:

    $$S(i) = O(i)/2+ P(i)/2 \ .$$

14. Equation (15) is used to calculate the temperature along the fiber length using the standard referencing approach and the forward intensity data . Column T contains these results, as follows:

    T(i) = @EXP((-R(i) + B)/A).

    Values for constants A and B are given in the text of the report.

15. Column U contains the temperature calculations along the fiber length using the new referencing approach and Equation (15), as follows:

    U(i) = @EXP((-S(i) +B)/A).

16. An alternate method of calculating the temperature profile, using the new referencing approach, is provided in Columns V, W, and X. This new approach involves inverting the dBs values determined from the backward intensity data after it has been referenced to the room temperature values. This alternate approach can

sometimes further reduce noise in the OTDR data. To perform this alternate calculation, Column V contains an inversion of the backward dBs values, hence:

V(6) = Q(215)

V(7) = Q(214), ...etc.

17. Column W is similar to Column S in that dBs is calculated, however, in this case the data from Column V is used to reduce OTDR noise, therefore:

    W(i) = R(i) / 2 + V(i) / 2.

18. Column X contains temperature calculations along the fiber length using the modified version of the new referencing approach and Equation (15) as follows:

    X(i) = @EXP((-W(i) + B) / A).

Given the formulas and Macros listed above and in Figures A1 and A2, one should be able to construct a new LOTUS 1-2-3 (or EXCEL) program to analyze the data. Further, any other computer language could be generated to provide the same program functionality.

WARNING: This Document contains information classified under U.S. Export Control regulations as restricted from export outside the United States. You are under an obligation to ensure that you have a legal right to obtain access to this information and to ensure that you obtain an export license prior to any re-export of this information. Special restrictions apply to access by anyone that is not a United States citizen or a Permanent United States resident. For further information regarding your obligations, please see the information contained below in the section titled "Export Control Restrictions."

Export Control Restrictions

Access to and use of EPRI Intellectual Property is granted with the specific understanding and requirement that responsibility for ensuring full compliance with all applicable U.S. and foreign export laws and regulations is being undertaken by you and your company. This includes an obligation to ensure that any individual receiving access hereunder who is not a U.S. citizen or permanent U.S. resident is permitted access under applicable U.S. and foreign export laws and regulations. In the event you are uncertain whether you or your company may lawfully obtain access to this EPRI Intellectual Property, you acknowledge that it is your obligation to consult with your company's legal counsel to determine whether this access is lawful. Although EPRI may make available on a case by case basis an informal assessment of the applicable U.S. export classification for specific EPRI Intellectual Property, you and your company acknowledge that this assessment is solely for informational purposes and not for reliance purposes. You and your company acknowledge that it is still the obligation of you and your company to make your own assessment of the applicable U.S. export classification and ensure compliance accordingly. You and your company understand and acknowledge your obligations to make a prompt report to EPRI and the appropriate authorities regarding any access to or use of EPRI Intellectual Property hereunder that may be in violation of applicable U.S. or foreign export laws or regulations.

About EPRI

EPRI creates science and technology solutions for the global energy and energy services industry. U.S. electric utilities established the Electric Power Research Institute in 1973 as a nonprofit research consortium for the benefit of utility members, their customers, and society. Now known simply as EPRI, the company provides a wide range of innovative products and services to more than 1000 energy-related organizations in 40 countries. EPRI's multidisciplinary team of scientists and engineers draws on a worldwide network of technical and business expertise to help solve today's toughest energy and environmental problems.

EPRI. Electrify the World

TR-101950-V2

Printed on recycled paper in the United States of America

EPRI • 3412 Hillview Avenue, Palo Alto, California 94304 • PO Box 10412, Palo Alto, California 94303 • USA
800.313.3774 • 650.855.2121 • askepri@epri.com • www.epri.com